HIGH THROUGHPUT DISCOVERY OF NOVEL POLYMERS TO PREVENT BIOFILM FORMATION ON BLOOD-CONTACTING MEDICAL DEVICES

Taranjit Singh, MPharm(Hons) MRPharmS AMRSC

Thesis submitted to the University of Nottingham for the degree of Doctor of Philosophy

September 2016

Abstract

Biofilm formation on blood-contacting medical devices is a major healthcare problem causing significant morbidity, mortality and economic burden on healthcare systems around the world. In this thesis, a high throughput material microarray approach was used to screen a library of novel acrylate and methacrylate based polymer materials for bacterial attachment, haemostasis and immune system interactions. Polymer microarray printing was first optimised to produce confined spots of each material, confirmed by ToF-SIMS. The polymer microarray was incubated in human blood and analysed for blood proteins, cells and immune component attachment on each spot of the microarray. The blood exposed microarray was then incubated in RPMI-1640 media containing *Pseudomonas aeruginosa* and *Staphylococcus aureus* in two separate experiments to model a bacterial challenge on blood-contacting devices. These high throughput screening experiments identified nine haemocompatible bacterial resistant 'hit' materials for further analysis.

The 'hit' materials identified from microarray screening were then scaled up and used as coatings on silicone catheters for further *in-vitro* bacterial attachment and haemocompatibility testing. The *in-vitro* bacterial attachment assays were similar to the assays carried out by Hook *et. al.* [1] with an added complication of blood pre-conditioning step to simulate blood-contacting devices. All of the scaled up materials showed a significantly lower surface bacterial attachment when compared with uncoated silicone and commercially available silver incorporated catheters. Co-polymer of isobornyl acrylate with tri(ethylene glycol) methyl ether methacrylate (75:25) showed

71% and 77% lower coverage of *P. aeruginosa* and 67% and 58% lower coverage of *S. aureus* when compared with uncoated silicone and silver incorporated catheters, respectively. A number of scaled up materials showed a good haemocompatibility, in particular the co-polymer containing 2-ethylhexyl methacrylate and di(ethylene glycol) methyl ether methacrylate (75:25), which showed a very low coagulation and immune system activation.

The *in-vivo* foreign-body infection model results showed an order of magnitude reduction in bacterial attachment for co-polymer isobornyl acrylate (75%) tri(ethylene glycol) methyl ether methacrylate (25%) over five day period for *P. aeruginosa* and *S. aureus* when compared with a silicone surface. This reduction in bacterial numbers was also observed in the tissue surrounding the catheter. Furthermore, isobornyl acrylate–co-tri(ethylene glycol) methyl ether methacrylate also showed good biocompatibility without a foreign-body reaction. The future work involves testing these 'hit' materials in an animal model under blood flow conditions to validate *in-vivo* performance, a successful outcome of which would warrant a big step towards its clinical use.

Acknowledgements

After three years of blood (from healthy volunteers!), sweat and tears, I would like to take this opportunity to thank a number of individuals for their help, guidance and support throughout this project. Firstly, I am extremely grateful to the University of Nottingham for funding my project via the Vice-Chancellor's Scholarship for Research Excellence for International students. This scholarship was vital for carrying out my research at the University of Nottingham.

I would like to thank my supervisors Prof. Morgan Alexander, Prof. Martyn Davies and Prof. Paul Williams for their support and guidance throughout my PhD. The monthly supervisors' meetings were key to the success of this project.

During my PhD I had an opportunity to travel to Dresden (Germany) to work with Leibniz Institute of Polymer Research, Max Bergmann Center of Biomaterials Dresden. My visit was made possible with the funding from Graduate school travel prize from the University of Nottingham. I would like to thank my host Prof. Carsten Werner, along with Dr. Manfred Maitz and Dr. Claudia Sperling for their help with my project.

I am very grateful to Mike Taylor, Robert Cavanagh, Fabian Bülow and Morgan Alexander for donating their precious blood for my experiments. The help and support with polymer chemistry from Dr. Derek Irvine and Dr. Kevin Adlington is kindly acknowledged. Help and support with *in-vivo* experimental work from Dr. Jeni Luckett is kindly acknowledged.

The support and guidance with experimental work from post-docs was very helpful. I would like to thank Dr. Andrew Hook, Dr. Ewan Murray, Dr. Jean Dubern, Dr. David Scurr, Dr. Adam Celiz, Dr. Asha Patel, Dr. Peter Magennis and Dr. Vincenzo Taresco.

Help with XPS analysis from Dr. Emily Smith and NEXUS facility at Newcastle University is kindly acknowledged. Help and support with SEM analysis from Christine Grainger-Boultby is kindly acknowledged.

Office D20 in Boots Science Building was the place to discuss the work with fellow PhD students as well as learn new English slang words! I would like to thank my friends Mike, Stephen, Adam, Sunil, Rob, Yasin, Toba, Alessandro, Paula, Vicky, Leigh-Ann and Mo for pleasant time in D20. The support from the technicians – Paul, Christy, Tom and admin staff – Gail and Julia in Boots building is kindly acknowledged.

Finally, I would like to thank my parents Kulwinder and Avtar, my sister Harpreet for their love, prayers and encouragement to achieve my goals in life. I would also like to thank my uncle and aunt - Balwant Singh Tumber and Baljit Kaur and their family – Jasbir, Sharon, Amrik, Didar and Harvinder for supporting and helping me throughout my time in the UK.

Table of Contents

Abstract ii

Acknowledgements iv

Table of Contents vi

List of Figures xvi

List of Tables xxiii

List of Abbreviations xxiv

1 Chapter 1 - Introduction 1

1.1 Blood-contacting medical devices 2

1.1.1 Biofilm formation on medical devices 2

1.1.2 Protein adsorption and thrombosis on medical devices 7

1.2 Current clinical best practice to prevent catheter associated biofilm infections 10

1.2.1 Antibiotics 10

1.2.2 Antiseptic coated catheters 12

1.2.3 Heparin coating 13

1.3 Molecular microbiology approaches to combat biofilms . 15

1.4 Emergent surface chemistry modification strategies to combat biofilms 16

1.4.1 Surface modification using poly-sulfobetaine (zwitterionic polymer) 16

1.4.2 Polymer embedded with electro-conductive materials 17

1.4.3 Polycationic antimicrobial hydrogel with microbe membrane suctioning effect 18

1.4.4 High throughput screening using material microarrays to identify bacterial adhesion resistant materials 19

1.5 Table of key molecules described in the Thesis 22

1.6 Aim and objectives 23

2 Chapter 2 – Materials and methods 24

2.1 Materials 24

2.2 Microarray substrate slide preparation for printing 25

2.3 Microarray printing 26

2.4 Time of Flight Secondary Ion Mass Spectrometry (ToF-SIMS) 28

2.5 X-ray Photoelectron Spectroscopy (XPS) 35

2.6 Water Contact Angle measurements 39

2.7 Details of bacterial strains used in this project 41

2.8 Bacterial incubation and high throughput bacterial attachment assay 41

2.9 Fluorescence confocal microscopy 43

3 Chapter 3 – Optimisation of microarray printing 46

3.1 Introduction 46

3.1.1 Aim and objectives 47

3.2 Experimental 48

3.2.1 pHEMA dip coating on epoxy functionalised glass slides 48

3.2.2 Microarray Printing 48

3.2.3 ToF-SIMS 49

3.2.4 Contact angle measurements 50

3.2.5 Optical microscopy 51

3.3 Results 52

3.3.1 Optimising microarray printing for well-defined spot formation by varying solvent concentration 52

3.3.2 ToF-SIMS analysis of microarray printed at 4 different DMF concentrations 55

3.3.3 Measurement of the contact angle of DMF solutions on pHEMA surface 58

3.3.4 The effect of the thickness of pHEMA background coating on spot diameter and spreading 60

3.3.5 Investigating the mixing of spots containing two monomers using ToF-SIMS 62
3.4 Discussion 67
3.4.1 The effect of increasing solvent (DMF) concentration on microarray printing 67
3.4.2 The effect of uniformity and thickness of pHEMA background coating 68
3.4.3 ToF-SIMS analysis of the composition of printed polymer spots 69
3.5 Conclusions 71
4 Chapter 4 – Haemocompatibility assays on polymer microarrays 72
4.1 Introduction 72
4.1.1 Aim and objectives 74
4.2 Experimental 75
4.2.1 Whole blood incubation assay 76
4.2.2 Leukocyte detection 77
4.2.3 Platelet detection 77
4.2.4 Fibrinogen and IgG detection 78
4.2.5 Complement C3b detection 78
4.3 Results 79

4.3.1 XPS analysis to determine protein adsorption on polymer microarray from human blood 79
4.3.2 Fibrinogen adsorption assay 82
4.3.3 Immunoglobulin G (IgG) adsorption on microarray 85
4.3.4 Leukocyte attachment assay 86
4.3.5 Complement C3b adsorption assay 86
4.3.6 Platelet attachment assay 87
4.4 Discussion 89
4.4.1 Protein adsorption from whole blood 89
4.4.1.1 XPS protein overlayer thickness 89
4.4.1.2 Fibrinogen adsorption assay 91
4.4.2 Estimating the immune system response to materials 92
4.5 Conclusions 95
5 Chapter 5 – Bacterial attachment assays on polymer microarrays 96
5.1 Introduction 96
5.1.1 Aim and objectives 98
5.2 Experimental 99
5.2.1 Whole blood incubation 99

5.2.2 Bacterial strain preparation and high throughput bacterial attachment assay setup 100

5.2.3 Fluorescence scanner imaging and analysis 100

5.3 Results 102

5.3.1 The effect of blood proteins on bacterial attachment to existing catheter materials 102

5.3.2 Pseudomonas aeruginosa (PA01-N) attachment to micro arrays 103

5.3.3 Staphylococcus aureus attachment assay 105

5.3.4 The relationship between surface bacterial attachment and wettability 106

5.3.5 Combining haemocompatibility and bacterial attachment results to identify hit materials from microarray screening 108

5.4 Discussion 111

5.4.1 Bacterial attachment assays 111

5.4.2 The effect of surface wettability on bacterial attachment 112

5.4.3 Selecting 'hit' polymer compositions via high-throughput screening 113

5.5 Conclusions 115

6 Chapter 6 – Bacterial attachment and haemocompatibility testing of scaled-up 'hit' polymer compositions 116

6.1 Introduction 116

6.1.1 Coagulation activation (F1+2) 117

6.1.2 Platelet and leukocyte decay and platelet-leukocyte conjugates 118

6.1.3 Platelet activation PF-4 (platelet factor 4) 118

6.1.4 Aim and objectives 120

6.2 Experimental 121

6.2.1 Materials 121

6.2.2 Scale-up polymerisation of microarray 'hit' compositions 121

6.2.3 Oxygen plasma treatment of silicone catheters and dip coating in polymer solution 122

6.2.4 Confocal microscopy bacterial attachment assay on hit material coated silicone catheters 123

6.2.5 Whole blood incubation of scaled up materials under quasi-static conditions 124

6.2.6 Whole blood incubation of scaled up materials under flow conditions to evaluate haemocompatibility 126

6.2.7 LIVE/DEAD™ staining 127

6.3 Results 128

6.3.1 Bacterial attachment assay on polymer coated silicone catheters 128

6.3.2 LIVE/DEAD™ staining on hit material coating 129

6.3.3 Haemocompatibility assays on 'hit' polymers 131

6.3.3.1 Haemostasis parameter assays 131

6.3.3.2 Inflammation parameter assays 133

6.3.4 Combining haemocompatibility data to identify the best performing material 134

6.4 Discussion 137

6.4.1 Bacterial attachment on polymer coated catheters 137

6.4.2 Haemocompatibility assessment of scaled up polymer materials 138

6.5 Conclusions 141

7 Chapter 7 – In-vivo mouse infection model to assess hit material performance 142

7.1 Introduction 142

7.1.1 Aim and objectives 144

7.2 Experimental 145

7.2.1 Polymer coating on silicone catheters 145

7.2.2 Mouse catheter implant model 145

7.2.3 Scanning Electron Microscopy (SEM) 147

7.3 Results 148

7.3.1 Foreign-body reaction on isobornyl acrylate (75%) tri(ethylene glycol) methyl ether methacrylate (25%) [2(75%)B(25%)] 148

7.3.2 In-vivo bacterial attachment assays on isobornyl acrylate (75%) tri(ethylene glycol) methyl ether methacrylate (25%) [2(75%)B(25%)] 149

7.3.3 Viability of the 'hit' polymer coating on silicone catheter 152

7.4 Discussion 155

7.4.1 Foreign-body response to the polymer coated catheter 155

7.4.2 In-vivo foreign-body infection model 156

7.4.3 Suitability of the 'hit' polymer as a coating on medical devices 158

7.5 Conclusions 160

8 Chapter 8 – Conclusions and future work 161

8.1 Summary 161

8.2 Recommendations for future work 163

9 Appendices 167

9.1 Appendix A: Bacterial attachment on scaled up polymer materials, silicone and silver containing catheters with and without blood pre-incubation. 167

9.2 Appendix B: In-vivo bacterial attachment on 2-ethylhexyl methacrylate (75%) di(ethylene glycol) methyl ether methacrylate (25%) [8(75%)A(25%)]..... 168

9.3 Appendix C: Comparison of foreign-body response pre-conditioning vs whole blood pre-conditioning on in-vitro biofilm formation..... 171

9.4 Appendix D: AIBN mediated polymerisation to scale up 'hit' compositions..... 174

9.5 Appendix E: Polymerisation % conversion and molecular weights 177

9.6 Appendix F: The effectiveness of washing procedure following plasma/blood incubation..... 178

9.7 Appendix G: Fluorescence scanner and software reproducibility test 181

10 References..... 182

List of Figures

Figure 1: Main stages of biofilm formation on the surface of a vascular catheter 5

Figure 2: Staphylococcus aureus biofilm on the inner surface of an indwelling medical device. 6

Figure 3: Blood coagulation pathway. 9

Figure 4: An overview of polymer microarray screening and scale up of 'hit' material compositions for in vitro and in vivo testing. 21

Figure 5: Monomers used in this thesis. 25

Figure 6: Automated dip coater used to dip coat glass slides with pHEMA solution. 26

Figure 7: A schematic representation of polymer microarray printing 28

Figure 8: ToF-SIMS schematic illustration of primary ion bombardment and ejection of secondary ions from a surface. . 29

Figure 9: Schematic of a ToF-SIMS instrument 32

Figure 10: ToF-SIMS total ion image of a microarray 33

Figure 11: Schematic representation of mechanism of action of an XPS instrument 35

Figure 12: An example of a survey or broad XPS spectrum obtained from an oxygen and carbon containing polymer material. 38

Figure 13: Measuring water contact angle on polymer microarray spots using a DSA100 instrument 40
Figure 14: Steps involved in bacterial attachment assay experimental setup. 43
Figure 15: Schematic representation of a confocal microscope. 44
Figure 16: The process to extract surface chemistry of each polymer spot from ToF-SIMS chemical image. (a) ToF-SIMS total ion chemical image of a microarray, (b) selected ROIs to acquire a ToF-SIMS spectrum for each polymer spot, shown by (c). (Average spot diameter 400 μm). 50
Figure 17: Optical microscope images (stitched, shown on left side) and ToF-SIMS chemical image of the array printed at a range of solvent concentrations. 53
Figure 18: The effect of DMF concentration on microarray printing. 54
Figure 19: ToF-SIMS chemical mapping of a microarray printed at various DMF concentrations based on ion fragments from three different monomers and pHEMA background. (ToF-SIMS data accusation was carried out by Dr. David Scurr). 56
Figure 20: Monomer composition map of microarray printed at 50% v/v solvent (DMF) concentration. 57
Figure 21: ToF-SIMS ion image based on an ion marker for pHEMA background to assess the extent of spreading 58

Figure 22: (a) Contact angle measured for monomer 11 (Cyclohexyl methacrylate) mixed with DMF on pHEMA surface at various concentrations (%v/v); (b) The effect of increasing DMF concentration from 0% v/v to 75% v/v on spot diameter (n=3 for both plots). 59

Figure 23: The effect of pHEMA coating thickness on solvent droplet spreading compared to bare glass. 60

Figure 24: (a) Optical microscope images (stitched using Cell ProfilerTM software from individual images), average spot diameter is 400 μm, scale bar = 1 mm. (b) ToF-SIMS chemical image of polymer microarray built using pHEMA background ion marker, m/z = 45.02 –> $C_2H_5O^+$ and normalised by total counts (au on scale). 61

Figure 25: Zoomed in high-resolution ToF-SIMS image of the printed polymer spot 62

Figure 26: ToF-SIMS chemical images of the microarray built using a unique ion marker for each of two monomers (monomer 8 and monomer B). 64

Figure 27: High spatial resolution ToF-SIMS images of the microarray polymer spots (400 μm diameter) made up from monomer 8 mixed with monomer B at three different concentrations (%v/v). 65

Figure 28: ToF-SIMS ion intensity of the UV-cured surface of polymer spots made up of various combinations of the two

monomers $C_3H_7O_2^-$ (monomer B) and $C_8H_{17}O^-$ (monomer 8) printed in a microarray format (n = 3, on three separate blocks). (ToF-SIMS data accusation was carried out by Dr. David Scurr). 66

Figure 29: The complex complement pathway system showing Classical, Lectin and Alternative pathways. 73

Figure 30: Polymer microarray printing on 25 mm circular slides fixed on standard glass slide. 75

Figure 31: Quasi-static blood incubation chamber experimental setup 76

Figure 32: Protein overlayer thickness (nm) after two hour incubation in human whole blood, estimated from [N] (at%) measured using XPS. 81

Figure 33: Relationship between protein adsorption and surface wettability (water contact angle). 82

Figure 34: Heat map representation of fluorescence intensity (au) from antibody based assays to detect (a) Fibrinogen adsorption, (b) IgG adsorption, (c) Leukocyte attachment and (d) Complement C3b adsorption on polymer microarray following whole blood incubation for two hours at 37 ^oC. 84

Figure 35: Platelet adsorption on polymer microarray spots following two hour incubation in human whole blood at 37 ^oC. A low attachment (comparable to pHEMA surface) was observed on

most of the polymer spots as compared to PTFE control surface. 88
Figure 36: Blood incubation and bacterial attachment assay experimental setup on polymer microarray. 99
Figure 37: The effect of blood on bacterial attachment on silicone and silver catheters. 103
Figure 38: Heat map representation of P. aeruginosa (PA01-N) attachment on each polymer spot on the microarray 105
Figure 39: Heat map representation of S. aureus attachment on each polymer spot on the microarray 106
Figure 40: The effect of surface wettability on P. aeruginosa attachment. 107
Figure 41: The effect of surface wettability on S. aureus attachment. 107
Figure 42: The combination (Ω) of bacterial (α), immune (β) and protein (γ) components to choose 'hit' materials from microarray screening..... 109
Figure 43: Blood incubation and bacterial attachment experimental setup on 'hit' material coated silicone catheter sample. 124
Figure 44: Custom made blood incubation flow chamber experimental setup 126
Figure 45: Bacterial attachment on 'hit' compositions coated silicone catheters as compared to silicone uncoated and

commercially available silver containing catheters following 72 hour incubation in planktonic bacteria. 129
Figure 46: Live/dead staining on hit material (2(75%)B(25%)) coated and uncoated silicone catheters..... 130
Figure 47: Haemostasis parameter assays to assess haemocompatibility of scaled up 'hit' materials under static and flow conditions. 132
Figure 48: Inflammation parameter assays to assess immunogenicity of scaled up 'hit' materials under static and flow conditions. 134
Figure 49: (a) Haemostasis and (b) Inflammation parameters to rate polymer performance using the most relevant parameters of the haemocompatibility test. 135
Figure 50: An optical microscope image of foreign-body reaction on subcutaneously implanted polymer (2(75%)B(25%)) coated and silicone uncoated catheters. 149
Figure 51: P. aeruginosa (PA01-L) bioluminescence measured on a polymer coated catheter compared with a silicone catheter in an in-vivo foreign-body mouse infection model over five-day period. 150
Figure 52: S. aureus (Xen29) bioluminescence from a polymer coated catheter compared with a silicone catheter in an in-vivo foreign-body mouse infection model over a five day period. .. 152

Figure 53: Isobornyl acrylate-co-tri(ethylene glycol) methyl ether methacrylate (75:25 %v/v) coated silicone catheter before and after seven days in PBS at 37°C under static conditions. 153
Figure 54: Scanning electron microscope images of the 'hit' polymer coating before and after in-vivo testing compared with silicone catheter. 154
Figure 55: In-vivo performance of polymer material in a foreign-body response model used by Hook et. al. for a comparison with the 'hit' polymer material used in this thesis. 157
Figure 56: IVIS scanner images showing in-vivo biofilm experimental setup for polymer 8(75%)A(25%) over five day period. 169
Figure 57: Bioluminescence from two repeats of polymer coated and control samples subcutaneously implanted in mice, measured using an IVIS spectrum camera and quantified using living image software package over five day period. 170

List of Tables

Table 1: Estimated economic burden and mortality associated with healthcare-associated infections in US based on systematic reviews of the literature. 3

Table 2: List of key molecules described in the Thesis, with their description and key characteristics. 22

Table 3: The description and origin of bacterial strains used in this project. 41

Table 4: Bacteria resistant haemocompatible 'hit' polymer compositions selected based upon their bacterial resistance and haemocompatibility properties from high throughput microarray screening for scale up studies. 110

List of Abbreviations

AIBN

2,2’-azobis-(2,4-dimethyl-4-methoxyvaleronitrile) 121

c-di-AMP

cyclic diadenosine monophosphate 15

c-di-GMP

cyclic diguanosine monophosphate 15

CE

Conformité Européene 1

CFUs

colony forming units 146

CRBI

Catheter Related Bloodstream Infections 3

CVCs

Central venous catheters 2

DCM

Dichloromethane 122

DEGMA

diethylene glycol methyl ether methacrylate 159

DMF

Dimethylformamide 49

E. Coli.

Escherichia coli. 12

EPM

Extracellular Polymeric Matrix 4

F1+2

Prothrombin fragment 1+2 117

FDA

Food and Drug Administration 13

FITC

Fluorescein isothiocyanate 77

ICU

Intensive Care Unit 2

IgG

Immunoglobulin G 85

ISO

International Organization for Standardisation 72

LB

Luria-Bertani 42

MRSA

methicillin-resistant Staphylococcus aureus 12

OD^{600}

Optical Density at 600nm 42

P. aeruginosa

Pseudomonas aeruginosa 41

PBS

Phosphate buffered saline 42

PDMS

Polydimethylsiloxane 37

PEG

poly(ethylene glycol) 18

PF4

Platelet factor 4 125

PFA

Paraformaldehyde 77

pHEMA

poly(2-hydroxyethyl methacrylate) 48

PLS

Partial Least Square regression 165

PolySB

poly-sulfobetaine 16

PTFE

Polytetrafluoroethylene 76, 87

ROIs

Regions of Interest 50

S. aureus

Staphylococcus aureus 17

SAMs

self-assembled monolayers 90

SEM

Scanning Electron Microscope 6

Tg

Glass Transition temperature..... 158

ToF-SIMS

Time-of-Flight Secondary Ion Mass Spectrometry 49

UHV

ultra-high vacuum..... 35

UV

ultraviolet 49

vWF

von Willebrand factor 116

WCA

Water contact angle 39

XPS

X-ray Photoelectron Spectroscopy 35

1 Chapter 1 - Introduction

Infections associated with medical devices are a major healthcare problem causing significant mortality and morbidity for hospitalised patients. Biofilm formation is strongly correlated with these infections; it is a complex process and the current understanding of bacterial-device surface interactions is limited. The present clinical best practice measures are insufficient to prevent biofilm formation on indwelling devices. The surface of existing medical devices such as silicone catheters is prone to bacterial attachment. Due to ever increasing antibiotic resistance, novel approaches are needed to combat medical device associated infections. Furthermore, blood-contacting medical devices such as venous catheters need to prevent thrombosis formation to avoid occlusion and increase device life-time. The work presented in this thesis explores high throughput polymer microarray screening methods to screen a library of biomaterials to identify bacterial resistant, haemocompatible materials for application as coatings on blood-contacting medical devices. It starts from the point of a polymer library already successfully screened for materials undergoing approval for use in humans as urinary catheters by CE mark [2, 3].

1.1 Blood-contacting medical devices

Blood-contacting medical devices such as vascular catheters and venous access ports are increasingly used in contemporary healthcare systems. The use of these devices has revolutionised modern medicine by improving the quality of care provided to the patients in oncology, nephrology and intensive care unit (ICU) [4]. Central venous catheters (CVCs) and totally implantable venous access ports are the most commonly used medical devices in intensive care settings. These devices are used to administer medication, sample blood, feed intravenously and carry out dialysis to name a few. Despite being the lifeline of patients in ICU, these implantable devices are associated with considerable complications such as infections (biofilms), occlusion and blood clot (thrombosis) [5, 6].

1.1.1 Biofilm formation on medical devices

Biofilm formation on medical devices such as vascular catheters is a major healthcare problem, which often put patients at risk of local and systemic infectious complications, such as local site infections, device related bloodstream infections and endocarditis [7]. Medical device associated infections account for a large proportion of all healthcare associated infections as evident from Table 1.

Table 1: Estimated economic burden and mortality associated with healthcare-associated infections in US based on systematic reviews of the literature. (Table from [8], adapted from US Department of Health and Human Services)

Infection type	Annual infections (n)	Mean hospital cost per infection (US$)	Mean deaths per year
Surgical-site infection	290,485	25,546	13,088
Ventilator-associated pneumonia	250,205	9,966	35,967
Central-line-associated bloodstream infection	248,678	36,441	30,655
Catheter-associated urinary tract infection	561,677	1,006	8,205

Biofilms are responsible for about 80% of device-associated infections acquired in hospitals [9]. Several studies have been conducted to estimate the morbidity and mortality associated with the use of catheters. For example, in the United States, 15 million CVC days (the total number of days of exposure to CVC by all patients) occur in ICU each year [10]. In addition, the American Centres for Disease Control has estimated an average rate of CVC-associated bloodstream infections of 5.3 per 1,000 catheter days in ICU, with approximately 80,000 CVC associated bloodstream infections occurring in ICU each year in the United States [11]. In the UK alone 210,000 central venous and arterial catheters are inserted annually and 8,940 Catheter Related Bloodstream Infections (CRBI) reported at an incidence rate of 4.2 per 1,000 catheter days in ICU with a total annual cost of up to £36 million [12]. According to NHS Scotland [13], in critically ill patients (e.g. in ICU) catheter-related bloodstream infections are a significant cause of mortality (25%) and morbidity (increased length of stay of up to three weeks) with an estimated average cost burden of £20,000 per episode. Biofilm formation on a CVC

can lead to a local as well as a systemic infection. This adds further therapeutic complications in patient care especially in a hospital setting (ICU) where a patient who is already ill has to be treated for a local or a systemic infection.

Biofilm forming bacteria commonly isolated from central venous catheters are: *Staphylococcus aureus*, *Pseudomonas aeruginosa*, Coagulase-negative *staphylococci*, *Enterococcus faecalis* and *Klebsiella pneumoniae* [14, 15]. These bacteria originate from a patient or a healthcare professional or from a contaminated device and migrate from the skin via catheter port to colonise the device surface [10, 16-18].

A biofilm is a complex aggregation of one or more species of micro-organisms (mainly bacteria) on a substrate forming a highly hydrated coating in which bacteria are protected by an Extracellular Polymeric Matrix (EPM) from the surrounding environment [19]. Micro-organisms colonise and form biofilms on a wide variety of surfaces, including living tissues, indwelling medical devices, industrial or potable water system piping, or natural aquatic systems [20]. The initial key step in a biofilm formation is the attachment of free-floating (planktonic) micro-organisms to a surface. These first colonists adhere to the surface initially by using weak reversible van der Waals forces [21]. Early reversible interactions have to be converted into strong irreversible interactions in order for bacteria to remain adhered. Thus, bacteria utilize cell adhesion molecules on their surface such as pili or fimbriae. The structure of Pili consists of hair like extensions (~1-4 μm long and ~5 nm in diameter) from the surface of a bacterial cell made up of proteins [22-24]. Bacteria use pili to adhere to surfaces or host cell membrane [23].

The first colonists facilitate the arrival of other bacterial cells by constructing an EPM that holds the biofilm together (Figure 1) [25].

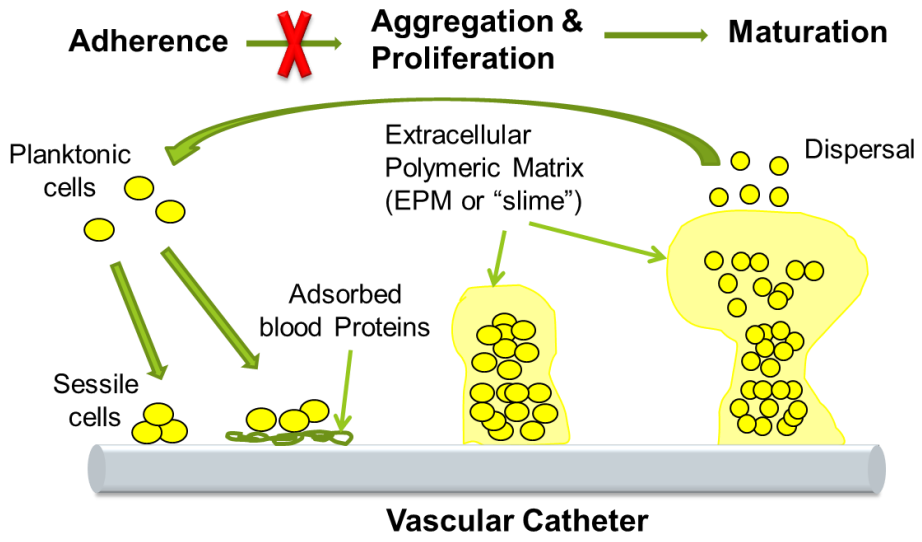


Figure 1: Main stages of biofilm formation on the surface of a vascular catheter and the stage at which a bacterial resistant material would act to stop the process (marked by red cross). (Figure modified from [10] and [26]).

Biofilm EPM is a dynamic environment with the major components being microbial polysaccharides, proteins, extracellular DNA, lipids together with other excreted cellular products [27]. These complex features and co-ordination make bacteria within the biofilm up to 1,000 times more tolerant to antimicrobials and host defence system as compared to their planktonic counterparts [28, 29]. Following colonisation of micro-organisms, the biofilm grows through a combination of cell division and other bacterial cell recruitment (e.g. quorum sensing). The timescale of biofilm formation depends upon the number of species present in the biofilm and their co-ordination within the EPM.

Bacteria in a biofilm exhibit a difference in expression of surface molecules, virulence factors and antibiotic resistance than their planktonic counterparts [30]. Furthermore, a number of genes have been shown to be up- or down-regulated upon initial contact of bacterial cells with the substrate [31-33]. In addition, minimal shear together with a close cell-to-cell contact inside a biofilm environment provides an ideal niche for exchange of extrachromosomal DNA (plasmids). The plasmid transfer can help bacterial co-ordination and transfer of antibiotic resistance. Bacteria use sex (F) pilus to transfer plasmids from one cell to another for the purpose of transferring genetic material and code for antibiotic resistance. Same mechanism is also used to inject toxins into host cell to establish infection [23].

The micro-organisms present in a biofilm are able to form micro-colonies which co-operate to perform specialised tasks such as to construct the extracellular matrix. Figure 2 shows a bacterial biofilm on the inner surface of an indwelling medical device such as a vascular catheter using a scanning electron microscope (SEM) and a confocal microscope.

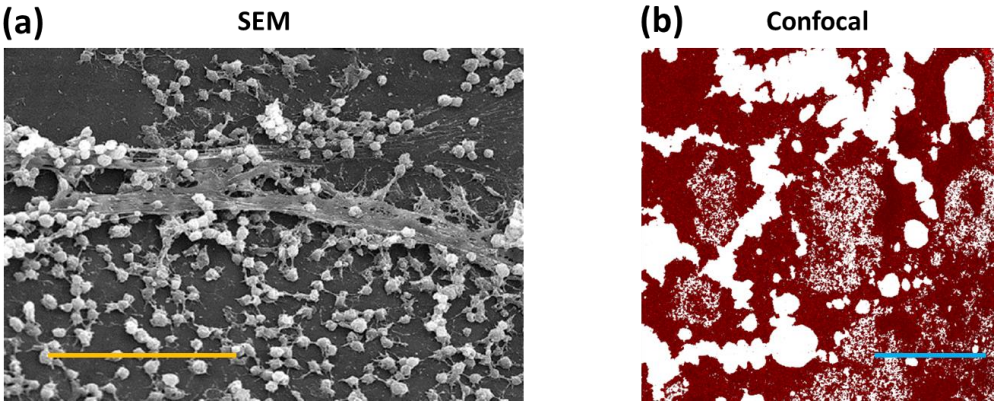


Figure 2: *Staphylococcus aureus* biofilm on the inner surface of an indwelling medical device. **(a)** A scanning electron microscope image of the biofilm showing bacterial cells and extracellular polymeric matrix (scale bar = 20 μm) (image adapted from [20]). **(b)** A confocal microscope image (taken during current project) of a

biofilm showing fluorescently labelled *S. aureus* bacteria (scale bar = 200 μm) (bacteria labelled red and surface appears white).

If biofilm formation continues unabated together with unfavourable environmental conditions such as nutrient deprivation, then a mature biofilm develops. The mature biofilm continues growing and also starts releasing microbes from the biofilm into the surrounding area (Figure 1). The mature biofilm acts as microbial reservoir, resulting in bacterial dispersal, surface re-colonisation and infection. The dispersal may happen either by bacteria shedding from actively growing biofilm, detachment due to nutrient levels or quorum sensing, or shearing of biofilm aggregates caused by flow effects [20]. All these features of biofilms make the eradication of infection notoriously difficult.

1.1.2 Protein adsorption and thrombosis on medical devices

Important parameters which need to be considered when designing a bacterial resistant material for blood-contacting medical devices (e.g. vascular catheter) are blood protein adsorption and blood cells adhesion on the surface. The material should also possess good haemocompatibility for the application on blood-contacting medical devices. Once in contact with blood, the surface of the device is rapidly covered by a thin film of blood proteins: albumin, fibrinogen, fibrin, collagen, elastin and von Willebrand factor, that promote microbial adhesion and as a result biofilm formation [26]. Hence, the material should also be resistant to protein adsorption as well as bacterial adhesion.

Furthermore fibrinogen, fibrin and von Willebrand factor are also associated with blood clotting and it has been widely reported in the literature that insertion of a venous (and arterial) catheter leads to an increased risk of thrombosis due to foreign-body response by the body [34-36]. The foreign surface contact with blood also leads to the activation of immune system which promotes inflammation at catheter insertion site. The normal homeostasis response of the body is to stop bleeding by clot formation; as a result, the insertion of venous catheter leads to activation of complex clotting cascade and thrombosis formation (Figure 3).

From Figure 3, it can be seen that thrombosis formation via intrinsic pathway is dependent on surface contact. Surface contact activates Factor XII proteins in the blood, which subsequently activates another inactive precursor factor by proteolytic cleavage and this chain reaction go on to produce fibrin clot (thrombosis). Thrombosis formation can also be initiated by tissue factors expression by cells using extrinsic pathway (involves complex cell mechanisms), however, both pathways converge to a single pathway to form fibrin clot. Therefore, the surface contact is the key process in foreign-body mediated thrombosis, modification of which can reduce the incidence of medical device (venous catheter) mediated thrombosis.

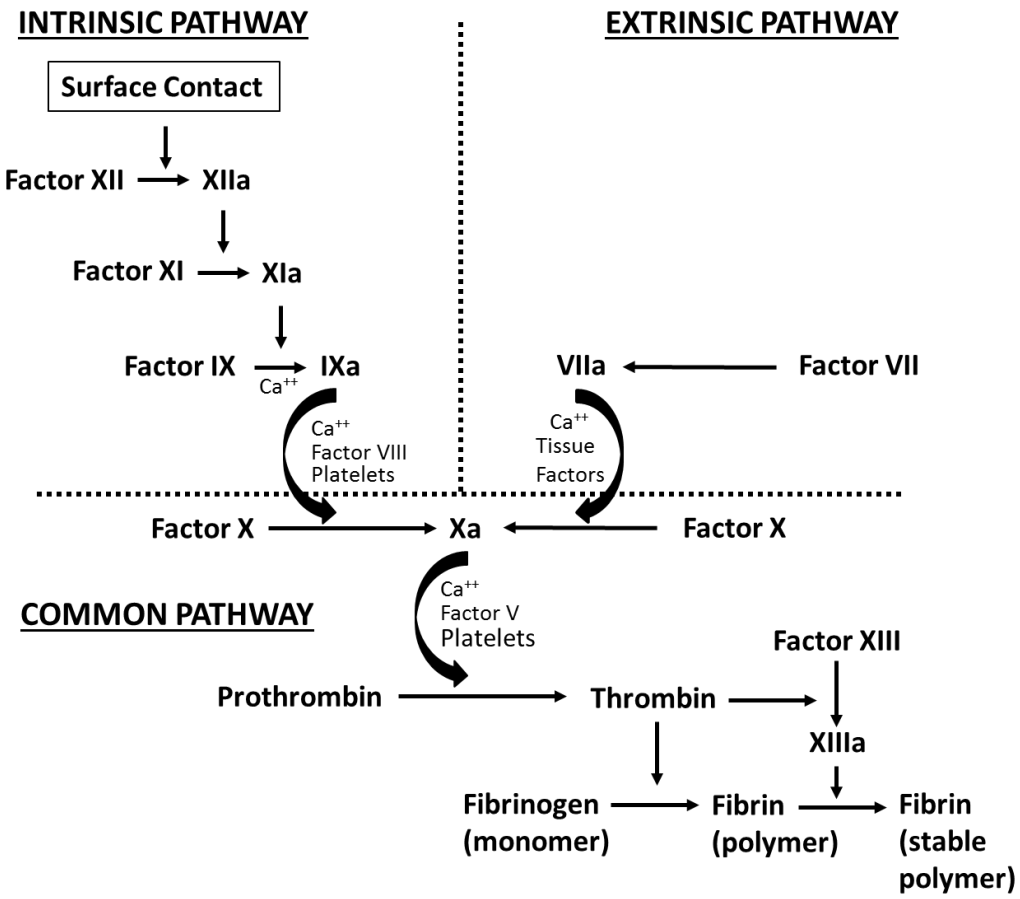


Figure 3: Blood coagulation pathway. starting from foreign surface (e.g. medical device such as catheter) contact with blood leading up to the formation of stable fibrin clot (Figure based on [37])

The size of plasma proteins also plays a role in protein adsorption. The surface of device rapidly gets covered with the smaller and most mobile blood plasma proteins in a matter of seconds [38, 39]. On longer timescales, it is known that the Vroman effect [40, 41], whereby larger proteins with stronger binding affinity can displace smaller and less strongly adsorbed proteins from the surface, plays an important role as well [42, 43]. In this context, albumin having a smaller molecular weight (66 kDa) and most abundant plasma protein (35-40 g/L) gets adsorbed on the surface first [44]. These non-specifically adsorbed proteins may be replaced by larger proteins (e.g. fibrinogen with molecular weight 340 kDa) with

stronger binding affinity for a surface. The binding affinity of a protein towards the surface depends upon the surface chemistry [45]. In this thesis, polymer microarrays were used to screen hundreds of polymers materials with different surface chemistries for protein adsorption.

1.2 Current clinical best practice to prevent catheter associated biofilm infections

There is currently no fully efficient strategy to prevent bacterial colonisation and biofilm formation on medical devices. The traumatic and costly replacement of the device is the only fully efficient method to treat biofilms on medical devices [46]. A range of prevention and treatment strategies (with a limited success) are clinically used to prevent and treat device associated biofilms.

1.2.1 Antibiotics

Antibiotics have been widely explored for reducing biofilm formation on medical devices due to their bacteriostatic and bactericidal properties. Antibiotic lock solutions are clinically used to prevent and treat uncomplicated catheter related infections [47]. An antibiotic lock solution is made up of a mixture of a highly concentrated antibiotic and an anticoagulant [48]. This lock solution is used to fill the catheter lumen (‘locked’), while the catheter is not in use, to prevent bacterial colonisation or for catheter sterilisation [48]. Various antibiotics have been used as lock solutions with

promising results [49-51], however, increasing antibiotic resistance limited their clinical use.

An alternative approach incorporated broad spectrum antibiotics (rifampicin and amoxicillin) into the device at the manufacturing stage [52]. However, this can be limited by insufficient antibiotic incorporated into the device and the lack of a sustained bactericidal concentration of antibiotic being released over the life-time of the device. Presence of an extracellular polymeric matrix in mature biofilm also reduces the penetration of antibiotic into the biofilm. Furthermore, the incorporation of antibiotics must not interfere with the function and properties of the device such as host compatibility.

An alternative approach is to covalently link antibiotics onto the backbone of the polymers as a main-chain monomer, from which the medical devices are made up of. In a study by Woo *et. al.* [53], fluoroquinolone antibiotics (e.g. ciprofloxacin) were covalently linked onto the backbone of degradable polyurethanes. The macrophage-derived enzyme cholesterol esterase was used to release the antibiotic from the polymer backbone by degradation of the polymer chains. This approach showed some success in killing bacteria. However, it was difficult to control the specificity of the cleavage sites in the polymer and further work was required to determine the structures of other degradation products released, which can compromise the material biocompatibility.

Another approach has utilised antibiotic-loaded liposomes sequestered within a biocompatible matrix (liposomal hydrogel) that was retained on the surface of the catheter. This resulted in a reduced bacterial adhesion to silicone urinary

catheters. The system consisted of a poly(ethylene glycol) - gelatin hydrogel in which liposomes containing the antibiotic ciprofloxacin were sequestered [54].

Bayston *et. al.* developed an antimicrobial impregnation method to prevent bacterial colonisation on hydrocephalus shunt catheters [55] and silicone peritoneal catheters [56]. The method involved immersion of silicone tubing into a 2% w/v solution of antibiotics (rifampicin and clindamycin) in chloroform for one hour at room temperature. The tubing was swollen to twice the original volume, incorporating antibiotics throughout the silicone tubing following the evaporation of chloroform. The tubing was then rinsed with ethanol, air dried and autoclaved. The catheters were then tested for antimicrobial activity against gram negative (*Escherichia coli.*) and gram positive (methicillin-resistant *Staphylococcus aureus* or MRSA) bacteria. The impregnated catheters showed an ability to kill 100% of bacteria in multiple high-count challenges. Furthermore, the impregnated catheters also showed continuous antibacterial activity for 280 days *in-vitro*. However, *Escherichia coli* colonisation was observed after 13th challenge over 100 day period. This approach was taken forward by Medtronic Ltd. to develop Ares^{TM} antibiotic-incorporated catheter [57], which is currently clinically used. Despite a good initial efficacy of this antibiotic combination approach, emerging multi-antibiotic resistance has limited the use of this approach.

1.2.2 Antiseptic coated catheters

Antimicrobials such as silver salts and chlorhexidine have also been used as coatings on the catheters to prevent bacterial colonisation [58]. Despite showing a good efficacy *in-vitro*, the *in-vivo* performance of these antimicrobial coatings is limited by leaching and potential to cause anaphylaxis. A number of hypersensitivity as well as anaphylaxis reactions have been reported worldwide following the use of silver and chlorhexidine based catheters. In one case the insertion of a silver sulfadiazine central venous catheter immediately caused an anaphylactic shock in two patients in China [59]. Similarly three cases of anaphylaxis following insertion of chlorhexidine central venous catheters were reported on a cardiac ward in the UK [60]. These incidents led to the issue of a public health notice by US Food and Drug Administration (FDA) alerting all healthcare professionals regarding the possibility of anaphylaxis with the use of chlorhexidine incorporated medical devices [61].

1.2.3 Heparin coating

Heparin is a commonly used anticoagulant in a hospital setting for the prevention as well as the treatment of thrombosis. Heparin is a mucopolysaccharide made up of sulphated D-glucosamine and D-glucuronic acid with sulfaminic bridges [62, 63]. Paulsson *et. al.* [34] coated (physisorbed) central venous catheters with heparin to explore its ability to prevent bacterial adhesion to the surface of the catheter. The idea behind this approach was to reduce platelet attachment to the surface of central venous catheter (due to anticoagulant properties) that often facilitates subsequent bacterial colonisation. However, heparin coating failed to inhibit

microbial adhesion for a number of micro-organisms such as *Staphylococcus* species that possess surface proteins to which heparin competitively binds and hence, facilitate the bacterial adhesion [64]. Liang *et. al.* [64] showed that the binding of heparin to *S. aureus* was time-dependent, saturable and depends upon pH and ionic strength. Furthermore, other glycosaminoglycan of comparable size such as chondroitin sulfate and anionic polysaccharides such as dextran sulfate, competitively inhibited heparin binding to various extents.

1.3 Molecular microbiology approaches to combat biofilms

Biofilm formation and the survival of microbes are dependent on the ability of these organisms to sense their environment and adapt to it by modifying their physiological processes [65]. Bacteria use cell-to-cell communication via various diffusible signalling molecules to synchronise gene expression as a function of bacterial cell population density [66]. This is termed 'quorum sensing' and plays a critical role in co-ordinating gene expression leading to the co-ordinated production of various virulent factors and biofilm development. Therefore, various research groups have explored the idea of using quorum sensing inhibitors to target quorum sensing to inhibit biofilm maturation. In one such study, O'Loughlin *et. al.* [67] used synthetic molecules to inhibit two *P. aeruginosa* quorum sensing receptors and virulence factor pyocyanin and inhibited biofilm development. Similarly a novel quorum sensing inhibitor (coded 'yd 47') showed a good *in-vivo* activity in a guinea pigs study by reducing *S. pneumoniae* biofilm on cochlear implants [68].

Nucleotide signalling molecules such as cyclic diguanosine monophosphate (c-di-GMP) and cyclic diadenosine monophosphate (c-di-AMP) which act as second messengers, have been investigated as potential targets for anti-biofilm drugs [69]. It has been shown that nucleotide signalling plays key role in bacterial motility and pathogenicity, particularly c-di-GMP, which has been shown to be closely linked to Gram-negative bacterial biofilm development [70, 71]. Therefore, the current anti-biofilm drug development is focussed on c-di-

GMP modification and quorum sensing control to inhibit bacterial cell-to-cell communication [65].

1.4 Emergent surface chemistry modification strategies to combat biofilms

The current best practice guidelines used clinically provide insufficient protection against the biofilms [72]. In light of a global push to minimise the use of antibiotics to prevent resistance, the current research is now focussed on surface chemistry modification. This approach is based on the idea that surface chemistry of a device is directly linked to the biological performance (e.g. bacterial attachment or protein adsorption). Various research groups have shown that the modification of surface chemistry leads to improved biological performance [73-75].

1.4.1 Surface modification using poly-sulfobetaine (zwitterionic polymer)

Smith *et.al.* of Semprus Biosciences [76] modified the surface of commercially available polyurethane catheters using zwitterionic poly-sulfobetaine (PolySB), which possesses both positive and negative charge in close molecular proximity on the surface. Both internal and external surfaces of catheters were modified with PolySB by grafting the polymer onto the surface using redox polymerisation process to form a polymer layer. This PolySB surface showed a good resistance to bacterial as well as cell attachment *in-vitro* and *in-vivo*. These bacterial as well as host cell repellence properties were

suggested to be due to the zwitterionic structure of PolySB, which interacts with water molecules by ionic interactions and co-ordinates both bound and free water molecules to create a hydrophilic surface. This hydrophilic surface was shown to be highly resistant to protein as well as host cells due to binding on to the surface requires displacement of water, which is thermodynamically unfavourable.

1.4.2 Polymer embedded with electro-conductive materials

An approach explored by Liu *et. al.* [36] involved the development of electro-conductive polymers by incorporating carbon particles into the polymer matrix. Two modified catheters were placed vertically in a nutrient agar plate and connected to an electrical device which generated a 10 μA electric current, with one catheter acting as a cathode and the other as anode. Following overnight incubation with *S. epidermidis* and *S. aureus* at 37 ^{o}C, a zone of inhibition of bacterial growth was detected around the cathode. This bactericidal activity possessed by negatively charged electro-conducting polymers was due to the establishment of electrostatic repulsions between the negatively charged bacterial cell wall and the polymer. However, this approach is limited clinically due to complex design requirements of the polymer as well as a small current involved.

1.4.3 Polycationic antimicrobial hydrogel with microbe membrane suctioning effect

Li *et. al.* [77] developed an antimicrobial coating made up of dimethyl decylammonium chitosan (with high quaternisation) – graft – poly(ethylene glycol) methacrylate and poly(ethylene glycol) diacrylate hydrogel and investigated its antimicrobial properties against *P. aeruginosa*, *E. coli.*, *S. aureus* and *F. solani*. Jia *et. al.* [78] has shown that quaternised chitosan derivatives have higher antimicrobial activity and water solubility compared to pristine chitosan. Accordingly, chitosan was modified by adding a hydrophobic alkyl side-chain and a cationic charge through quaternisation of amino group of chitosan. The resultant hydrogel was covalently grafted on to a fluoropolymer substrate surface to create thin uniform coating. The results showed that the hydrogel coating exhibits an excellent antimicrobial activity against all four pathogen tested with 99% growth killing of each pathogen tested. The mechanism proposed for exceptional antimicrobial activity was that the polycationic hydrogel carries a positive charge on the surface and hence, acts as an 'anionic sponge' to draw negatively charged (anionic) phospholipids out of bacterial cell membrane into the nanometre size hydrogel pores. It was proposed that because the mammalian cell membrane lacks anionic lipids and consequently lacks an 'anionic sponge' effect, a good biocompatibility was shown for *in-vivo* studies using rabbit conjunctiva. Furthermore, hydrogel charge density as well as the pore size was shown to plays an important role in killing efficacy of the coating.

1.4.4 High throughput screening using material microarrays to identify bacterial adhesion resistant materials

Microarray technology has been extensively used in genomics and proteomics by respectively using DNA/RNA and proteins as probe molecules for high throughput screening applications [79-81]. Inspired by the success of DNA, protein and small molecule microarrays, Anderson *et. al.* developed first polymer microarray in 2004 [82, 83] by replacing biomolecules with monomers and forming a combinatorial library of polymer spots using UV initiation of polymerisation on-slide. The polymer microarray format allows hundreds of polymers to be presented on a single glass slide that can be screened in a parallel, high throughput manner. Anderson *et. al.* used a robotic contact (pin) printer to print a range of monomers (pre-mixed with a photoinitiator) onto a substrate slide. The robotic printer dipped the pins into monomer solutions and spotted on a substrate slide to produce a microarray. Upon printing, the monomers were photopolymerised on stage using UV light. This method of 'on slide' polymerisation is advantageous for some polymer materials that are insoluble, cross-linked and cannot be transferred by printing once polymerised [75]. Furthermore, a large combinatorial library can be generated by mixing monomer solutions in a well plate before printing and polymerisation. This also offers the flexibility to follow the leads rapidly, without the need to carry out conventional polymerisation and separation steps. The polymer microarray was used to create a combinatorial library of novel acrylate based materials to study material-cell interactions for stem cell applications.

Various other research groups have used polymer microarray technique for a range of applications. The Bradley group has developed high throughput screening methods using polymer microarrays to screen a library of polymers for mammalian cell attachment and differentiation [84-87] as well as bacterial resistant polymer material [88]. The polymer microarray format has also been used as a tool for high throughput surface characterisation of a library of polymers [73, 75]. Similarly, Hook *et. al.* [1, 2, 75] screened hundreds of polymers for bacterial attachment using polymer microarrays. The material microarrays were screened for *P. aeruginosa, S. aureus* and *E. coli.* This high throughput approach identified a number of 'hit' materials from a library of acrylate and methacrylate based materials. This approach discovered novel bacterial resistant materials that could not have been predicted based upon current knowledge of bacterial interactions with surfaces. The 'hit' materials identified from microarray screening were then scaled up and used to coat a commercially available silicone urinary catheter. The coated catheter device showed up to 30-fold reduction in surface bacterial coverage when compared to commercial silver incorporated device [1]. Furthermore, the coated material also showed resistance to bacterial attachment in an *in-vivo* mouse implant infection model, where live animal imaging was used to follow bioluminescence from labelled bacterial strain over four day period. The proposed mechanism of low bacterial attachment was the presence of the ester group and the weakly amphiphilic structure of these hit polymers. The presence of ring structures was also shown to be a determining factor for low bacterial attachment to hit polymers [1].

An overview of this thesis is shown in Figure 4 below, which shows various experimental steps from microarray to scale up, leading up to *in-vivo* testing.

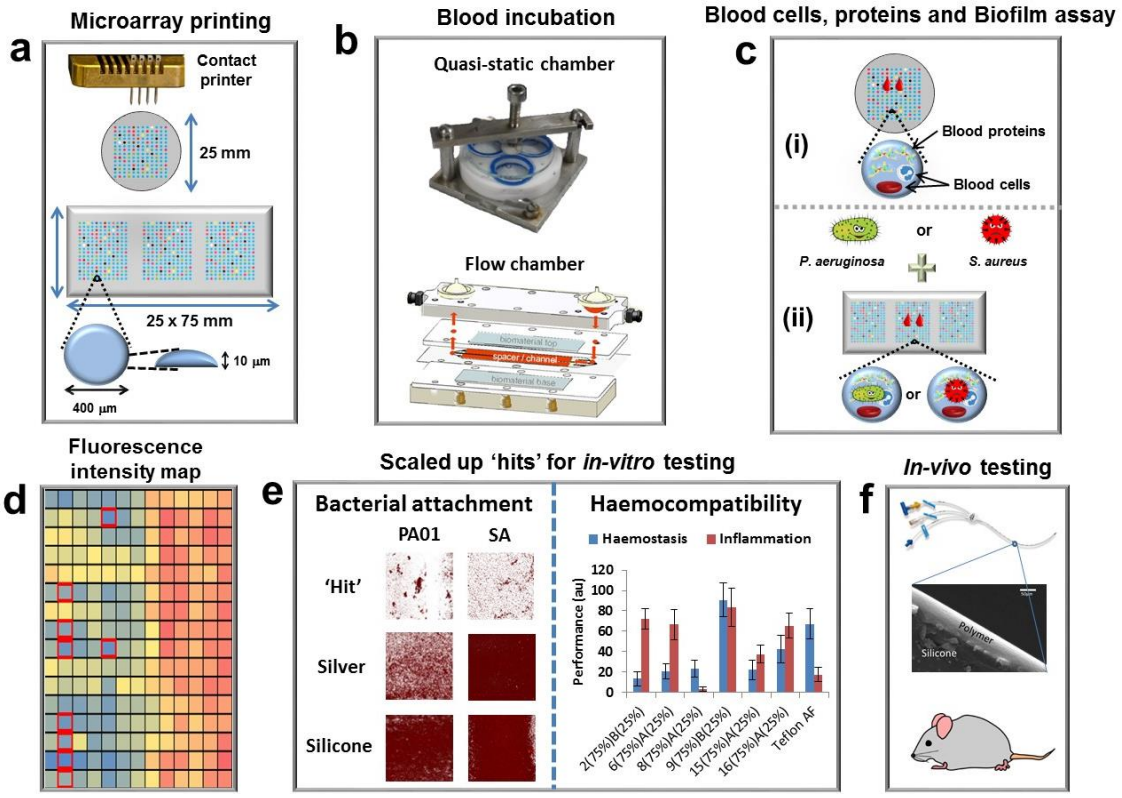


Figure 4: An overview of polymer microarray screening and scale up of 'hit' material compositions for in vitro and in vivo testing.**(a)** Polymer microarray printing using a robotic contact printer on pHEMA coated round and rectangular slides. **(b)** Quasi-static and Flow chambers used for human whole blood incubation for two hours. **(c) (i)** Quantification of protein adsorption and blood cell attachment on each polymer spot; **(ii)** Incubation of blood exposed microarray in RPMI-1640 medium containing *P. aeruginosa* and *S. aureus* (in two separate experiments). **(d)** A heat map representation of blood cells, proteins and bacterial attachment data to select 'hit' material compositions. **(e)** Confocal microscope images showing surface bacterial coverage of lead 'hit' material compared against commercially available silver and silicone uncoated catheters; Haemocompatibility testing involving haemostasis and inflammation parameters on scaled up hit materials. **(f)** Coating of scaled up 'hit' compositions on silicone catheters (confirmed by SEM) and *in-vivo* testing of lead material in a murine infection model.

1.5 Table of key molecules described in the Thesis

The key molecules mentioned in this Thesis are listed in Table 2, with their description, size and shape parameters and molecular weight (Mw) obtained from the literature [89-96].

Table 2: List of key molecules described in the Thesis, with their description and key characteristics.

Molecule	Description	Size and Shape	Mw (kDa)
Heparin	Mucopolysaccharide	Linear and polydisperse chains	3 – 30
Fibrinogen	Plasma glycoprotein	Rod-shaped protein comprising 3 polypeptide pairs – two Aα, two Bβ and two ϒ coiled structure linked by disulphide bonds, with dimensions - 9 nm × 47.5 nm × 6 nm	340
Human serum albumin	Globular plasma protein	Ellipsoid tertiary structure (67% α-helices) composed of 3 homologous domains linked by disulphide bonds, with dimensions of 8 nm x 8 nm x 3 nm	66
Immunoglobulin G (IgG)	Antibody	Y-shaped molecule made up of two types of polypeptide chains – Heavy chain and Light chain, linked thogether by disulphide bonds, with dimensions of 14.5 nm x 8.5 nm x 4.0 nm	150
von Willebrand factor	Plasma glycoprotein	Multimeric structure with shape alteration from irregularly coiled to extended thread-like in response to shear and hydrodynamic force. The dimensions of elongated vWF strings measured *in-vivo* range from 20 – 100 µm	500 – 20,000
Complement C3	α_2-macroglobulin protein	α- and β-chains arranged as 13 domains linked by disulphide bonds	200

1.6 Aim and objectives

The aim of this thesis was to identify new polymers which resist bacterial attachment in venous catheter environment. The objectives were as follows:

1. Optimise polymer microarray printing to create a library of biomaterials, identified from previous research [1] to have bacterial resistant properties.
2. Carry out blood incubation assays on microarrays and analyse protein adsorption and blood cell attachment on each polymer material.
3. Setup biofilm assays, on blood incubated microarrays, using two key biofilm forming bacteria *P. aeruginosa* (Gram-negative) and *S. aureus* (Gram-positive) strains.
4. Scale up 'hit' materials identified from high throughput screening and coat silicone catheters to carry out *in-vitro* and *in-vivo* biofilm and biocompatibility studies.

2 Chapter 2 – Materials and methods

2.1 Materials

All monomers used in this project were obtained from Sigma Aldrich and used as-received. Solvents employed were ordered from Fisher Scientific UK and used as-received. The chemical structures of monomers used are shown in Figure 5. A range of 16 acrylate and methacrylate based monomers with aliphatic, cyclic and aromatic groups were combinatorially mixed with short and long chain glycol based monomers to create a polymer microarray. The monomers used in this project were chosen from a library of mono (meth)acrylates based on their bacterial resistant properties identified from a number of previous screening cycles under urinary catheter physiological conditions [2, 3]. The chosen materials were not previously tested for bacterial resistant properties in the presence of blood. In addition, three zwitterionic monomers (E, F and G) were also tested for haemocompatibility and bacterial attachment. The zwitterionic materials were chosen due to their ability to resist non-specific protein adsorption, foreign-body reaction [97, 98] as well as bacterial resistant properties [76].

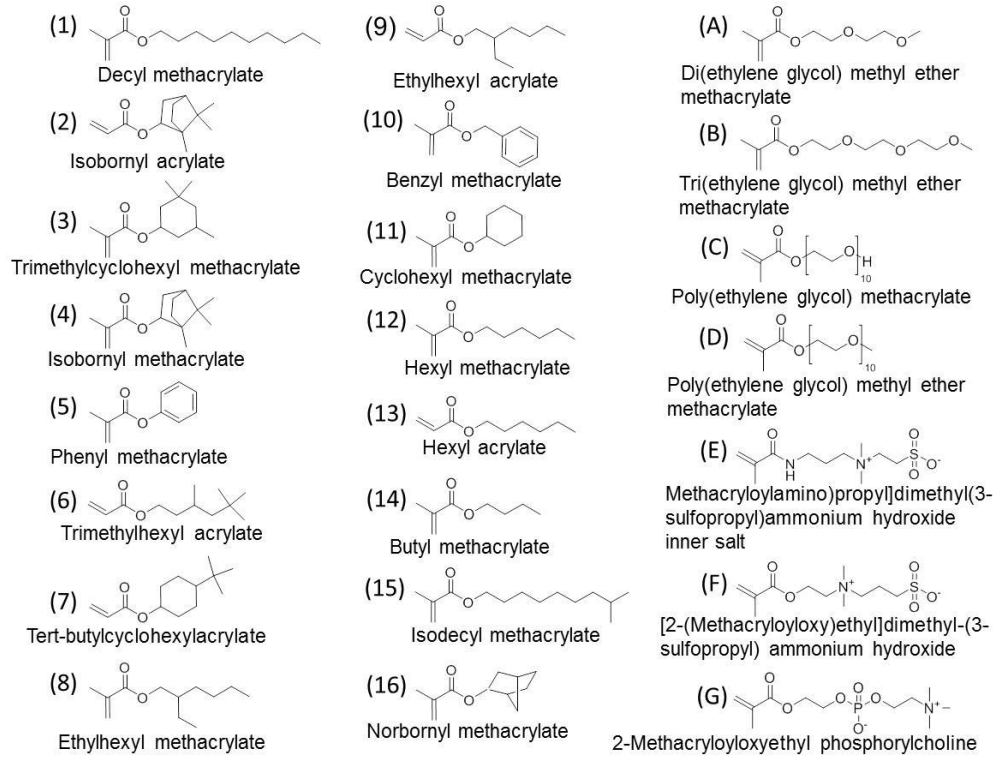


Figure 5: Monomers used in this thesis.

2.2 Microarray substrate slide preparation for printing

Dip coating is a technique commonly used to apply a thin coating of a material on to a substrate. The simplest method of dip coating is by manually dipping and removing the substrate from a volatile solution of a material (for example using ethanol as a solvent) and by subsequent evaporation of the solvent. The thickness of a coating produced by dip coating depends upon the speed at which the substrate is withdrawn from the solution, the viscosity of the solution and the number of dips. There is a direct relationship between withdrawal speed and the coating thickness, whereby increasing the withdrawal speed leads to a thicker coating [99]. This is due to a viscous coating solution having less time

to drain off the slide at a faster withdrawal speed as compared to a slower withdrawal speed. Manual dip coating produces poor slide to slide reproducibility of the coating thickness and uniformity. Hence, an automated dip coater (Holmarc, India) (Figure 6) was used to dip coat epoxy functionalised glass slides with 6% w/v poly(2-hydroxyethyl methacrylate) (pHEMA) in 95%/5% v/v ethanol/water. pHEMA was chosen as a substrate due to the low fouling properties of the material [100, 101]. Therefore, by keeping all other factors, such as viscosity of the solution, constant a reproducible and uniform coating can be applied.



Figure 6: Automated dip coater used to dip coat glass slides with pHEMA solution.

2.3 Microarray printing

The microarray printing was carried out using a XYZ3200 pin printing workstation on a Biodot® contact printer (CA, USA) (Figure 7). The monomer solutions were mixed (using a multi-channel pipette) at various concentrations in a polypropylene

384 well plate. Three 946MP3B slotted metal pins (Arrayit, USA) with a tip diameter of 110 μm were used to transfer approximately 1 nL of pre-mixed monomer solution from 384 well plate onto pHEMA coated substrate slides. The metal pins as well as printer pin head (pin holder) were cleaned by sonication in dichloromethane for 10 minutes prior to printing. This is necessary to prevent the pins getting stuck in the holder during the printing run due to dust or contamination from previous run. The array fabrication run was designed using Biodot macro on the Biodot software. The printing was done using three metal pins, organised such that three monomer solutions were printed in each printing loop followed by pin washing prior to the next three monomers.

The basic components of each run were (a) The quilled metal pins were filled with monomer solution by dipping the pins into well plate at a set speed of 25 mm/s, remained in solution for 2.5 seconds and lifted out of the solution at 25 mm/s, (b) The filled pins were blotted 10 times on blank glass slides to remove excess monomer solution from the outside of the pins, (c) The monomer solutions were printed onto pHEMA coated slides by making the pin contact the surface for 10 ms, (d) The pins were washed in the flow bath of DMF twice, before continue with the next loop. The monomer solutions printed on the slide were then irradiated with ultraviolet (UV) light (30 watt, λ = 365 nm) for 10 seconds between each print loop. After pin printing all the solution compositions, the slides were irradiated (photo-polymerised) for 10 minutes using UV light (30 watt, λ = 365 nm) for complete polymerisation. The printing was done in a sealed chamber with oxygen concentration below 2000 ppm (to prevent free radical quenching by oxygen), at 30-40% humidity and at room

temperature. Upon photo-polymerisation, the polymers were placed under vacuum (<50 mTorr) for one week to remove DMF and any unpolymerised monomers.

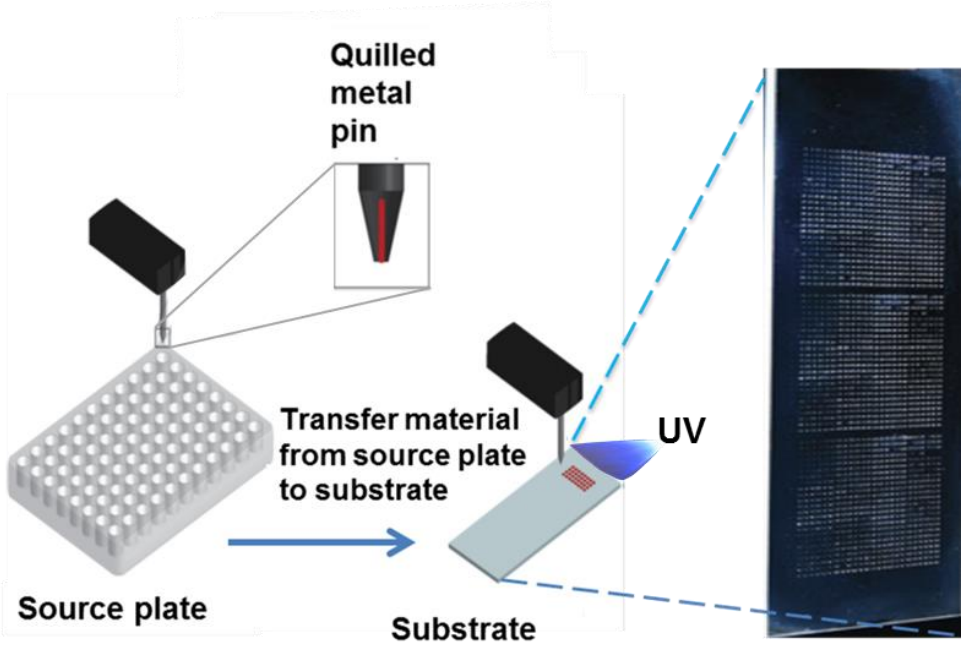


Figure 7: A schematic representation of polymer microarray printing and a photograph of a microarray showing three replicate blocks of polymer spots (average spot diameter is 400μm). (Figure adapted from Hook *et. al.* [102]).

2.4 Time of Flight Secondary Ion Mass Spectrometry (ToF-SIMS)

ToF-SIMS is a surface sensitive technique used to obtain a mass spectrum from the surface of a material at a depth of approximately 1 to 2 nm [103]. This spectrum contains a great detail of information about the molecular structure of the material's surface. In case of the polymer spots, ToF-SIMS provides information about chemical groups present on the surface and hence, details of orientation of the monomer units within the polymer structure.

In order to obtain a mass spectrum, the surface of a material is bombarded with a high energy (usually between 10 and 40 keV) beam of primary ions (Figure 8). The kinetic energy of primary ions gets transferred to the atoms on the surface of the material by a collision cascade which can be likened to a billiard-ball-type collision process [104]. This results in a large number of bond breakage and fragmentation at the collision site leading to the emission of positive and negatively charged secondary ions (ca. 1%) together with a large amount of unionised or neutral fragments [104]. The secondary ions are the only species that are detected and analysed by the mass spectrometer, which allows a thorough chemical analysis of a surface to be performed.

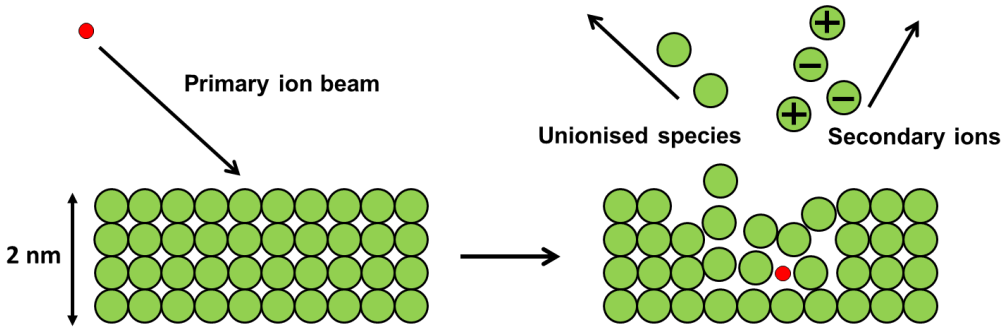


Figure 8: ToF-SIMS schematic illustration of primary ion bombardment and ejection of secondary ions from a surface. (The majority of fragments ejected from a surface are unionised or neutral – not all are shown in the schematic).

Since SIMS is destructive, the primary ion dose used in static SIMS is usually kept below 1 x 10^{12} ions/cm^2 to limit the ion dose such that analysis does not normally come from previously impacted areas (1%) of the surface [105].

The working mechanism of a ToF-SIMS instrument is shown in Figure 9. The primary ion beam produced by the ion gun is

pulsed over a very short period of time, which is then focussed and rastered on the sample surface as shown in Figure 9. The commonly used liquid metal ion sources include Ga^+, Bi_n^+ (n= 1-7) and Cs^+. Gas ion sources such as Ar^+, O^+ and large cluster primary ion sources (C_{60} and Ar_{5000}) are also used. The work presented in this thesis was carried out using Bi_3^+ primary ion source, which offers a good secondary ion yield as well as better detection limits as compared to traditionally used sources such as gallium.

As ToF-SIMS technique is based on the detection of secondary ions, the ionisation of the species emitted from the surface following primary ion bombardment is a key process. The ionisation of molecules, typically ca. 1%, is strongly influenced by the electronic state of the material being analysed [106]. When this is influenced by the surrounding molecules this phenomenon is called the matrix effect, complicating quantitative analysis using SIMS.

The pulsing of the primary ion beam produces discrete 'packets' of secondary ions from the surface. These 'packets' of ionised species emitted from the surface are extracted into a drift tube and accelerated over a very short distance resulting in all the ions possessing identical kinetic energies, which is important to the working of the Time-of-Flight spectrometer. Upon acceleration, the secondary ions with identical kinetic energies separate according to their mass due to lighter ions travelling with a higher velocity than the ions with higher mass [35].

This effect can be described based upon the relationship between kinetic energy, mass and velocity as represented in Equation 1 below:

$$\boldsymbol{E_k = \frac{1}{2} m V^2} \quad \text{(Equation 1)}$$

Where E_k is the kinetic energy, m is the mass and V, is the velocity of a secondary ion. Therefore, the ions with identical kinetic energy have different velocity based upon their mass. Due to this difference in velocity, the ions arrive at the analyser at different times. Hence, based upon the time taken by an ion to travel through a known length of the flight path to reach the detector, the mass of an ion can be calculated using Equation 2:

$$\boldsymbol{t - t_0 = L \left(\frac{m}{2E_k} \right)^{1/2}} \quad \text{(Equation 2)}$$

Where t_0 is the start time and t is the arrival time of an ion at the detector, L is the length of the flight path, m is the mass and E_k is the kinetic energy of an ion. The mass resolution obtained from a Time-of-Flight instrument is much greater than older systems, which employ Quadrupole detectors. Furthermore, the Time-of-Flight instrument also uses a reflectron (ion mirror), which compensates for any spread in the kinetic energies (following acceleration) of the ions of same mass [105]. A reflectron is essentially a retarding electric field, which permits the ions of higher kinetic energies to penetrate further into the reflectron before reflecting to the detector, which in turn minimises the spread of kinetic energies of ions with same mass. Owing to the above features,

a Time-of-Flight instrument allows the collection of whole mass spectrum in parallel and minimises the primary ion dose required. ToF-SIMS can be operated in positive and negative polarity mode to generate a positive and a negative spectrum of the surface based on the detection of positively and negatively charged ions.

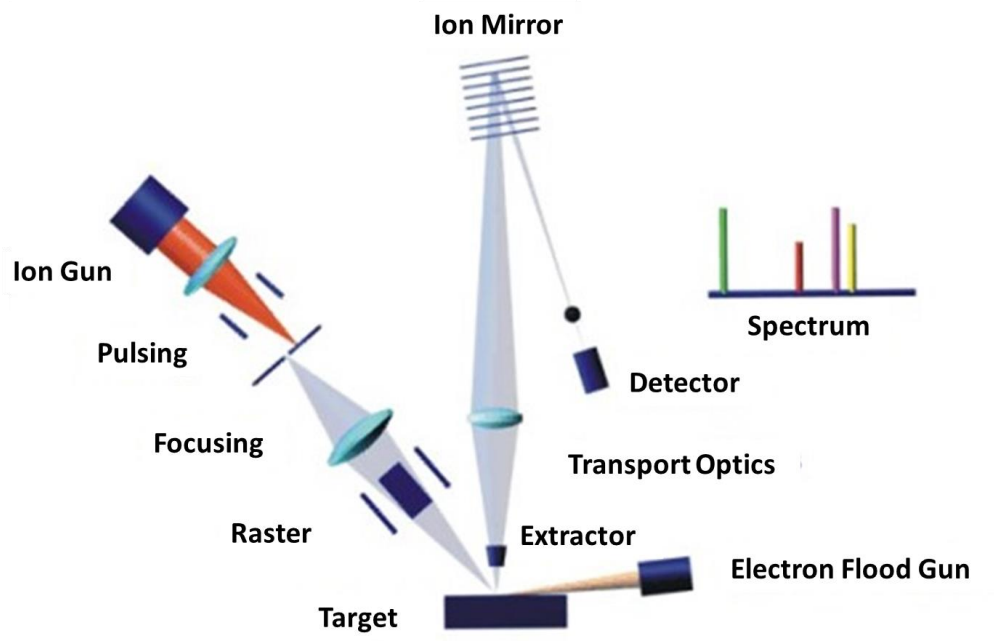


Figure 9: Schematic of a ToF-SIMS instrument showing main parts of the machine from ion gun to detector and production of a mass spectrum (image adapted from Ion ToF [107]).

The use of an electron flood gun is required when analysing insulating materials such as polymers. This is because the sample gains a net positive charge due to bombardment with positively charged primary ions as well as the emission of the secondary electrons [35]. This build-up of positive charge on the sample surface interferes with the function of ToF-SIMS and leads to a poor quality spectrum. An electron flood gun stabilise the surface potential by 'flooding' the sample surface with low energy electrons.

In addition to the mass spectrum of a surface, the ToF-SIMS technique also allows a chemical map / image of a surface to be constructed based upon selected atomic or molecular species. These SIMS images can be used to assess the surface distribution of the atomic or molecular species of interest. An area ranging from a few micrometres to millimetre size can be imaged to obtain SIMS images that consist of a full mass spectrum per pixel of the image. Hence, SIMS image can be used to retrospectively visualise any ion in the spectrum. For the work presented in this thesis ToF-SIMS images of microarrays were acquired as 500 x 500 μm patches with 100 pixels/mm resolution (Figure 10), that were then stitched together by SurfaceLab 6 software to form a chemical image of the whole microarray surface.

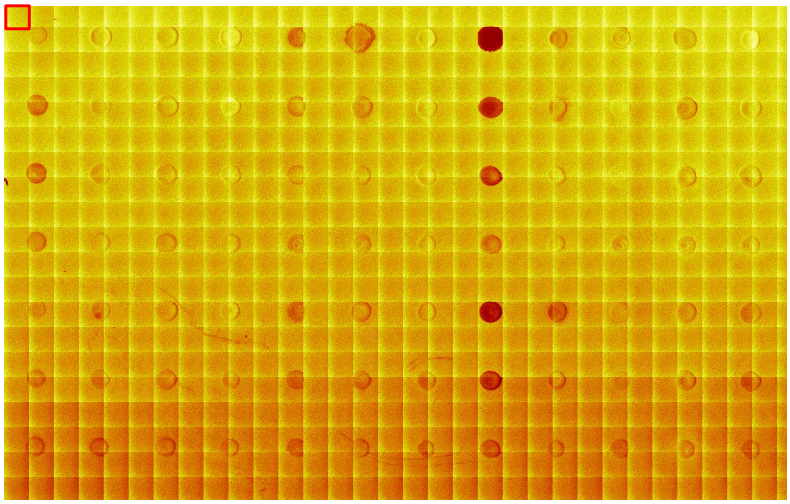


Figure 10: ToF-SIMS total ion image of a microarray made up of 500 x 500 μm patches (Red box shown on top left of the image) acquired using ION TOF IV instrument and SurfaceLab 6 software (Field of view = 15.5 x 10 mm).

The limitations of ToF-SIMS technique for surface analysis is that it is a vacuum based destructive analysis technique and

leads to surface damage. Therefore, a sample used for ToF-SIMS cannot then be used for other experiments such as surface bacterial attachment studies or contact angle measurement.

2.5 X-ray Photoelectron Spectroscopy (XPS)

XPS is a highly surface sensitive technique (top 1 to 10 nm of a surface) capable of providing quantitative data such as elemental composition of all the elements present on the surface (except Hydrogen and Helium) [108]. XPS is also known as electron spectroscopy for chemical analysis (ESCA). The key components and the working mechanism of an XPS instrument are shown in Figure 11.

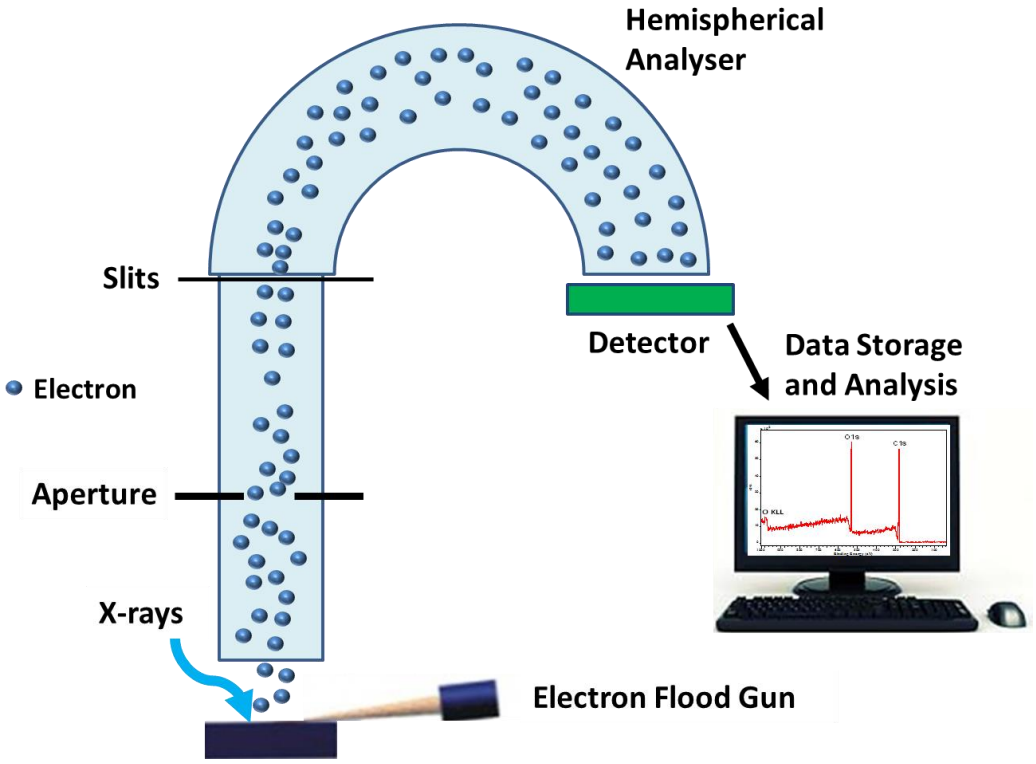


Figure 11: Schematic representation of mechanism of action of an XPS instrument showing key components of the instrument.

XPS involves placing a sample in ultra-high vacuum (UHV) and irradiating the sample surface with photons of X-ray energy range (Magnesium K alpha (MgKa) = 1486.6eV and Aluminium K alpha (AlKa) = 1253.6eV). An anode (usually made up of

aluminium or magnesium) is bombarded with high energy electrons from a heated filament to generate X-ray beam. The X-rays produced are commonly monochromated with a smaller energy range, improving the resolution of the technique [109].

Following the irradiation of a surface, three potential outcomes are possible; firstly the photon can pass through an atom with no interactions, secondly the photon can be scattered by the electrons leading to a partial loss of energy and thirdly the photon can collide and transfer its energy to an atomic orbital electron resulting in emission of an electron from an atom [106]. The first two scenarios lead to no electron ejection from the surface but the third possibility leads to the ejection of electrons from a surface and is the basis for XPS analysis. However, the emission of an electron from core energy levels in atoms on or near the surface is determined by the binding energy (E_B) of an electron. The binding energy of an electron in a particular orbital can be defined as the force of attraction by which the negatively charged electron is attracted to the positively charged nucleus. For example, the closer an electron to the nucleus, higher the force of attraction and higher will be the binding energy. Therefore, in order to eject an electron from an atomic orbital, the X-ray energy has to be high enough to overcome the binding energy of an electron. Furthermore, only a small amount of the electrons ejected from an atom emerge from the surface without losing the energy through collisions on their way through the sample bulk. The probability of an electron reaching the surface without any energy loss reduces as the distance from the surface increases. Due to this loss of electron energy, although the X-rays can penetrate to a distance of microns in the

sample bulk, only the electrons from top 10 nm are detected by the detector.

The Binding energy of the emitted electrons can be calculated based upon the energy of the X-ray source (known) and the kinetic energy of the electrons (measured by the detector), using the Einstein equation:

$$\boldsymbol{E_B = hv - E_K - \phi_{sp}} \quad \text{(Equation 3)}$$

Where $\boldsymbol{E_B}$ is the binding energy of an electron, $\boldsymbol{hv}$ is the energy of the X-ray source, $\boldsymbol{E_K}$ is the kinetic energy of the emitted electron measured by the detector and ϕ_{sp} is the work function of the spectrometer [108]. Since the binding energies of core electrons from an atom are unique for each atom, the XPS spectrum can be used to determine which atoms (elements) are present on the sample surface. In a typical XPS analysis, initially a survey XPS scan (broad spectrum) covering entire binding energy range (usually 0 to 1000 ev) is carried out. This broad XPS spectrum (Figure 12) shows binding energy of the electrons plotted against the electron counts per second (CPS). This allows a relative quantification of each atom on the surface by integrating the area under each peak on the spectrum. Hence, the survey scan provides useful information about what elements are present on the surface and together with their relative quantities. Furthermore, a survey spectrum also gives information about common contaminants such as polydimethylsiloxane (PDMS) or surface oxidation products or other hydrocarbons on the surface. Therefore, due to high surface sensitivity of XPS, a great care

should be taken in sample preparation and storage prior to the XPS analysis to prevent surface contamination.

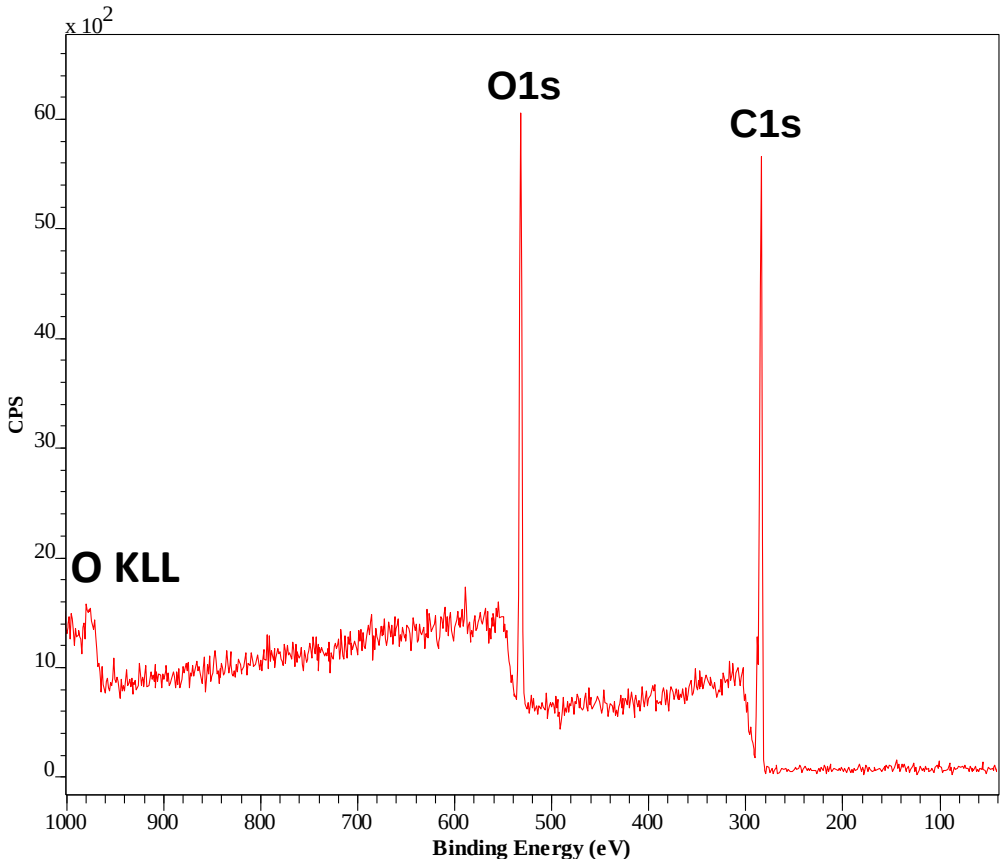


Figure 12: An example of a survey or broad XPS spectrum obtained from an oxygen and carbon containing polymer material.

As the case with ToF-SIMS, sample charging can also affect XPS spectrum and causes a shift in binding energies of the electrons. This is because sample gains a net positive charge due to removal of negatively charged electrons from the surface. Hence, an electron flood gun is employed to minimise the charging of the surface. Charge correction of the spectrum must also be carried out before data analysis and shifting the data to C-C at 285.0 eV is the most commonly used protocol.

The XPS analysis presented in this thesis was carried out using a Kratos Axis Ultra spectrometer. A mono-chromated

Aluminium X-ray gun (AlKα = 1253.6 eV) was used with a charge-compensating electron flood gun. The data acquisition was automated by loading XY co-ordinates of the microarray into the instrument software. Photoelectrons were sampled from a 110 μm diameter (aperture) in the centre of each polymer spot, to prevent any contribution from the pHEMA background and the substrate. To permit the analysis of whole microarray in a high-throughput manner, the data acquisition was carried out in a snapshot mode for the C1s, N1s and O1s core levels. The acquisition time was limited to 30 seconds for N1s and 20 seconds for C1s and O1s scans, using pass energy of 160 eV. The main purpose of the XPS analysis was to quantify N1s atomic percentage that could then be linked to the amount of protein adsorbed on the surface. Following the data acquisition, elemental quantification was carried out using CASA XPS software (version 2.3.16 PR 1.6).

2.6 Water Contact Angle measurements

Water contact angle (WCA) measurement can give information about the relative hydrophilicity/ hydrophobicity of a surface. WCA data can be used to determine a relationship between biological properties of a surface and its hydrophilicity/ hydrophobicity (wettability). WCA has been used in some studies to explain bacterial behaviour towards materials [110, 111]. Contact angle measurements on each polymer spot on the microarray were taken using ultra-pure water (18.2 MΩ resistivity at 25 °C). Due to small diameter of each microarray spot (~400 μm), a DSA100 (Krüss) instrument with a piezo-doser head unit was used [112]. The piezo-doser head

dispensed 100 pL droplets of water onto the centre of each polymer spot as shown in Figure 13.

Data acquisition was carried out by recording the side profile of each back lit spot in an automated fashion. In order to ensure the alignment of the piezo-doser head with the spot surface, a dual camera system was used. The side high-definition camera recorded a profile of the spot and the top camera was used to record a bird's eye view of the spot to ensure that the water droplet was deposited in the middle of each polymer spot, as shown in Figure 13 (a). The video clips recorded for each polymer spot were analysed using DSA100 software (Krüss) by using a circle fitting method [112].

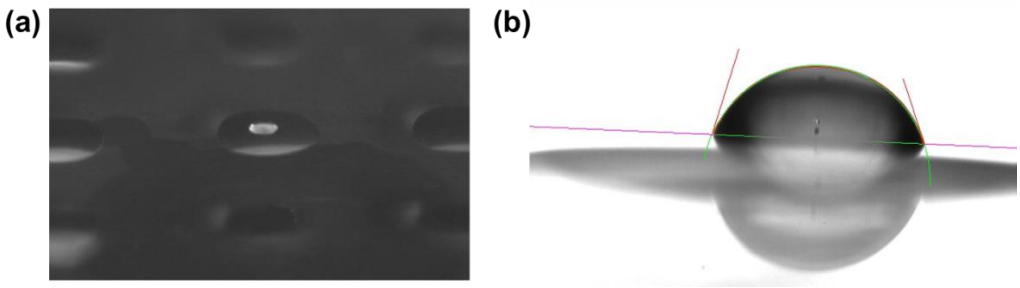


Figure 13: Measuring water contact angle on polymer microarray spots using a DSA100 instrument **(a)** Bird's eye view (from top camera) of a 100 pL water droplet in the middle of a polymer microarray spot (400 μm diameter). **(b)** A circle fitting on the profile of a 100 pL water droplet on a polymer microarray spot to determine contact angle (Figure adapted from [113]).

2.7 Details of bacterial strains used in this project

P. aeruginosa and *S. aureus* strains used in this project are listed in Table 3 below.

Table 3: The description and origin of bacterial strains used in this project.

Bacterial strain	Description	Origin
***P. aeruginosa* PA01-N**	Nottingham strain with plasmid pME6032ΔlacIQ::mCherry Tc resistant for constitutive expression of mCherry fluorescent tag	Hollway BW (1955) J Gen Microbiol 13:572-581
***P. aeruginosa* PA01-L**	Lausanne strain with plasmid pME6032ΔlacIQ::mCherry for constitutive expression of mCherry fluorescent tag	From Dr. Jean Dubern's lab collection
***S. aureus* SH1000**	Wild type with PBS10 mKat plasmid with Ery resistant for constitutive expression of mKat fluorescent tag	From Dr. Ewan Murray's lab collection

2.8 Bacterial incubation and high throughput bacterial attachment assay

The bacterial incubation work was carried out in a category 2 microbiology lab. Plasmids expressing mCherry and mKat were transformed into *P. aeruginosa* (PA01-N) and *S. aureus* (SH1000) bacterial strains, respectively and maintained using appropriate antibiotics in the culture media [114]. These red fluorescence proteins were chosen to tag bacteria over green fluorescence protein (GFP) due to high autofluorescence

observed from the polymers at GFP wavelength (488nm). The key steps involved in the bacterial attachment assay are shown in Figure 14. The transformed bacterial strains were streaked out on LB (Luria-Bertani, Oxford, UK) agar plates and were allowed to grow overnight at 37 ^{o}C to form colonies. Using a sterile plastic loop, a single colony of bacteria, grown on LB agar plate, was then used to set up an overnight culture in 10 mL of LB broth in a 50 mL Falcone tube at 37 ^{o}C with 200 RPM shaking. The OD^{600} of this bacterial culture was measured to be around 2 units. The overnight culture in LB medium was then centrifuged at 9995 rpm at 22 ^{o}C for 10 minutes to separate the media from the bacteria. The LB media was discarded and replaced with 10mL of RPMI-1640 chemically defined medium (Sigma, UK). The bacteria were re-suspended into RPMI-1640 medium using a vortex mixer. The above centrifugation and re-suspension steps were repeated to completely remove LB medium from the bacterial culture.

The polymer microarray slides were UV-sterilised for 10 minutes and were placed in a sterile petri dish. The microarray slides were then incubated in human whole blood for two hours at 37 ^{o}C with 60 rpm shaking. Following incubation, the slides were rinsed once with sterile PBS to remove unadsorbed blood proteins/cells and once with sterile deionised water to remove salts. The slides were then incubated in 15 mL of RPMI-1640 medium inoculated with diluted (OD^{600} = 0.01) bacteria from overnight culture (bacteria suspended in RPMI-1640 medium) and was grown at 37 °C with 60 rpm shaking for 72 hours.

After 72 hours, the slides were removed from their respective incubation conditions and were rinsed once using sterile PBS

and sterile deionised water before imaging the slides using a fluorescence scanner.

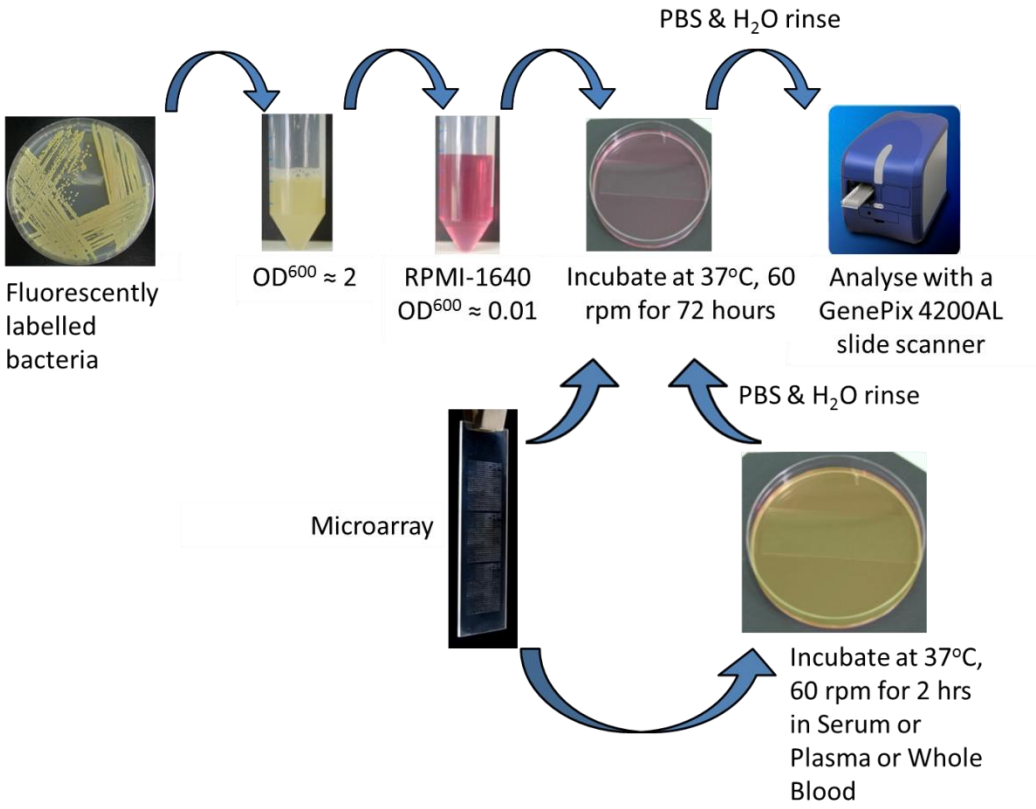


Figure 14: Steps involved in bacterial attachment assay experimental setup. Fluorescently labelled bacteria streaked on an agar plate (top left) were first transferred into LB media for an overnight culture and then incubated in RPMI-1640 media for three day biofilm assay. Polymer microarray incubated in serum or plasma or whole blood was then transferred into RPMI-1640 medium containing bacteria to allow surface bacterial attachment. The final step was to analyse bacteria incubated microarray using a fluorescence scanner.

2.9 Fluorescence confocal microscopy

The basic principle of fluorescence confocal microscopy is same as the conventional fluorescence microscopy. A sample consisting of a fluorophore (a chemical compound that fluoresce when illuminated by light of a particular wavelength) is illuminated using high energy (shorter wavelength) light.

The fluorophore absorbs the energy and emits a lower energy (longer wavelength) light, which is detected by the detector to form an image [115]. Confocal microscopy technique allows high resolution, high contrast imaging by reducing the background signal and improving signal to noise ratio [116]. A schematic of a confocal microscope is shown in Figure 15. A laser light source of a particular wavelength is used to illuminate the sample. A confocal microscope consists of a dichromatic (dichroic) mirror, which reflects the laser light with a shorter wavelength (excitation light) towards the sample and allows the emitted fluorescence light with a longer wavelength to pass through to the detector as shown in Figure 15. The selection of a dichromatic mirror is an important step to minimise interference from the excitation light.

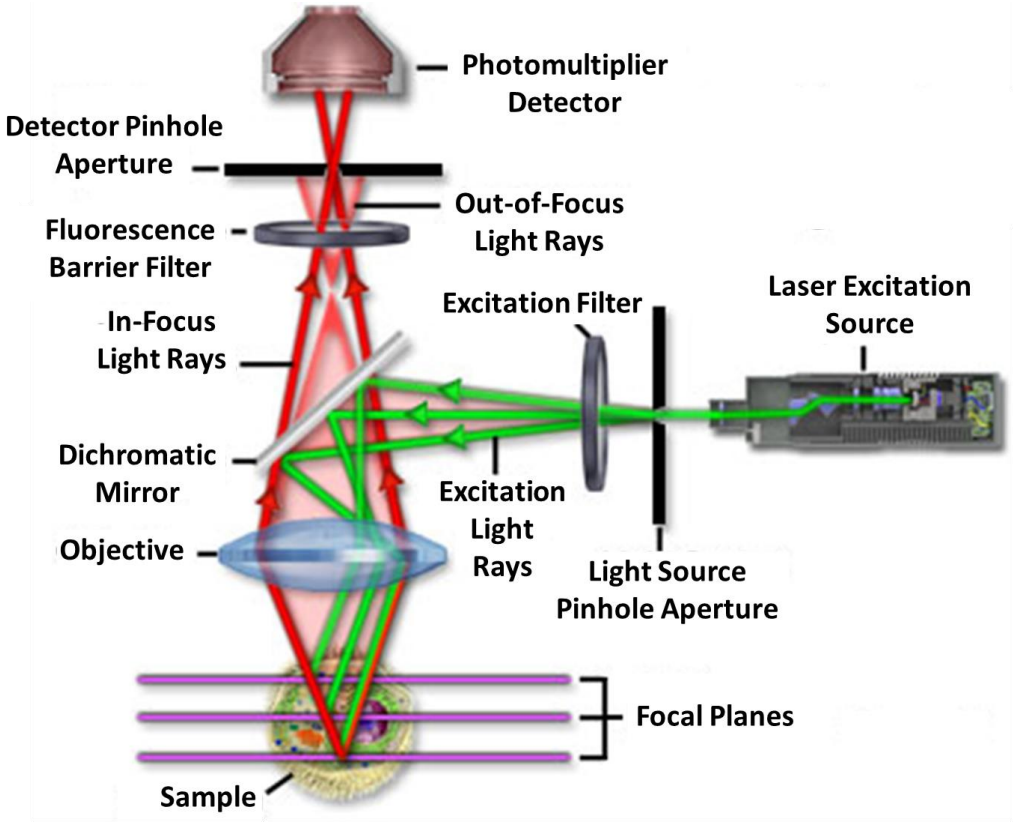


Figure 15: Schematic representation of a confocal microscope. (Image adapted from [116])

The objective lens is used to focus the excitation and emitted light on the sample and the detector, respectively. Unlike conventional fluorescence microscopy, in which the entire sample surface is illuminated by the excitation light, confocal fluorescence microscope uses pinholes to block scattered light from above and below the focal plane, resulting collection of light from a highly focussed point [115]. Therefore, the images acquired using a confocal microscope have high contrast and low background noise. An increase in pinhole size leads to increase in z-slice thickness and poor contrast. The downside of having small pinholes is blockage of majority of fluorescence signal. A photomultiplier detector is used to amplify the fluorescence light signal from the sample. The signal intensity can also be increased by increasing the gain, which increases the sensitivity of the detector. However, a high gain leads to higher background noise. Similarly, the detector exposure time should be fine-tuned to prevent detector saturation, which makes quantitative analysis difficult and less reliable. The confocal microscopy allows cross section slices of a sample to be combined to re-construct a 3D image of the sample.

The work presented in this thesis was carried out using Zeiss LSM 700 confocal microscope (Carl Zeiss, Germany). A 555 nm laser was used as an excitation source to detect mCherry and mKat labelled *P. aeruginosa* and *S. aureus,* respectively using 10x objective.

3 Chapter 3 – Optimisation of microarray printing

3.1 Introduction

The polymer microarray technique is an excellent tool for high throughput screening of a library of biomaterials for a particular biomedical application. However, there were a number of challenges associated with microarray printing, which needed to be addressed before proceeding further. The main challenge in this high throughput work was to produce a microarray with a wide range of polymers (using monomers with diverse physiochemical properties, e.g. viscosity and hydrophilicity) that are spatially confined on a glass slide to prevent materials merging into one another. The separation of the array spots is vitally important to accurately carry out subsequent biological assays, i.e. bacterial attachment quantification on each spot in a high throughput manner. The quality of a polymer microarray printing depends upon a range of parameters such as concentration and the physiochemical properties of the monomers to be printed and the support material. This Chapter focusses on the microarray optimisation experiments to produce an optimised polymer microarray, fit for bacterial attachment and blood incubation experiments.

3.1.1 Aim and objectives

The aim of these optimisation experiments was to obtain a defined and reproducible microarray. To do this these objectives were tackled:

1. Identify optimal conditions for polymer microarray printing.
2. Produce a polymer microarray with well-defined spots without spot to spot spreading.
3. Confirm the microarray printing quality using optical microscopy as well as chemical images using ToF-SIMS.

3.2 Experimental

3.2.1 pHEMA dip coating on epoxy functionalised glass slides

A 6% w/v pHEMA solution was prepared by dissolving pHEMA into 95%/5% v/v solution of ethanol and water. Adding 5% v/v water enhances the solubility of pHEMA in ethanol. Epoxy coated glass slides (Molecular devices, Sunnyvale, CA, USA), with dimensions of 75 mm x 25 mm, were then dip coated in pHEMA solution using an automated dip coater (Holmarc Ltd, India). The epoxy group is a reactive functional group that covalently links with pHEMA by a ring-opening addition reaction to form a low-fouling substrate [83, 100, 101]. The dip and retrieval speeds were set at 9 mm/s and 2 mm/s, respectively. The process of dip coating was optimised to produce a thick enough pHEMA coating that holds the spots on their place and helps reduce spreading of monomer spots printed on it. The glass slides were dip coated four times into 6% w/v pHEMA solution to produce a coating of 6.5 μm thickness. The dip-coated slides were then dried for two hours before being left at room temperature for further one week to allow solvent evaporation.

3.2.2 Microarray Printing

The pHEMA coated epoxide functionalised glass slides were used to print microarrays using a XYZ3200 pin printing workstation on a Biodot contact printer (CA, USA). The

monomer solutions were mixed at various concentrations in a polypropylene 384 well plate. The composition of the solution in each well in 384 well plate was 75% v/v monomer mixture, 25% v/v Dimethylformamide (DMF) (was optimised to 25% v/v monomer and 75% v/v DMF after optimisation) and 1% w/v initiator (2,2-dimethoxy-2-phenylacetophenon). Three 946MP3B slotted metal pins (Arrayit, USA) with a tip diameter of 110 μm were used to transfer approximately 1 nL of pre-mixed monomer solution from 384 well plate onto pHEMA coated substrate slides. The monomer solutions printed on the slide were then irradiated with ultraviolet (UV) light (30 watt, λ = 365 nm) for 10 seconds between each print loop. After pin printing all the solution compositions, the slides were irradiated (photo-polymerised) for 10 minutes using UV light (30 watt, λ = 365 nm) for complete polymerisation. The printing was done in a sealed chamber with oxygen concentration below 2000 ppm (to prevent free radical quenching by oxygen), at 35-40% humidity and at room temperature. Upon photo-polymerisation, the polymers were placed under vacuum (<50 mTorr) for seven days to remove DMF and any unpolymerised monomers.

3.2.3 ToF-SIMS

A ToF-SIMS IV (ION TOF GmbH) instrument was operated using a Bi_3^+ primary ion source, operated at 25 kV in "bunched mode". A 0.3 pA primary ion beam was applied and both positive and negative secondary ions were collected. The whole microarray area of 14 mm × 12 mm (including background) was scanned in 500 μm × 500 μm area patches, 15 frames acquired per patch at 1 shot/pixel. The primary ion

dose was maintained below 1 × 10^{12} ions/cm^2 to maintain static SIMS conditions. As the polymer samples (as well as glass substrate) are insulating in nature, it was necessary to employ a charge compensation device. This is because the sample gains a net positive charge due to dosing with positively charged primary ions [35]. Ion masses were determined using a high resolution ToF analyser allowing accurate mass assignments. ToF-SIMS data was acquired and analysed using SurfaceLab 6 software (ION TOF, GmbH). The resulting microarray chemical images were then used to select Regions of Interest (ROIs), shown as various coloured dots, for each polymer spot to acquire ToF-SIMS spectra, as shown in Figure 16. These individual ToF-SIMS spectra can be used to link surface chemistry of each material to their biological performance such as bacterial attachment.

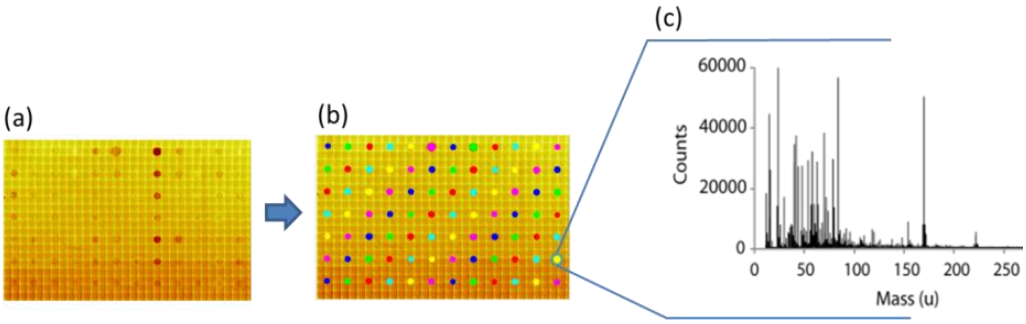


Figure 16: The process to extract surface chemistry of each polymer spot from ToF-SIMS chemical image. **(a)** ToF-SIMS total ion chemical image of a microarray, **(b)** selected ROIs to acquire a ToF-SIMS spectrum for each polymer spot, shown by **(c).** (Average spot diameter 400 μm).

3.2.4 Contact angle measurements

Contact angle of a mixture of monomer and DMF at various concentrations (%v/v) was measured on a pHEMA coated glass slide using CAM200 contact angle equipment (KSV

Instruments Ltd., Finland & USA). A 5 μL volume droplet of DMF mixed with monomer solution was placed on pHEMA surface. The contact angle was calculated using the Young–Laplace drop shape applied to the profile of 5 μL drops, measured using CAM200 sessile drop instrument.

3.2.5 Optical microscopy

An inverted optical microscope (IMSTAR®, S.A.) was used to acquire optical images using 10x objective lens. Image mosaics were then reconstructed and Pathfinder™ software was used to measure diameter of microarray spots.

3.3 Results

3.3.1 Optimising microarray printing for well-defined spot formation by varying solvent concentration

Initial printing of monomer spots on a pHEMA coated surface was carried out using the printing conditions used previously, described in method section above. ToF SIMS imaging clearly indicated that this lead to drop spreading and merging of the resulting polymer spots but this was not clear from a visual inspection of the light microscopy images alone (as evident in Figure 17). Because well-separated and reproducible polymer spots on the microarray are essential for this study, optimisation to form good quality polymer spots was undertaken. Many different parameters such as humidity in the printing chamber (and consequent pHEMA swelling), thickness of pHEMA background coating, pin blotting settings, concentration of the initiator and solvent (DMF) and amount of monomer solution in the 384 well plate were changed to optimise the microarray printing. None of these changes produced a significantly improved microarray. The previous method used was to employ 25% v/v DMF concentration to print microarrays. However, the monomers used in this project were more prone to spreading than those investigated previously. Consequently, the effect of DMF concentration on printing quality was investigated.

A microarray was printed using five monomers (prone to spreading) by varying the solvent concentration from 10% v/v to 50% v/v as shown in Figure 17 Each row in the map

consists of homopolymer (first and second column) and monomers mixed with ethylene glycol methacrylates of varying chain length. The microarray printed at range of solvent concentrations was analysed using optical microscopy and ToF-SIMS to visualise physical and chemical spreading of printed spots, respectively. The printed microarray was imaged using an optical microscope with 10x magnification to obtain high resolution images of polymer spots. The images obtained from the optical microscope were stitched together using Cell Profiler™ software to represent a microarray format as shown in Figure 17.

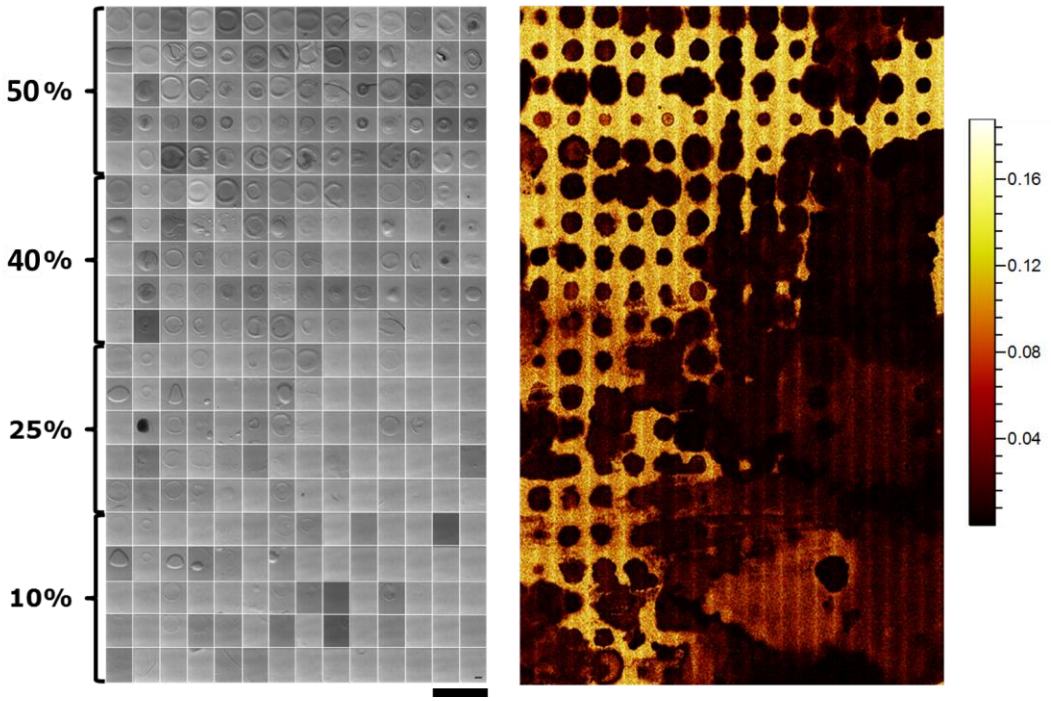


Figure 17: Optical microscope images (stitched, shown on left side) and ToF-SIMS chemical image of the array printed at a range of solvent concentrations. Optical images were stitched together using Cell Profiler™ software. (Scale bar = 1 mm). Right side image shows a ToF-SIMS chemical image built using chemical fragment $C_2H_5O^+$ at m/z 45.02, which is a fragment of pHEMA and acts as a background marker for pHEMA coating. The monomers printed on the surface appear as black dots (image normalised by total counts (au, as shown on scale). ToF-SIMS data accusation was carried out by Dr. David Scurr). (The difference in contrast seen on the optical microscope images was due a different contrast setting

automatically applied to each image by the microscope software. This problem was corrected in later images shown in Figure 24).

From these high-resolution images, it can be seen that a very few spots were printed at 10% v/v DMF as compared to a 50% v/v DMF concentration, which produced the most well-defined spots. It is clear that number of spots printed increased as the concentration of DMF was increased from 10% v/v to 50% v/v as presented in Figure 18.

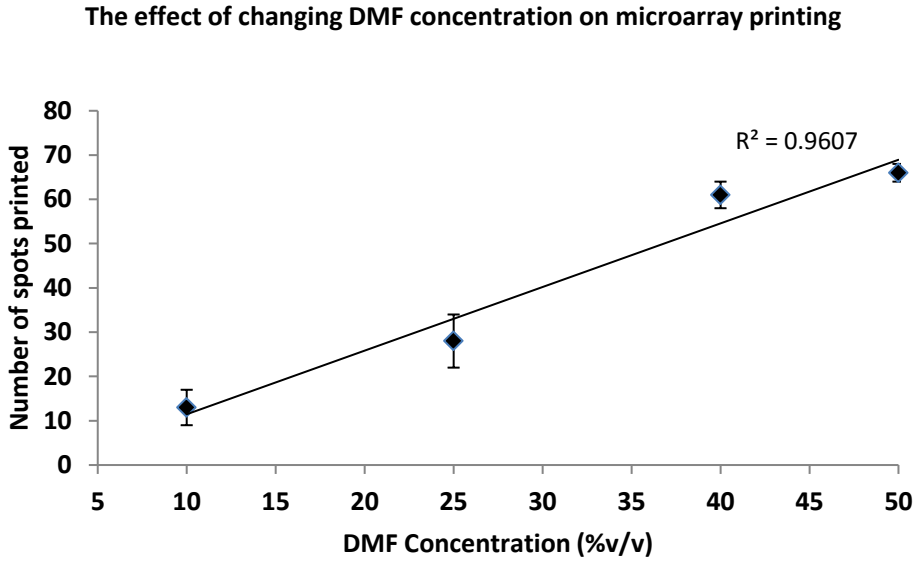


Figure 18: The effect of DMF concentration on microarray printing. Average number of spots (n=3) printed in microarray format on pHEMA coated glass slide at four different DMF concentrations. More polymer spots were printed at higher DMF concentrations.

Although the optical microscopy shows the position of the printed spots and whether the spot is printed or not, it does not give any information about the chemical characteristics of the printed spot. Therefore, the microarray was then analysed using ToF-SIMS to understand the surface chemistry of the printed / missing spots. The key question probed using ToF-SIMS was to understand if a missing spot was actually not present on the surface or thinly spread over the surface.

3.3.2 ToF-SIMS analysis of microarray printed at 4 different DMF concentrations

The ToF-SIMS technique allows a chemical map / image of a surface to be constructed based upon a particular ion fragment. If the structure of a monomer is known and can be related to an ion fragment, ToF-SIMS software (SurfaceLab 6) allows building a chemical image of the surface unique to a particular ion fragment. The printed microarray was analysed by ToF-SIMS to build a chemical map of the surface as shown in Figure 17 (right hand side image) to confirm the extent of spreading at various DMF concentrations. Ion fragment $C_2H_5O^+$ at m/z = 45.02 is a marker for pHEMA, which was used to represent pHEMA background. The bright background on the chemical image corresponds to the high abundance of $C_2H_5O^+$ ion fragments in pHEMA, with dark spots representing polymer spots printed on it. This ion map of the microarray re-emphasises the observations made from the optical images meaning 50% v/v DMF concentration produced better defined microarray spots with reduced spreading and merging of monomers. At lower solvent concentrations most of the printed monomer solutions failed to produce a defined spot and as a result merged with neighbouring spots to coat the pHEMA surface. Therefore, the missing spots appeared in optical microscopy (Figure 17) were due to the spreading and failure of the printed materials to form defined spots.

ToF-SIMS chemical images of a surface were also reconstructed based on key ion fragments from the printed materials to visualise the printing quality of a microarray as

presented in Figure 19. The chemical map shows that the monomer spots printed on pHEMA surface have higher ion intensity for a particular ion fragment (hence, the spots light up on a dark background) as compared to the background pHEMA coating. These chemical images shown in Figure 19 also reinforce the beneficial effect of 50% v/v DMF concentration on printing quality of the microarray, by showing well defined spots at 50% v/v DMF concentration as compared to the 10% v/v, where the spots merged together.

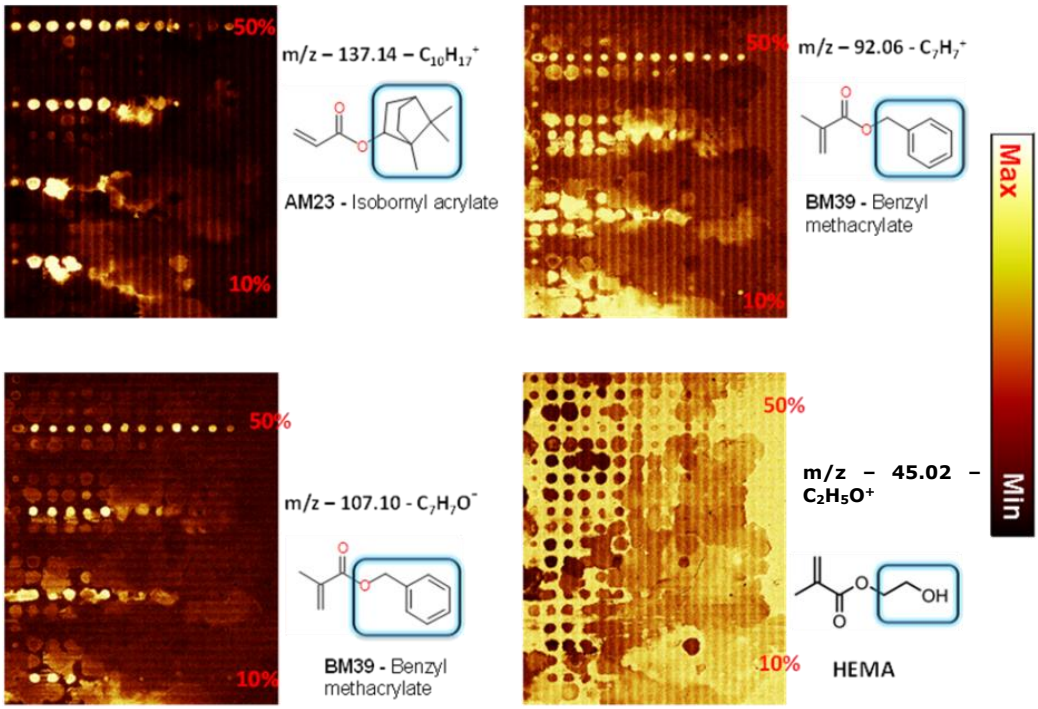


Figure 19: ToF-SIMS chemical mapping of a microarray printed at various DMF concentrations based on ion fragments from three different monomers and pHEMA background. (ToF-SIMS data accusation was carried out by Dr. David Scurr).

Following on from these optimised printing conditions, microarray printing was then done using 50% v/v DMF and under standard conditions described in the method section above and as per the composition map shown in Figure 20. The resultant microarray was then analysed by ToF-SIMS and an ion map of the microarray was reconstructed to assess the

extent of spreading of the polymer spots (Figure 21). Although 50% v/v DMF concentration had led to a great reduction in spot spreading on the microarray, however, there was still a significant spreading present. The effect of DMF on spreading was further evaluated using contact angle of monomer and DMF mixture on pHEMA coated slide as described in the next section.

15	Blank	15(80)A	15(60)A	15(40)A	15(20)A	15(80)B	15(60)B	15(40)B	15(20)B	15(80)C	15(60)C	15(40)C	15(20)C
1	Blank	1(80)A	1(60)A	1(40)A	1(20)A	1(80)B	1(60)B	1(40)B	1(20)B	1(80)C	1(60)C	1(40)C	1(20)C
2	Blank	2(80)A	2(60)A	2(40)A	2(20)A	2(80)B	2(60)B	2(40)B	2(20)B	2(80)C	2(60)C	2(40)C	2(20)C
3	Blank	3(80)A	3(60)A	3(40)A	3(20)A	3(80)B	3(60)B	3(40)B	3(20)B	3(80)C	3(60)C	3(40)C	3(20)C
4	Blank	4(80)A	4(60)A	4(40)A	4(20)A	4(80)B	4(60)B	4(40)B	4(20)B	4(80)C	4(60)C	4(40)C	4(20)C
5	Blank	5(80)A	5(60)A	5(40)A	5(20)A	5(80)B	5(60)B	5(40)B	5(20)B	5(80)C	5(60)C	5(40)C	5(20)C
6	Blank	6(80)A	6(60)A	6(40)A	6(20)A	6(80)B	6(60)B	6(40)B	6(20)B	6(80)C	6(60)C	6(40)C	6(20)C
7	Blank	7(80)A	7(60)A	7(40)A	7(20)A	7(80)B	7(60)B	7(40)B	7(20)B	7(80)C	7(60)C	7(40)C	7(20)C
8	Blank	8(80)A	8(60)A	8(40)A	8(20)A	8(80)B	8(60)B	8(40)B	8(20)B	8(80)C	8(60)C	8(40)C	8(20)C
9	Blank	9(80)A	9(60)A	9(40)A	9(20)A	9(80)B	9(60)B	9(40)B	9(20)B	9(80)C	9(60)C	9(40)C	9(20)C
16	Blank	16(80)A	16(60)A	16(40)A	16(20)A	16(80)B	16(60)B	16(40)B	16(20)B	16(80)C	16(60)C	16(40)C	16(20)C
10	Blank	10(80)A	10(60)A	10(40)A	10(20)A	10(80)B	10(60)B	10(40)B	10(20)B	10(80)C	10(60)C	10(40)C	10(20)C
11	D	11(80)A	11(60)A	11(40)A	11(20)A	11(80)B	11(60)B	11(40)B	11(20)B	11(80)C	11(60)C	11(40)C	11(20)C
12	C	12(80)A	12(60)A	12(40)A	12(20)A	12(80)B	12(60)B	12(40)B	12(20)B	12(80)C	12(60)C	12(40)C	12(20)C
13	B	13(80)A	13(60)A	13(40)A	13(20)A	13(80)B	13(60)B	13(40)B	13(20)B	13(80)C	13(60)C	13(40)C	13(20)C
14	A	14(80)A	14(60)A	14(40)A	14(20)A	14(80)B	14(60)B	14(40)B	14(20)B	14(80)C	14(60)C	14(40)C	14(20)C

Figure 20: Monomer composition map of microarray printed at 50% v/v solvent (DMF) concentration. Bacteria attachment resistant monomers 1 to 16 were mixed with four glycol methacrylate monomers at 100:0, 80:20, 60:40, 40:60, 20:80 and 0:100 compositions and printed in a microarray format.

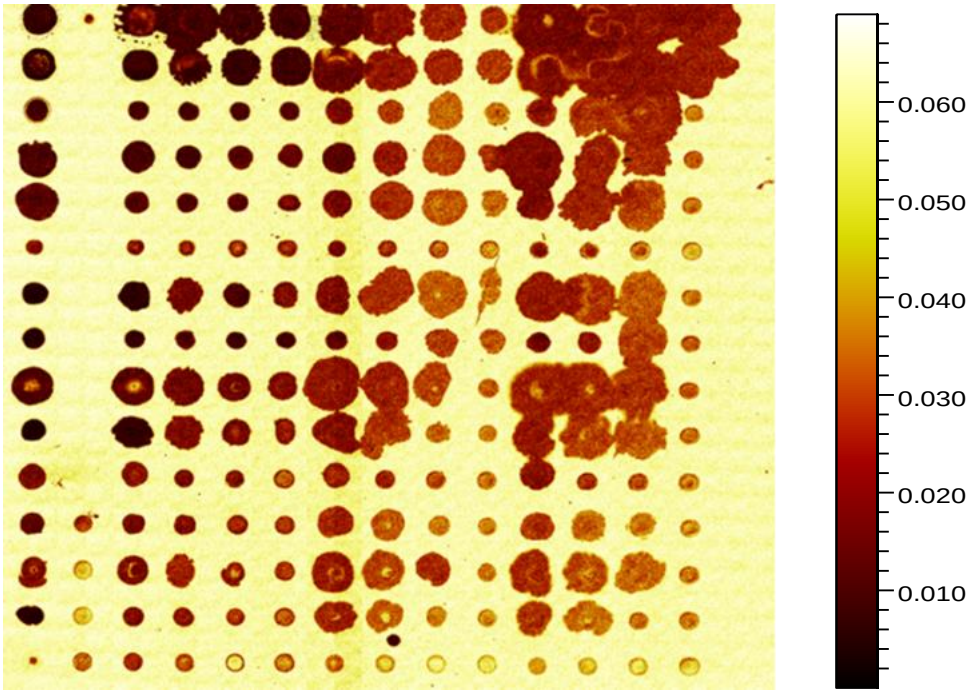


Figure 21: ToF-SIMS ion image based on an ion marker for pHEMA background to assess the extent of spreading (Image was constructed using pHEMA background ion marker, m/z = 45.02 –> $C_2H_5O^+$ and normalised by total counts (au)). (ToF-SIMS data accusation was carried out by Dr. David Scurr).

3.3.3 Measurement of the contact angle of DMF solutions on pHEMA surface

It was anticipated that the addition of solvent would decrease the solution contact angle, and thereby increase spreading, yet polymer spots became more defined upon monomer dilution. In order to understand the surface interaction properties of DMF, the contact angle of monomer-DMF mixtures were measured on pHEMA surface using CAM200 contact angle equipment as described in method section above. The results from this experiment helped to explain the effect of decreasing solute concentration on improved microarray printing. The contact angle experimental measurements (Figure 22 (a)) showed that as the

concentration of DMF was increased from 10% v/v to 50% v/v, the contact angle increased in a continuous manner from 11° to 19°.

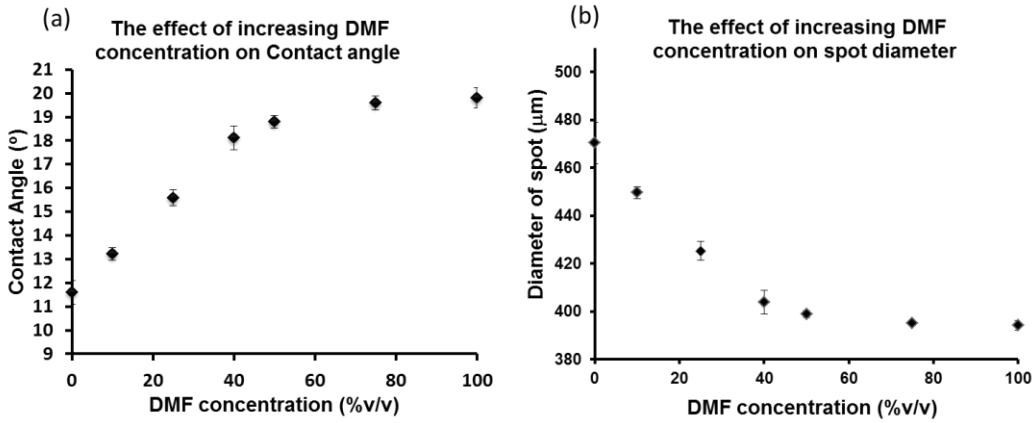


Figure 22: (a) Contact angle measured for monomer 11 (Cyclohexyl methacrylate) mixed with DMF on pHEMA surface at various concentrations (%v/v); **(b)** The effect of increasing DMF concentration from 0% v/v to 75% v/v on spot diameter (n=3 for both plots).

The effect of increasing DMF concentration on printed microarray spots was also analysed using an optical microscope. The diameter of the resultant microarray spots was measured and plotted as shown in Figure 22 (b), which shows that the spot diameter reduces linearly as the concentration of DMF is increased from 0% v/v to 75% v/v. It can be seen that 75% v/v DMF concentration produced a spot with a diameter of less than 400 μm, with a reduction of about 70 μm as compared to 0% v/v DMF (or 100% v/v monomer) solution. Hence, the effect of increasing DMF concentration to 75% v/v is very significant. This indicated that the surface tension of the DMF solvent was in fact greater than that of the monomers.

3.3.4 The effect of the thickness of pHEMA background coating on spot diameter and spreading

Besides 'low-fouling' properties, pHEMA background coating also acts as an anchoring material for microarray printing. The thickness of the pHEMA coating also plays a role in reducing the spreading of the printed monomer solution, before on-stage polymerisation. A simple experiment was conducted to observe the effect of the thickness of pHEMA coating on resultant spot diameter, by increasing the number of times a glass slide is dipped into pHEMA solution. A 5 μL droplet of DMF was placed on the surface of glass slides with a range of pHEMA thicknesses. The results showed an inverse relationship between pHEMA thickness and the diameter of the DMF droplet (Figure 23). Four times dip coated slide produced a spot diameter of 7.5 mm as compared to 20 mm on bare glass.

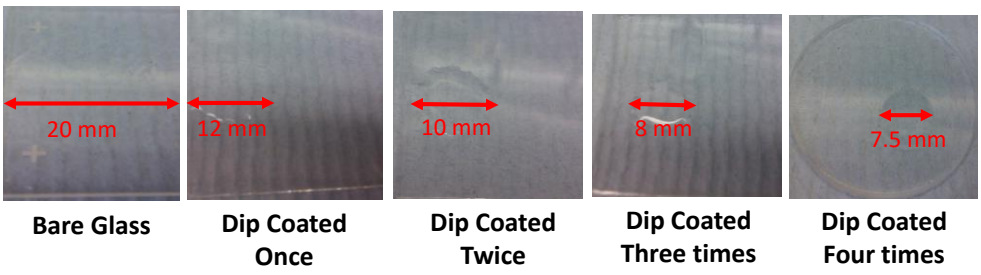


Figure 23: The effect of pHEMA coating thickness on solvent droplet spreading compared to bare glass. The slide was dip coated in pHEMA solution once, twice, three and four times and a 5 μL droplet of DMF was placed on each surface (The wave-like lines seen on some of the images were due to the paper towel present in the background, on which the slides were placed).

Hence, the optimised microarray printing was done using 25% v/v monomer solution mixed with 75% v/v DMF as a solvent and 1% w/v initiator. The glass slides were dip coated four

times in 6% w/v pHEMA solution to minimise the spreading. The newly printed microarray was also analysed using optical microscopy (Figure 24 (a)) and ToF-SIMS as a quality control method and ion map was constructed using an ion marker for pHEMA background as shown in Figure 24(b). From the optical microscopy images as well as ToF-SIMS ion map, it is evident that all the spots on the microarray are well defined and confined without merging. This ideal microarray allowed a confident spot to spot analysis of biological response (e.g. bacterial attachment or cell adherence) of each polymer material present on the microarray.

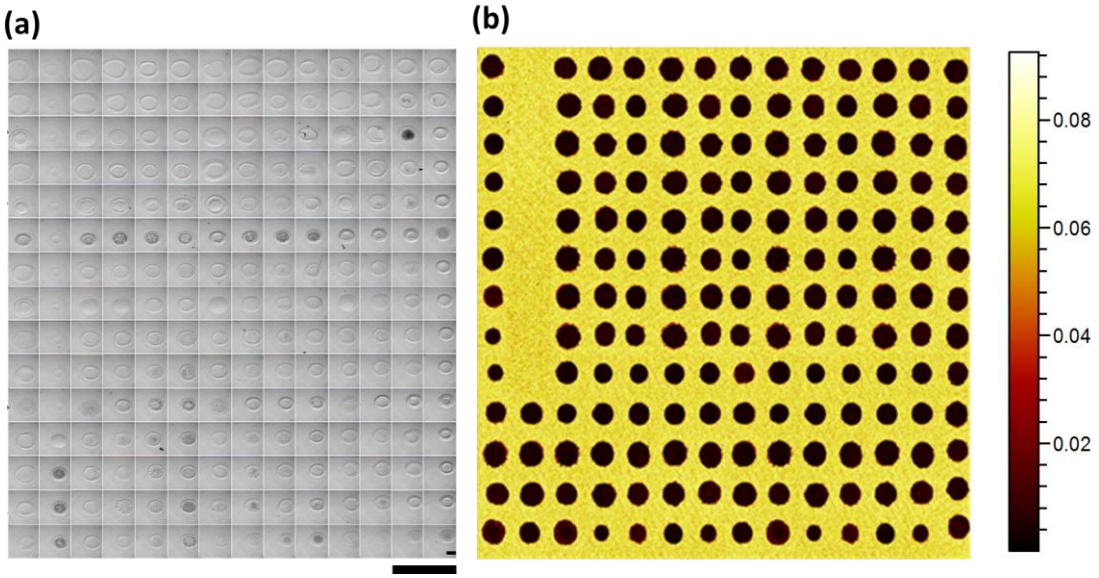


Figure 24: **(a)** Optical microscope images (stitched using Cell ProfilerTM software from individual images), average spot diameter is 400 μm, scale bar = 1 mm. **(b)** ToF-SIMS chemical image of polymer microarray built using pHEMA background ion marker, m/z = 45.02 –> $C_2H_5O^+$ and normalised by total counts (au on scale). The microarray was printed using optimised conditions (75% v/v DMF, smaller 3B pins and a uniform pHEMA background coating). (ToF-SIMS data accusation was carried out by Dr. David Scurr).

Following successful printing of the microarray at 75% v/v solvent concentration, the high spatial resolution ToF-SIMS images of the polymer spots were taken as shown in Figure

25. This was done to confirm a complete coverage of the surface of spots with the polymer material printed as well as the absence of background pHEMA on the surface of polymer spots. Due to time restaints and cost using ToF-SIMS, the high spatial resolution ToF-SIMS imaging was done for three spots randomly chosen on the microarray. ToF-SIMS chemical images showed a complete coverage of the surface of the printed area by the polymer material (appear as a bright colour spot (Figure 25 (a)) and the absence of pHEMA on the surface of printed spot (dark colour spot in Figure 25 (b)).

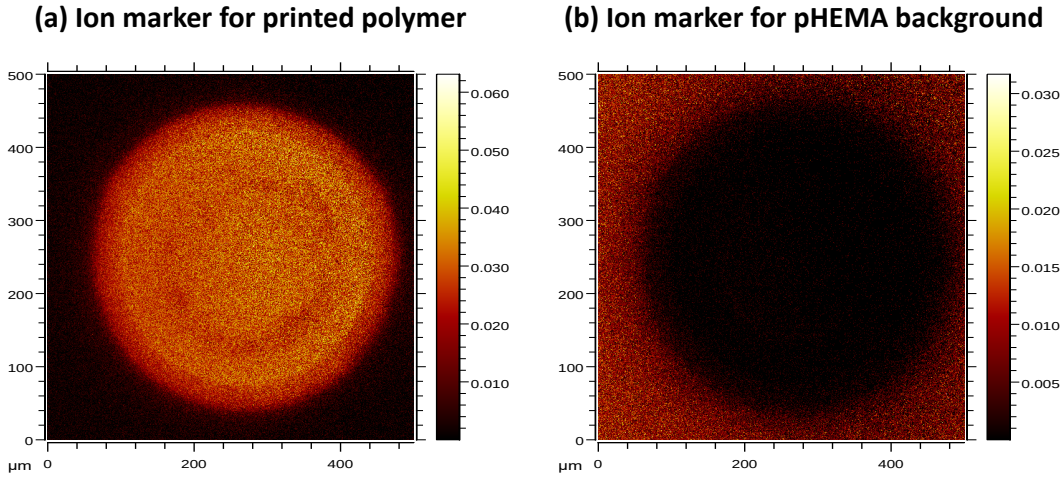


Figure 25: Zoomed in high-resolution ToF-SIMS image of the printed polymer spot based upon **(a)** an ion marker (m/z = 129.129, $C_8H_{17}O^-$) for a printed polymer material (monomer 8 or 2-ethylhexyl methacrylate) and **(b)** the pHEMA background (m/z = 45.023, $C_2H_5O^+$). (ToF-SIMS image normalised by total counts (au), data accusation was carried out by Dr. David Scurr).

3.3.5 Investigating the mixing of spots containing two monomers using ToF-SIMS

The final polymer microarray spots are made up of a combination of monomers mixed at three concentrations (25% v/v, 50% v/v and 75% v/v). The monomers were mixed in

384 well plate before printing and polymerisation on-slide. It was important to know if the final polymer spots had the same monomer composition on the surface of microarray as mixed in the well plate (bulk), since phase or surface segregation of monomers has previously been observed by Hook *et. al.* [117, 118]. ToF-SIMS was used to obtain a mass spectral image of each polymer spot on the microarray. Ion intensity maps (chemical images) were built for two monomers (monomer 8 and monomer B) mixed in a microarray format. Both chemical images shown in Figure 26 are from the same polymer microarray, but built using an ion marker for each monomer. The structure of each monomer is also shown in Figure 26 and related to the ToF-SIMS ion formed using a rectangular box. Monomer 8 produced an ion fragment at mass/charge (m/z) of 129.1292, which can be related to its structure as $C_8H_{17}O^-$ (deviation = 14 ppm) in negative ToF-SIMS spectrum. Similarly, monomer B produced an ion fragment at m/z of 75.0452 ($C_3H_7O_2^-$, deviation = 15 ppm), again coming from the offend of the pendant group of monomer B. Due to the difference in chemical structure of monomer 8 and monomer B, the ion fragments are unique to each monomer as represented in Figure 26. From the images, it can be seen that the ion intensity of monomer 8 increases as its concentration is increased from 25% v/v to 75% v/v. This increase in ion intensity of monomer 8 is also reflected by a decrease in ion intensity of monomer B as the concentration of monomer B is reduced from 75% v/v to 25% v/v (Figure 26).

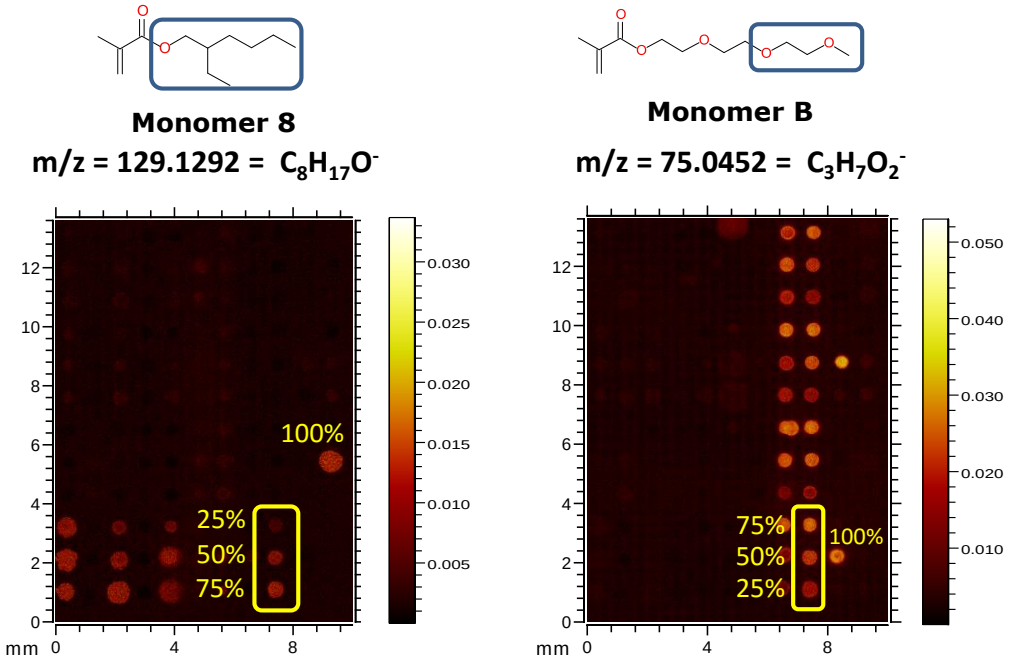


Figure 26: ToF-SIMS chemical images of the microarray built using a unique ion marker for each of two monomers (monomer 8 and monomer B). The polymer spots made up of a combination of two monomers at different %v/v concentrations are shown in yellow rectangular boxes (images were normalised to total counts (au)). (ToF-SIMS data accusation was carried out by Dr. David Scurr).

The microarray spots made up of monomer 8 and monomer B at three different %v/v compositions were further analysed by ToF-SIMS to obtain high spatial resolution images (512 pixels/mm) of these polymer spots as shown in Figure 27. These high resolution ToF-SIMS images were colour coded (Monomer 8 ion fragment images were coloured Green, monomer B ion fragment images were coloured Red) and overlaid (mixing of red + green = yellow) to observe the surface coverage of the monomers in the mixture. The purpose of this analysis was to observe whether the monomers were homogeneously mixed at the surface or phase separated. From Figure 27, it can be seen that both monomers were homogeneously mixed on the surface indicated by a yellow colour from the overlay of red and green colours. This was true for all the combinations of two monomers analysed.

Although at 25%/75% v/v and 75%/25% v/v ratios, the major monomer (75%) shows slightly higher presence due to a higher concentration compared to second monomer. The 50/50 mixture shows a clear yellow colour indicating a good mixing without a phase separation.

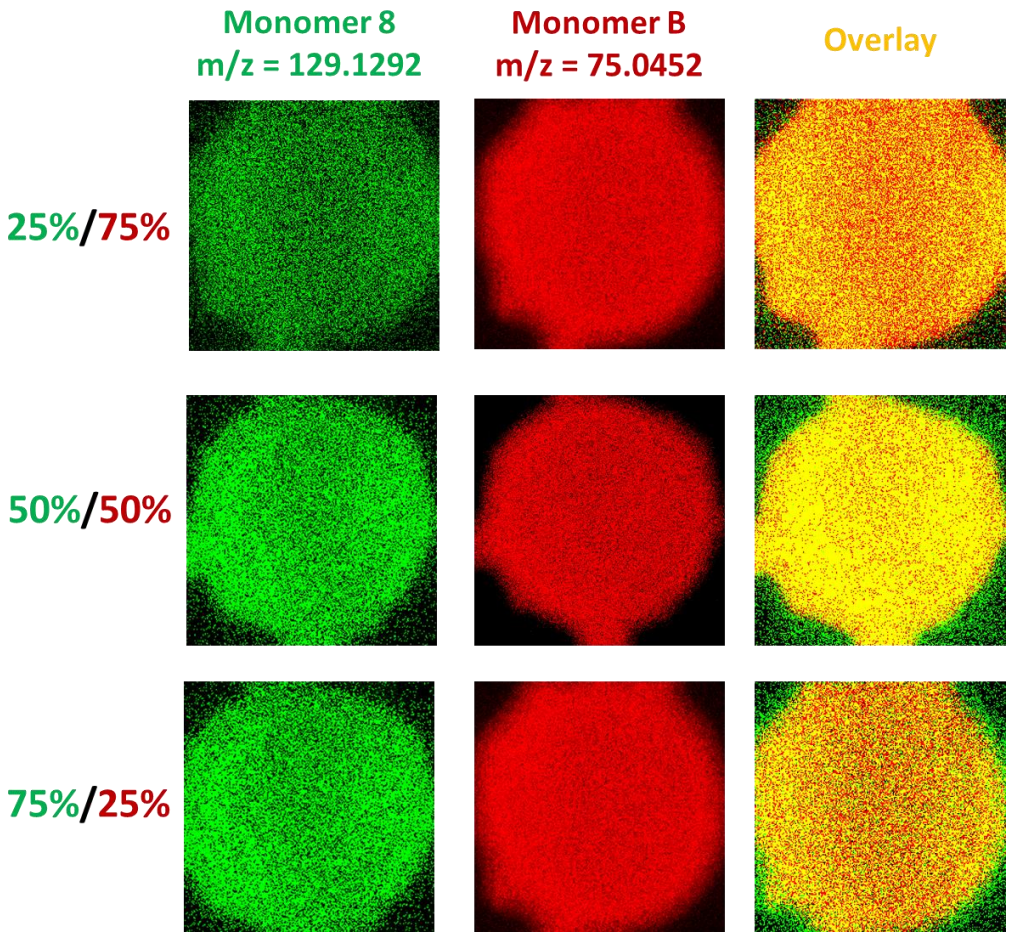


Figure 27: High spatial resolution ToF-SIMS images of the microarray polymer spots (400 µm diameter) made up from monomer 8 mixed with monomer B at three different concentrations (%v/v). The images show the surface distribution of monomer 8 (Green) and monomer B (Red) and the overlay images (yellow) of the two ions. (ToF-SIMS data accusation was carried out by Dr. David Scurr).

The intensity of the ion fragments representing monomer 8 ($C_8H_{17}O^-$) and monomer B ($C_3H_7O_2^-$) were obtained from the ToF-SIMS spectrum of each polymer spot and was normalised by total counts. The ion intensity of monomer 8 and monomer

B at three %v/v compositions is plotted as shown in Figure 28, which shows a good linear relationship between %v/v concentration of the monomers and their ion intensity. Hence, the monomers showed homogeneous mixing at the surface of the spots printed in a microarray format with no phase separation observed at the lateral resolution achieved in the images. A ring corona can be seen around the spot as the concentration of monomer 8 was increased from 25% to 75% v/v, which indicates phase separation on the edge of the spot.

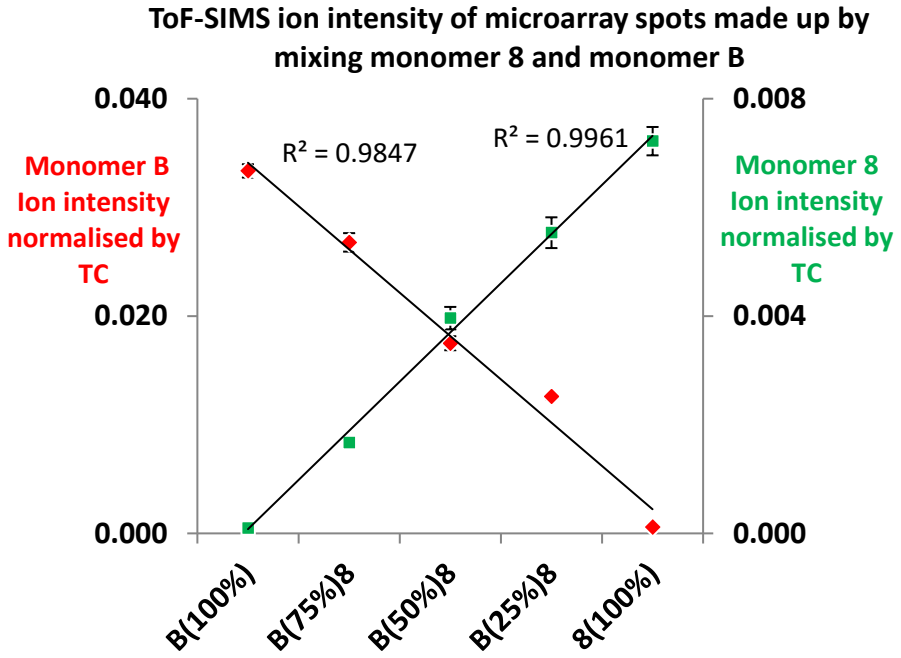


Figure 28: ToF-SIMS ion intensity of the UV-cured surface of polymer spots made up of various combinations of the two monomers $C_3H_7O_2^-$ (monomer B) and $C_8H_{17}O^-$ (monomer 8) printed in a microarray format (n = 3, on three separate blocks). (ToF-SIMS data accusation was carried out by Dr. David Scurr).

3.4 Discussion

A well-defined polymer microarray is the key to carry out meaningful high throughput biological assays. The printing conditions such as solvent concentration, size of pins and uniform background coating were optimised to produce spatially defined polymer spots. The optimised polymer microarray was printed using 25% v/v monomer and 75% v/v solvent (DMF) together with 1% w/v photoinitiator. The background pHEMA coating was also optimised for uniformity by using an automated dip coater to achieve reproducible film thickness compared to manual dip coating.

3.4.1 The effect of increasing solvent (DMF) concentration on microarray printing

Increasing the solvent concentration had the most positive impact on producing defined microarray spots. By increasing the concentration of the solvent, drop to drop spreading of printed monomers (hence, the polymerised spots) was reduced. This concentration effect was investigated by measuring the contact angle of monomer solution in solvent on pHEMA surface. The ability of DMF to increase the contact angle of monomer solution explains the good printing quality of a microarray. By holding the spots in place, microarray printed at 50% v/v DMF concentration produced well-positioned distinct spots and minimised the spreading of the monomer spots before the UV initiated on-slide polymerisation. Furthermore, using 75% v/v DMF and 25% v/v monomer solution lead to a slight increase in contact angle

compared to 50% v/v DMF. The beneficial effect of increasing the solvent (DMF) concentration can be explained on the basis of the surface tension of liquids. The surface tension of a liquid droplet determines the spreading of a droplet on a surface. A liquid with a high surface tension value would produce a well-defined droplet on the surface without spreading and wetting the surface. The surface tension of DMF is 37.10 mN/m and the surface tension of the monomer used in this experiment in Figure 22 (monomer 11 - Cyclohexyl methacrylate) is 30.5 mN/m [119-122]. As a result the addition of more solvent (reduction of monomer content of the solution) lead to an overall increase in the surface tension of the printed droplet and hence, an increase in the contact angle and reduced spreading. Furthermore the surface tension values of other monomers used in this project are: monomer 8 – 28.8 mN/m, monomer 9 – 29.2 mN/m, monomer 5 – 35 mN/m, monomer 14 – 29.8 mN/m, monomer 12 – 30.0 mN/m, monomer 4 – 32.4 mN/m, monomer 2 – 33.0 mN/m, monomer 7 – 30.4 mN/m [121]. All these surface tension values are less than the surface tension of DMF.

3.4.2 The effect of uniformity and thickness of pHEMA background coating

Apart from changing the solvent concentration, the uniformity of pHEMA coating was also investigated. Besides 'low-fouling' properties, pHEMA background coating also acts as an anchoring material for microarray printing [75, 123]. The thickness and uniformity of the pHEMA coating also plays a role in reducing the spreading of the printed monomer solution, before on-stage polymerisation. Using an automated

dip coater allowed a consistent pHEMA background coating that can be reproduced to avoid batch to batch variability. The simple experiment with DMF on pHEMA surfaces of varying thickness confirmed that the spreading of the monomer-DMF drop is dependent on the pHEMA thickness. A thinner coating provides less anchoring support for the droplet as compared to a thicker pHEMA coating (Figure 23).

3.4.3 ToF-SIMS analysis of the composition of printed polymer spots

Although ToF-SIMS is generally regarded as not readily quantitative, in some instances ToF-SIMS has been found to be quantitative [124, 125]. Furthermore, Weng *et. al.* [124] found that the influence of the matrix effect was less significant in negative mode as compared to positive mode of SIMS. For the experiments in this study, two monomers (monomer 8 and monomer B) were mixed at various concentrations (%v/v) before printing and on slide photo polymerisation and no surface segregation was observed from ToF-SIMS ion intensity maps (Figure 27).

A corona of monomer 8 ion intensity was observed around the spots (Figure 27) as the concentration of monomer 8 was increased from 25% to 75%. This effect may be due to the chemical properties of two monomers. Monomer 8 has a hydrocarbon chain, making it more hydrophobic (logP =4.88) than monomer B with glycol chains (logP = 1.102). As the mixture of two monomers were spotted on hydrophilic pHEMA surface, more hydrophilic monomer B may have diffused into the pHEMA, similar to partitioning of a substance between two

liquids, leaving hydrophobic monomer 8 around the edges of the spot appear as corona of monomer 8 in ToF-SIMS images. This effect is visible around the edges due to the dome shape of the spots. This effect has not previously been noted in micro array studies, where high resolution SIMS has not generally been undertaken. An example of this effect can be seen as the differential stem cell attachment on the edge of microarray spots as observed by Celiz et. al. [126]. This effect could may be due to ring corona effect as shown by high resolution SIMS imaging.

The relative ion intensity of each monomer on the surface was measured to understand if the ion intensity follows the same trend as the bulk composition of two monomers. The purpose of this investigation was to use ToF-SIMS as a semi-quantitative technique to understand the trend by which the ion intensity of each monomer varies at different concentrations rather than an absolute quantification of the amount of monomer present. The ion intensity of each monomer reflects their composition in 384 well plate before printing. Therefore, the biological performance of each polymer spot made up from the combination of two monomers can be accurately linked to concentration (%v/v) of each monomer. Due to a linear relationship between monomer concentration and ToF-SIMS ion intensity of the monomer, ToF-SIMS may be quantitative in this instance, which using these graphs as calibration curves would allow the surface composition to be determined.

3.5 Conclusions

- ToF-SIMS was successfully used to optimise polymer microarray printing by chemical mapping of the surface.
- The initial problem of spreading and merging of microarray spots was solved by decreasing the solute concentration from 75% v/v to 25% v/v, using smaller printing pins and having a uniform pHEMA background coating to produce an array without spot spreading.
- The surface homogeneity of the monomer mixture was confirmed using ToF-SIMS chemical mapping as well as using ion intensity plot of key ion peaks representing two monomers in a mixture.
- ToF-SIMS results showed a homogeneous mixing of the monomers on the surface of the microarray reflecting the bulk composition of the materials in the well plate before printing (e.g. 25% v/v to 75% v/v).

4 Chapter 4 – Haemocompatibility assays on polymer microarrays

4.1 Introduction

A bacterial resistant coating on blood-contacting medical devices needs to be haemocompatible. International Organization for Standardisation (ISO) standards on haemocompatibility cover thrombosis, coagulation, blood platelets, haematology and immunology [127, 128]. The experimental results presented in this Chapter assess the haemocompatibility of polymer materials presented on a microarray. This Chapter looks at protein adsorption on the surface of each polymer spot following whole blood incubation. Protein adsorption (e.g. fibrinogen) on blood-contacting medical devices plays a key role in blood clotting as well as bacterial attachment [26, 35, 36]. An ideal coating material should show a good resistance to protein adsorption as well as bacterial attachment. Otherwise, the polymer coating would be rapidly covered by blood proteins soon after the device gets in contact with blood [97, 129]. As a result, the bacteria could adhere to the adsorbed proteins negating the bacterial resistant properties of the material. Platelet attachment and clotting of red blood cells were also studied to find haemocompatible, non-thrombogenic polymer materials.

This study also investigated the attachment of the immune components of blood such as leukocytes (an important part of immune system), Immunoglobulin G (IgG) (most abundant immunoglobulin, plays key role in immune system activation)

and complement C3b (key component of innate immune system) on each polymer spot of the microarray. The complement system plays a key role in both innate and adaptive immune system to mediate inflammation, cell lysis and opsonisation (label foreign surfaces for leukocytes to attack) as shown in Figure 29. The alternative pathway of the complement system is activated by foreign surfaces such as pathogens or in our case, the surface of medical devices. The C3b component of alternative pathway was used to estimate the activation of complement system by a foreign surface. The classical pathway is responsible for antibody mediated complement system activation.

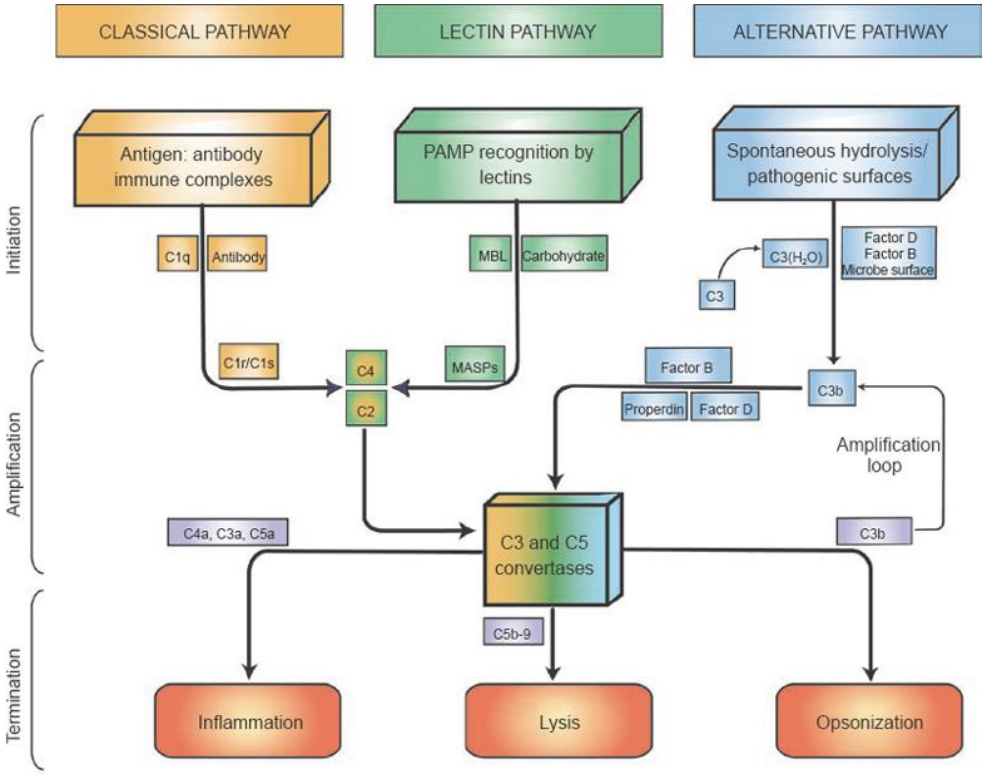


Figure 29: The complex complement pathway system showing Classical, Lectin and Alternative pathways. Alternative pathway is linked to foreign surfaces (e.g. medical devices) mediated activation. (Figure from [130]).

4.1.1 Aim and objectives

The aim of the experiments was to determine haemocompatibility of each material composition present on a microarray. The objectives of the experiments were as follows:

1. Quantify the amount of protein adsorbed on the surface of each material using XPS analysis.
2. Screen a library of materials for protein adsorption on the surface of each polymer material using fluorescence assays.
3. Investigate the platelet attachment on each polymer material.
4. Investigate immunogenicity of each material using markers for leukocytes, IgG and complement C3b components.

4.2 Experimental

Polymer microarrays were used to screen protein adsorption, blood cell attachment and immune system activation by carrying out assays using human whole blood. The microarrays were printed on 25 mm diameter pHEMA coated circular glass slides as shown in Figure 30 for the quasi-static incubation chamber as shown in Figure 31.

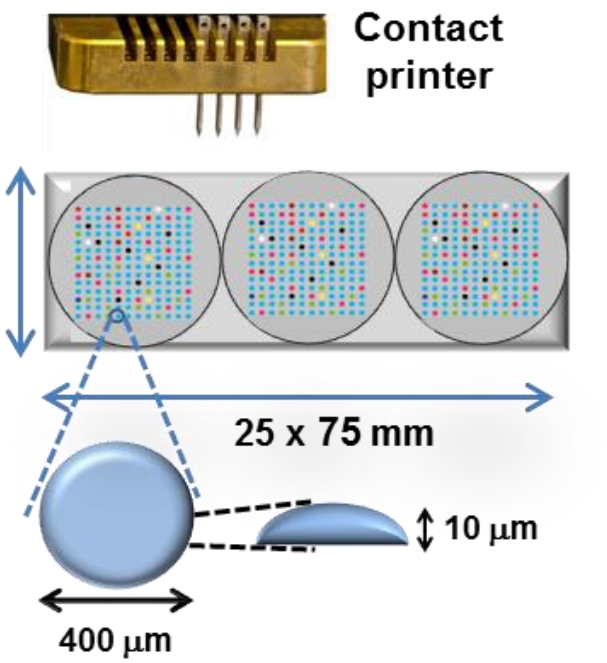


Figure 30: Polymer microarray printing on 25 mm circular slides fixed on standard glass slide. Circular slides were used in quasi-static blood incubation chamber in Figure 31.

The microarray incubation step was carried out using the quasi-static incubation chamber as shown in Figure 31.

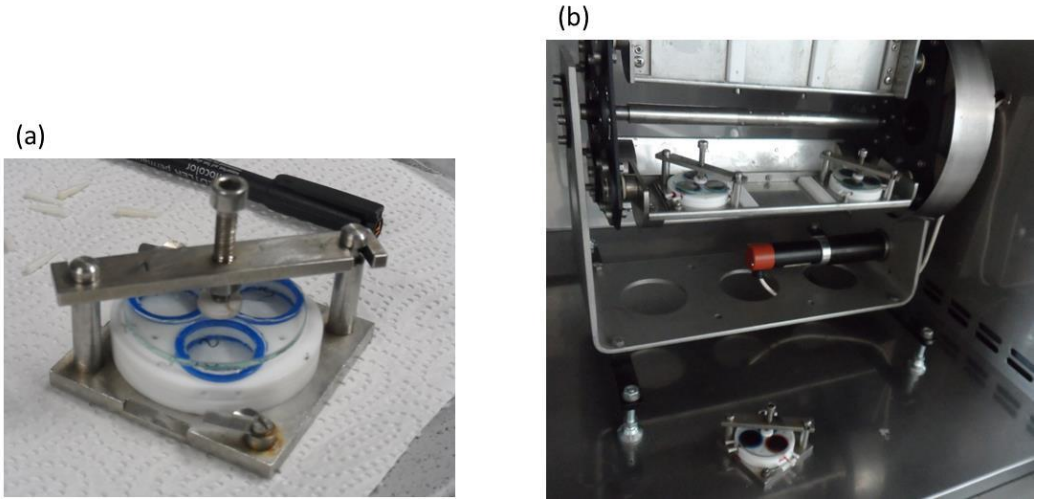


Figure 31: Quasi-static blood incubation chamber experimental setup, **(a)** Blood incubation chamber consisting of three slots for circular microarray repeats, **(b)** Horizontally rotating stage mounted with multiple incubation chambers at 37 ^{o}C.

4.2.1 Whole blood incubation assay

The microarrays were assembled as the top and bottom of autoclaved incubation chambers made up of Polytetrafluoroethylene (PTFE), with the printed side facing inwards (Figure 31(a)). Each incubation chamber holds 1.95 mL blood volume, producing a surface to volume ratio of 3.2 cm^{-1} [131]. The incubation chambers were filled with 0.9% NaCl solution and allowed to equilibrate at 37 ^{o}C prior to whole blood exposure. The NaCl solution was removed from the chamber after 30 minutes, before introduction of blood into the chamber.

Venous blood was obtained from healthy volunteers with no known medical conditions and who have not taken any medication 10 days prior to blood donation. A 19 G cannula was used to obtain venous blood. Blood was then anticoagulated with 2 IU/mL heparin and immediately used to

fill incubation chambers (pre-warmed at 37 ^{o}C), avoiding air bubbles in the chambers. The incubation chambers were then placed on a rotating stage (Figure 31 (b)) at 37 ^{o}C for two hours to prevent sedimentation of blood cells. Following the incubation, the blood was drained off from the incubation holder, the slides were carefully removed and washed twice with PBS and once with deionized water. The slides were then processed separately to detect leukocytes, platelets, fibrinogen, IgG and C3b.

4.2.2 Leukocyte detection

The microarray slides were incubated in 2% w/v Paraformaldehyde (PFA) in PBS for 1 hour to fix the leukocytes. The slides were washed in PBS to wash off PFA. The leukocytes were labelled with DNA-staining dye Sytox Green (1 μM) with 0.05% w/v Saponin (30-60 minutes). The slides were washed with PBS and were stored under PBS until analysis. The fluorescence measurements were taken using a fluorescence scanner (Fujifilm FLA-5100) at Excitation/Emission: 504/523 nm.

4.2.3 Platelet detection

The microarray slides were incubated in 2% w/v PFA in PBS for one hour for platelet fixation. The slides were washed in PBS to wash off excess PFA. The slides were then incubated for 30 minutes in blocking buffer (2% w/v dry milk powder, 0.05% w/v Tween-20 in PBS). Mouse anti-human CD41a FITC (Fluorescein isothiocyanate) (FACS-antibody, Becton

Dickinson) 1:10 in blocking buffer was used for platelet detection. The fluorescence was measured using Fujifilm FLA-5100 fluorescence scanner using Excitation/Emission: 495/519 nm.

4.2.4 Fibrinogen and IgG detection

Following the washing steps, the slides were incubated in blocking buffer (2% w/v dry milk powder (casein), 0.05% w/v Tween-20 in PBS) for 30 minutes. Rabbit anti-human fibrinogen (FITC) (Cedarlane) 1:30 in blocking buffer was used to detect fibrinogen by incubating for 1 hour. Similarly goat anti-human IgG (Rhodamin Red X) (Jackson Immuno) 1:50 in blocking buffer was used to detect IgG. Again, the fluorescence was measured using Fujifilm FLA-5100 fluorescence scanner at Excitation/Emission: 495/519 nm.

4.2.5 Complement C3b detection

The slides were incubated in blocking buffer (2% w/v dry milk powder, 0.05% w/v Tween-20 in PBS) for 30 minutes. Rabbit (rb) anti-human C3b 1:500 (primary antibody) and anti-rb IgG (Alexa 488) 1:200 (secondary antibody) were used to detect C3b by using Fujifilm FLA-5100 fluorescence scanner using Excitation/Emission: 496/519 nm.

4.3 Results

4.3.1 XPS analysis to determine protein adsorption on polymer microarray from human blood

XPS was used to measure the concentration of nitrogen on each spot on a polymer microarray using the intensity of the N1s core level. [N] (at%) can be used as a marker for proteins on polymer microarray spots. As none of the monomers used in this project contains any nitrogen in their structure (Figure 5), therefore any nitrogen detected by XPS indicates protein adsorption from whole blood. Hence, the amount of protein adsorbed can be quantified on each polymer spot. Furthermore, the [N] (at%) can be converted into protein overlayer thickness using Equation 4 described by Ray and Shard [132]. The relationship in Equation 4 assumes an estimated atomic fraction of 15% in the pure protein and the protein thickness is the thickness of a dry protein overlayer on a surface.

$$d_{\mathrm{N(1s)}} = -L_{\mathrm{N(1s)}} \cos\theta \ln\left(1 - \frac{[\mathrm{N}] - [\mathrm{N}]_0}{[\mathrm{N}]_\infty - [\mathrm{N}]_0}\right) \quad \text{(Equation 4)}$$

Where $d_{N(1s)}$ is protein thickness, L is electron attenuation length (3.02nm), $\cos(\theta=0^o) = 1$, [N] is measured nitrogen fraction, $[N]_\infty$ is atomic fraction of nitrogen in the pure protein (15%) and $[N]_0$ is nitrogen fraction on substrate (0%). Each rectangular block in Figure 32 represents a particular combination of two monomers, for example label A(25%)

represents a polymer spot made up of 25% v/v of monomer A and 75% of other monomer (1 to 16). The heat scale makes a clear distinction between low and high protein adsorption. A blue colour on the heat map represents a low protein adsorption and a red colour represents a high protein adsorption. Protein overlayer thickness results showed a higher protein adsorption on homopolymers of monomers 1 to 16. The addition of monomers B and C at various %v/v concentrations caused a reduction in protein overlayer thickness as compared to zwitterionic materials E, F and G. In contrast, the addition of monomer D (CH_3 terminated long chain glycol) did not show similar protein resistance to monomer C (OH terminated long chain glycol). As the average size of human serum albumin in solution is 3 nm [133, 134], the results in Figure 32 indicate a monolayer to sub-monolayers of proteins adsorbed polymer microarray spots. For example protein overlayer thickness of 1.5 nm would be equivalent to 50% surface coverage of 3 nm protein.

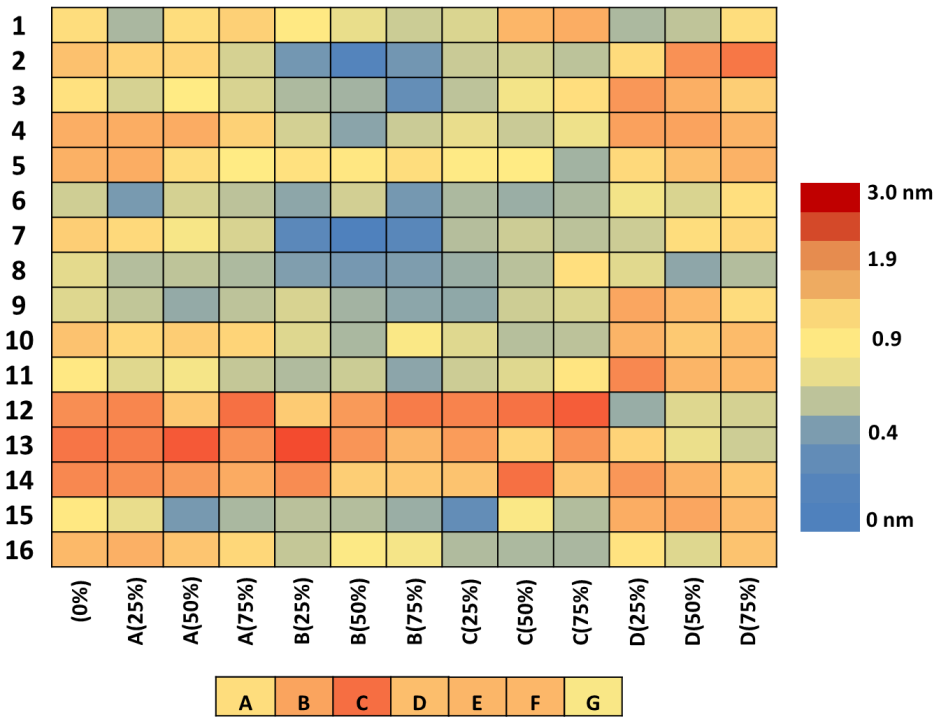


Figure 32: Protein overlayer thickness (nm) after two hour incubation in human whole blood, estimated from [N] (at%) measured using XPS. Blocks A to G represents homopolymers of A to G.

The relationship between protein adsorption on a surface and the respective wettability of that surface was also investigated. Water contact angle was measured on the surface of each spot on the polymer microarray. There was no correlation observed between protein overlayer thickness (amount of protein adsorbed) and the wettability of the surface as shown in Figure 33, indicating that the protein adsorption is not directly linked to the hydrophilicity/ hydrophobicity of a surface.

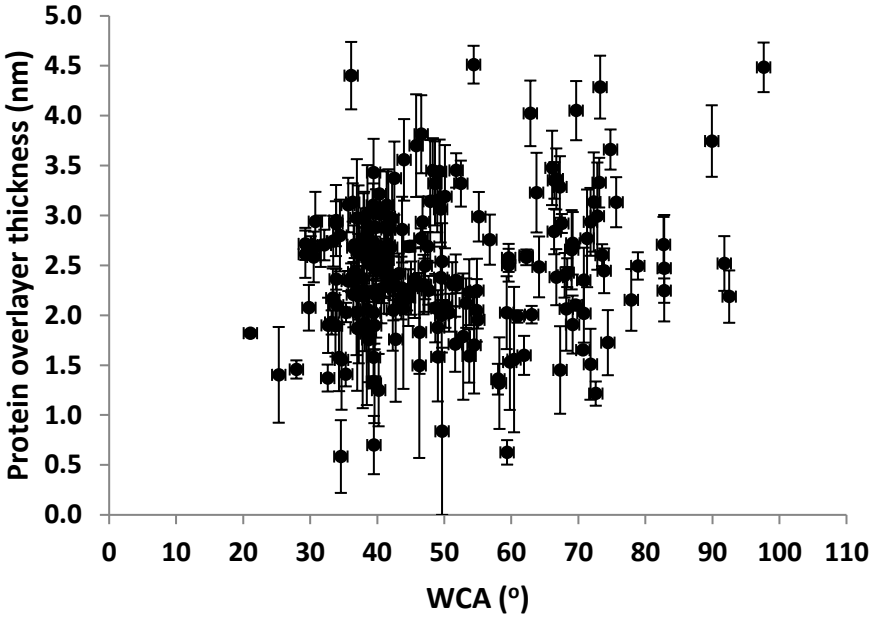


Figure 33: Relationship between protein adsorption and surface wettability (water contact angle). Protein overlayer thickness (nm) was calculated from XPS N1s at% on microarrays following incubation in human whole blood for two hours at 37 °C (n=3).

4.3.2 Fibrinogen adsorption assay

Fibrinogen is a key protein associated with blood clotting [37]. Polymers printed in a microarray format were assessed for fibrinogen adsorption using rabbit anti-human fibrinogen (FITC) labelled antibodies following whole blood incubation for two hours. The fluorescence intensity (au) measured from each spot is represented in a heat map format to provide an overview from the array in Figure 34 (a). From the results, it can be seen that material 1 to 8, 13, 14 and 16 showed a good resistance to fibrinogen adsorption as homopolymers as well as when mixed with monomer A. The zwitterionic materials E to G showed a moderate resistance to fibrinogen adsorption. In contrast, co-polymer of these materials with monomers C and D showed an increased surface fibrinogen adsorption, as shown in Figure 34 (a). These results suggest

that co-polymer of monomers 1 to 16 with smaller chain glycol monomers (A and B) are beneficial to reduce surface fibrinogen adsorption as compared to longer chain glycols (monomers C and D).

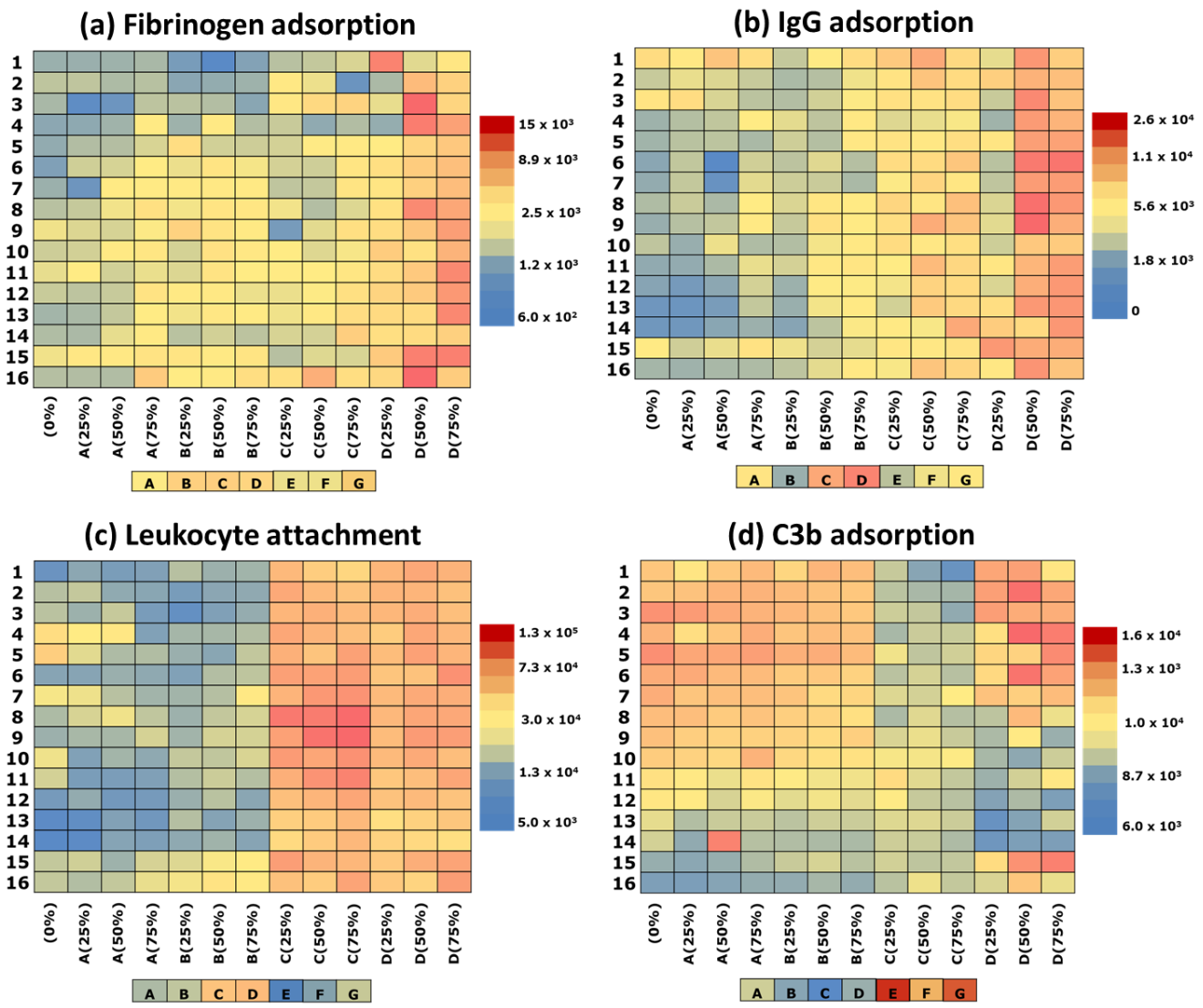


Figure 34: Heat map representation of fluorescence intensity (au) from antibody based assays to detect **(a)** Fibrinogen adsorption, **(b)** IgG adsorption, **(c)** Leukocyte attachment and **(d)** Complement C3b adsorption on polymer microarray following whole blood incubation for two hours at 37 °C. Red colour represents high fluorescence intensity (higher adsorption) (au) and blue colour represents low fluorescence intensity. Blocks A to G represent homopolymers of materials A to G.

4.3.3 Immunoglobulin G (IgG) adsorption on microarray

Immune system activation is a key consideration when screening for haemocompatible materials. IgG is the most abundant immunoglobulin in the blood and plays a key role in immune system activation [135]. Following the blood incubation step, the microarray was also screened for surface IgG adsorption using goat anti-human IgG (Rhodamin Red X) antibodies. It should be noted that a blocking buffer (2% w/v dry milk powder (casein) was used to prevent non-specific IgG adsorption on the polymer microarray. The blocking was confirmed by using a blank control (without blood incubation step) polymer microarray in each experiment. The fluorescence intensity (au) on the surface of each polymer spot was measured and represented in a heat map format as shown in Figure 34 (b). The results show a clear division between IgG adsorption on monomer 1 to 16 co-polymerised with monomer A and B (short chain glycols) and combination of 1 to 16 with C and D (longer chain glycol monomers). Monomer 1 and 15 showed a higher IgG adsorption as compared to rest of the materials when co-polymerised with monomers A to D at various %v/v concentrations. The homopolymers of B and E showed a good resistance to IgG adsorption as compared to homopolymers of A, F and G. Homopolymer D showed high IgG adsorption as was the case with co-polymers of monomers 1 to 16 with monomer D (D(50%) and D(75%) columns in Figure 34 (b)).

4.3.4 Leukocyte attachment assay

Leukocytes are vital part of the immune system and together with immunoglobulins, play a key role in fighting infection, inflammation and foreign-body reaction on implantable medical devices [136]. Therefore, the attachment of leukocytes on polymer microarray was also investigated using a DNA stain. The fluorescence intensity (au) from each spot was measured and is shown in Figure 34 (c). Similar to IgG results, the separation between monomers A & B and C & D is prominent. The addition of monomer A and B into monomers 1 and 16 shows lower leukocyte attachment as compared to monomers C and D. The addition of monomer B into monomer 4 led to a significant reduction in leukocyte attachment. Similar trends are shown by homopolymers of A and B showing low leukocyte attachment as compared to homopolymer C and D. Homopolymers of zwitterionic materials E and F showed a lower leukocyte attachment as compared to homopolymer G.

4.3.5 Complement C3b adsorption assay

Complement C3b adsorption on each polymer spot on microarray was measured and represented in a heat map format as shown in Figure 34 (d). Monomer C co-polymerised with monomers 1 to 12 at various %v/v concentrations showed lower C3b adsorption as compared to monomers A, B and D. In contrast monomers 13 and 14 showed a lower C3b adsorption regardless of co-polymerisation with other monomers (A to D), apart from an outlier 14+A(50%). The

zwitterionic materials E, F and G showed a considerably higher C3b adsorption as compared to all other material compositions. Homopolymer F showed similar C3b adsorption to most of the polymer material compositions printed on microarray.

4.3.6 Platelet attachment assay

Platelet aggregation is a key step in thrombosis (blood clot) formation. Following two hour incubation in human whole blood, no blood clotting was observed on any of the spots on the microarray. The platelet attachment on the microarray was compared against polytetrafluoroethylene (PTFE) or Teflon coated slide (as a control) as shown in Figure 35. Mouse anti-human CD41a FITC fluorescence measured from two samples shows a minimal platelet attachment on microarray as compared to PTFE control. Therefore, most of the materials printed on the microarray showed a very good resistant to platelet attachment relative to PTFE and hence, thrombosis formation as shown in Figure 35. In particular monomers 10 to 14 when mixed with monomer D, showed lower platelet attachment than other polymers compositions.

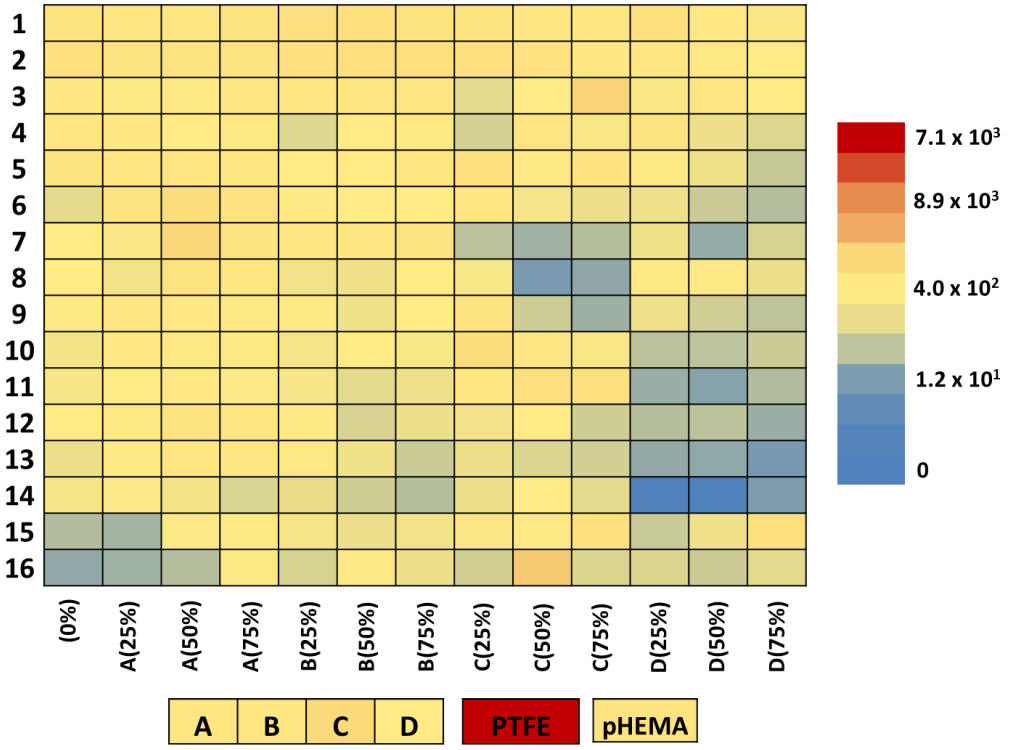


Figure 35: Platelet adsorption on polymer microarray spots following two hour incubation in human whole blood at 37 °C. A low attachment (comparable to pHEMA surface) was observed on most of the polymer spots as compared to PTFE control surface. Some polymer composition (10 to 14), when mixed with monomer D showed lowest surface platelet attachment.

4.4 Discussion

4.4.1 Protein adsorption from whole blood

Blood is a complex mixture of a range of molecules and cells with a variety of features and functions. The main components of blood plasma are proteins and there are around 300 types of proteins present in the blood [137]. The proteins are present at a range of concentrations for example 35-50 mg/mL for serum albumin (most abundant plasma protein) to only 0-5 pg/mL for interleukin 6 [138]. It is, therefore, not surprising that protein adsorption is the first key event in a sequence of events that occur on the surface of blood-contacting medical devices upon contact with blood [139-141]. The surface of device rapidly gets covered with the smaller and most mobile blood plasma proteins such as albumin, fibrinogen, fibronectin etc. in a matter of seconds [38, 39]. On longer timescales it is known that the Vroman effect [40, 41], whereby larger proteins with stronger binding affinity can displace smaller and less strongly adsorbed proteins from the surface, plays an important role as well [42, 43].

4.4.1.1 XPS protein overlayer thickness

In this Thesis, XPS has been used to quantify the amount of protein adsorbed from whole blood on a range of polymer surfaces in a high throughput manner. The protein overlayer thickness calculated [132] based on nitrogen atomic concentration measured, post protein exposure and rinsing, ranged from sub-monolayers to monolayers of proteins (3

nm). These adsorbed protein thickness values are consistent with a protein layer with a thickness of 2-10 nm on self-assembled alkanethiolate monolayers (SAMs) of organic surfaces on gold, measured using ellipsometric and infrared spectroscopic techniques [142]. However, the dehydrated nature of the XPS measurement (due to vacuum) may mean slightly thinner layer estimation than other ambient analytical techniques and almost certainly a reduction compared to the hydrated in situ state.

A number of array polymer compositions showed a very low amount of proteins adsorbed (Figure 32). As the XPS measurements were carried out after rinsing the microarrays with PBS and water to remove weakly adsorbed proteins and salts from the surface, this is likely only to retain the strongly adsorbed proteins [143]. The XPS protein overlayer thickness results reinforce the protein resistant properties of ethylene glycols, poly(ethylene glycol) or PEG has been widely studied for its protein resistant low-fouling properties [144-148]. An increase in ethylene glycol chain length showed a reduction in protein adsorption as evident from monomer B (tri (ethylene glycol) methyl ether methacrylate) and C (poly(ethylene glycol) methacrylate) series. In particular, the presence of monomer B produced a number of material compositions with a very low protein adsorption. In contrast, monomer D (methyl terminated long chain glycol) when mixed with monomers 1 to 16 failed to produce similar level of protein resistance as monomer C. The homopolymers of monomers 1 to 16 as well as materials A to G showed moderately higher protein adsorption when compared to combinations of these monomers. This suggests that the reduction in protein adsorption is due to combined surface chemistry of two

monomers when copolymerised together rather than from a single monomer alone.

The link between protein adsorption on a surface and its respective wettability was also studied using water contact angle. Unlike some studies in the literature suggesting a link between hydrophobicity of a surface and increased protein adsorption [149, 150], there was no correlation between protein adsorption and hydrophilicity or hydrophobicity of the wide library of materials investigated in this study (Figure 33). This may be due to a diverse library of materials with a range of physiochemical properties used in this thesis as compared to polyurethane and poly(propylene glycol) materials used in some studies in literature that looked at the hydration and dehydration of the polymers [149]

4.4.1.2 Fibrinogen adsorption assay

XPS protein overlayer thickness provided a quantitative measurement of the amount of protein adsorbed from whole blood on each polymer spot on the microarray. However, XPS is unable to differentiate between the amounts of different type of proteins, for example fibrinogen, albumin etc., adsorbed from whole blood. Fibrinogen has been shown to play a key role in platelet adhesion and blood coagulation [151], whereas other proteins such as fibronectin, von Willebrand factor and immunoglobulins play a supporting role in platelet activation and coagulation [152, 153]. Unlike the total protein overlayer thickness from XPS, most homopolymers of materials 1 to 16 showed a low fibrinogen adsorption as determined using antibody based assays in

Figure 34 (a). The addition of ethylene glycol monomers showed a higher fibrinogen adsorption when compared to homopolymers of 1 to 16. This was opposite to the effect of total protein adsorption shown by XPS, where the addition of glycol monomers reduced total protein adsorption. The protein adsorption is a competitive process [154] and an increase in total protein adsorption may have caused a lower fibrinogen adsorption as fibrinogen may be displaced by other proteins from whole blood.

Furthermore, the conformation of adsorbed proteins also play a key role in their biological activity. For example Sivaraman and Latour [155] showed that the conformation rather than the amount of adsorbed fibrinogen is important in platelet adhesion. A number of material compositions showed a lower fibrinogen adsorption than zwitterionic materials (Monomers E, F and G). A surface with lower overall protein adsorption as well as a lower fibrinogen adsorption is desirable as a coating on blood-contacting medical devices.

4.4.2 Estimating the immune system response to materials

The interactions of a material with different parts of the immune system are important considerations in the design phase of any medical device. It is particularly important for blood-contacting medical devices due to the risk of a systemic immune response. Immunoglobulins or antibodies play a key role in adaptive immune response and together with the complement system, identifies and presents foreign materials (opsonisation) in contact with blood to the immune system

[156, 157]. A lower IgG adsorption was observed on polymer spots made up of monomers 1 to 16 mixed with short chain glycols (monomers A - di(ethylene glycol) methyl ether methacrylate and monomer B - tri(ethylene glycol) methyl ether methacrylate) as compared to long chain glycol monomers (monomer C - poly(ethylene glycol) methacrylate and monomer D - poly(ethylene glycol) methyl ether methacrylate). Similar but more prominent separation between shorter chain and longer chain glycol monomers were observed in case of surface leukocyte attachment. These results show a link between IgG adsorption and leukocyte attachment. Increased opsonisation of foreign surfaces by IgG leads to increased leukocyte attachment [158]. In contrast a lower complement C3b adsorption shown by surfaces with monomers C showed a higher leukocyte attachment.

C3b adsorption and complement activation is complex process and it has been shown to be mediated by adsorbed proteins [159], negatively charged surfaces and denatured proteins [160]. The C3b results obtained from this study contrast with the previous studies listed in the literature, which state that the terminal hydroxyl (OH) group of PEG binds to C3b and activates complement system [161-163]. However, the results presented in this thesis showed a lower C3b adsorption on surfaces with monomer C (OH terminated PEG) (Figure 34 (d)). The difference in these results may be due to literature studies using self-assembled monolayers (SAMs) of ethylene glycol units of thiol PEG on gold rather than random polymerisation of PEG methacrylate on polymer microarray. An altered assembly of ethylene glycol units on the surface may lead to a different orientation of chemical groups present

on the surface. The polymer microarray spots may have a lower density of ‘OH’ on the surface as compared to SAMs.

Based on the blood incubation studies, the proposed material design rules to improve haemocompatibility of bacterial resistant materials would be the addition of short chain glycols. The addition of short chain glycol monomers to bacterial resistant monomers led to a lower surface protein adsorption as well as a lower immune system activation as compared to longer chain glycols.

4.5 Conclusions

- The protein adsorption on polymer microarray was quantified using XPS, which showed a sub-monolayer to a monolayer surface coverage of proteins from whole blood.
- No blood clotting was observed on the polymer microarray and most surfaces showed a very low platelet attachment.
- A lower fibrinogen adsorption was observed on homopolymers of monomers 1 to 16 and for compositions with short chain ethylene glycol units as compared to long chain ethylene glycols.
- A lower IgG adsorption and leukocyte attachment was observed on surface compositions with short chain ethylene glycol monomers (monomers A and B) when compared to polymer compositions with longer chain ethylene glycols.
- The complement C3b adsorption was lower on OH terminated ethylene glycol as compared to CH_3 terminated ethylene glycol surfaces.
- Some of the material compositions showed better haemocompatibility and lower immunogenicity than zwitterionic materials.

5 Chapter 5 – Bacterial attachment assays on polymer microarrays

5.1 Introduction

Polymer microarrays provide a high throughput platform to screen a library of materials for their biological properties such as bacterial attachment and biofilm formation. In the previous Chapter, the haemocompatibility of polymers printed in a microarray format was tested in a high throughput manner. In this Chapter, the polymer microarrays were screened for surface bacterial attachment using two common medical device colonising pathogens - *P. aeruginosa* (PA01-N) (Gram-negative) and *S. aureus* (SH1000) (Gram-positive).

The bacterial attachment assays were carried out on blood pre-conditioned microarrays to mimic the presence of blood proteins and cells. The surface of medical devices rapidly gets covered by blood proteins and cells following contact of the device with blood [164]. The effect of blood proteins on biofilm formation has been extensively studied and their presence leads to an increased bacterial attachment and biofilm formation [26, 165-167]. For example, fibrinogen-binding proteins, fibronectin-binding proteins (FnBPA and FnBPB) [168], collagen-binding protein [169] and clumping factor A and B (ClfA and ClfB) [170, 171] produced by *S. aureus* bind to plasma and host extracellular matrix components. Therefore, the bacterial attachment assays were carried out on blood pre-conditioned microarrays. The comparison of the 'hit' materials identified from high throughput screening with

silicone and silver will be made upon scale up in the next Chapter.

5.1.1 Aim and objectives

The aim of these experiments was to assess the bacterial attachment to the materials on polymer microarray following blood pre-treatment. The objectives of this Chapter were:

1. Screen a library of polymers (microarray) for bacterial resistant properties using *P. aeruginosa* (PA01-N) strain.
2. Screen a library of polymers (microarray) for bacterial resistant properties using *S. aureus* SH1000 strain.
3. Identify 'hit' materials from high throughput screening to scale up for further investigations.

5.2 Experimental

5.2.1 Whole blood incubation

Venous blood was obtained from healthy volunteers with no known medical conditions and who have not taken any medication 10 days prior to blood donation. The phlebotomy work was carried out in Clinical Research Facility (CRF), School of Medicine based at Queens Medical Centre hospital as per ethical approval (Ref: BT09052014 SoP SoLS). 2 u/mL Heparin was then added to Vacutainer® tubes (no additive) containing blood to prevent blood coagulation during the transfer of blood samples from CRF to Category 2 lab.

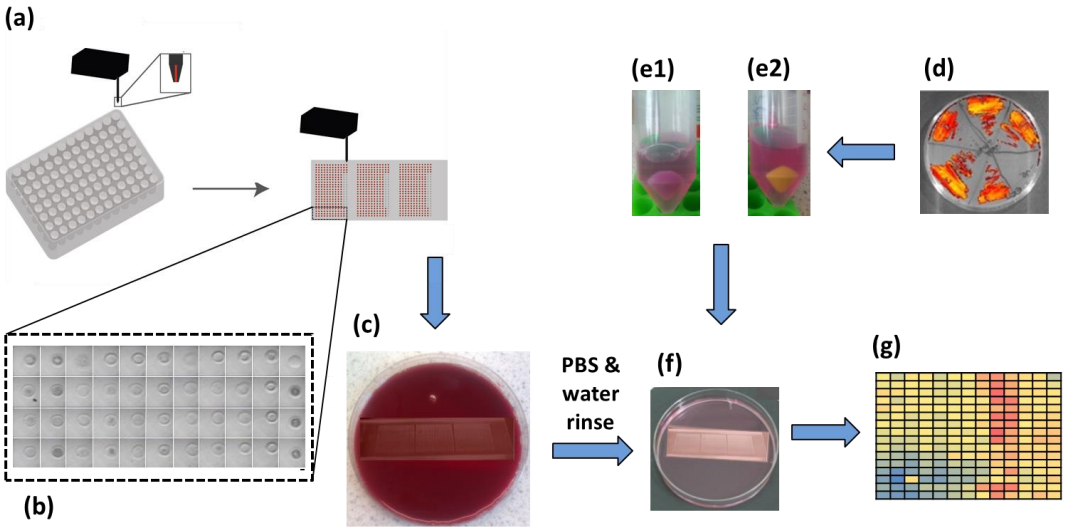


Figure 36: Blood incubation and bacterial attachment assay experimental setup on polymer microarray. **(a)** Microarray printing process, **(b)** Bright field images of microarray (individual images stitched together), **(c)** Microarray incubation in whole blood for two hours, **(d)** IVIS spectrum camera fluorescence image of mKat labelled S. aureus (SH1000) streaked on an agar plate, **(e1)** mCherry and **(e2)** mKat bacteria centrifuged following an overnight culture, **(f)** 72 hours bacterial attachment assay setup showing blood pre-incubated microarray in RPMI-1640 media at 37 °C at 60 rpm (OD_{600} = 0.01), **(g)** Heat map representation of the results.

The microarray slide (Figure 36 (a-b)) was then incubated in whole blood at 37 ^{o}C on a rotating stage at 60 rpm for two hours. The blood incubation work was carried out in a Category 2 laboratory (Figure 36(c)).

5.2.2 Bacterial strain preparation and high throughput bacterial attachment assay setup

The bacterial attachment experimental work was performed as per the protocol described in Section 2.8. Briefly, *P. aeruginosa* (PA01-N mCherry) and *S. aureus* (SH1000 mKat) were streaked out on an agar plate and placed at 37 ^{o}C overnight to allow bacteria form multiple colonies on the plate. The fluorescently labelled bacteria were confirmed using an IVIS spectrum camera (Caliper) as shown in Figure 36 (d). Thereafter, a single colony was transferred from agar plate into 15 mL LB medium for overnight culture at 37 ^{o}C at 200 rpm. The bacterial culture was then centrifuged and re-suspended (Figure 36(e1 & e2)) into RPMI-1640 medium for bacterial attachment assay. A 3-day bacterial attachment experiment was setup as described in Section 2.7.

5.2.3 Fluorescence scanner imaging and analysis

A Genepix 4200AL fluorescence scanner (Molecular Devices UK Ltd.) was used to quantify the fluorescence from the bacteria attached to each polymer spot on the microarray. *P. aeruginosa* (mCherry labelled) and *S. aureus* (mKat labelled) were detected using a laser on Genepix 4200AL scanner with

an excitation wavelength of 594 nm and emission filter set at 607-694 nm. The images obtained from the scanner were then analysed using Genepix Pro 6.1 software (Molecular Devices UK Ltd.) to output fluorescence intensity (au) from each polymer spot by drawing regions of interest on the fluorescence image. The numerical data obtained from the software was processed using Microsoft Excel and represented in form of heat maps for ease of visualisation of trends.

5.3 Results

5.3.1 The effect of blood proteins on bacterial attachment to existing catheter materials

It was interesting to look at the effect of blood proteins on bacterial attachment on a surface. Previous research suggested that the presence of blood proteins leads to an increased bacterial attachment on a surface [26, 141, 172, 173]. To test this hypothesis, silicone and commercial silver incorporated catheters were tested for bacterial attachment with and without a blood pre-incubation step. The presence of blood incubation step leads to an increase bacterial attachment for both materials as shown in Figure 37. The effect of the presence of adsorbed blood proteins is more prominent for the silver impregnated hydrogel coated catheter. Silver being a bactericidal compound, showed a low bacterial attachment of both *P. aeruginosa* and *S. aureus* in the absence of blood proteins on the surface. However, the presence of blood proteins from whole blood incubation showed a dramatic increase in bacterial attachment as evident from Figure 37. This may be due to inability of silver ions to diffuse and kill bacteria attached to the surface. As the surface gets rapidly covered with blood proteins and cells, the ability of silver to kill bacteria dramatically reduces due to bacterial attachment onto the adsorbed proteins rather than directly onto silver impregnated surface.

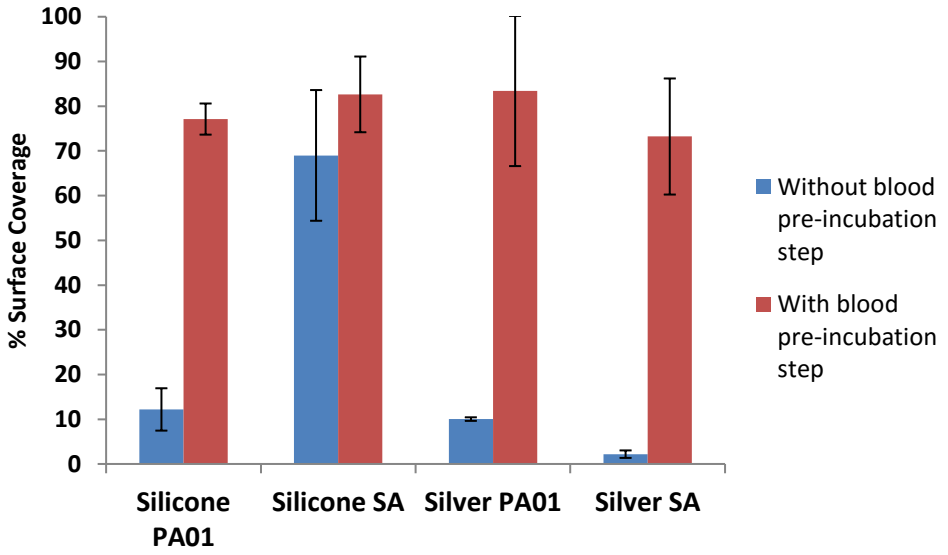


Figure 37: The effect of blood on bacterial attachment on silicone and silver catheters. PA01 indicates *P. aeruginosa* (PA01-N) and SA represents *S. aureus* (SH1000) bacterial strains. Half of the catheter samples (n=3) ('With blood pre-incubation step' samples) were incubated in human whole blood for 2 hours prior to bacterial assay. The %surface coverage was estimated from confocal microscopy images of surfaces after 72 hours incubation in RPMI-1640 media containing bacteria.

Due to this synergistic effect of blood proteins and bacterial attachment on the surfaces, polymer microarray biofilm assays were carried out with whole blood pre-incubation step.

5.3.2 *Pseudomonas aeruginosa* (PA01-N) attachment to micro arrays

P. aeruginosa attachment to each polymer spot on the microarray was measured and presented in the form of a heat map as shown in Figure 38. Monomers 1 to 16 were co-polymerised with monomers A to D at 25%, 50% and 75% v/v concentrations. Each block in Figure 38 represents a particular combination of two monomers, for example label A(25%) represents a polymer spot made up of 25% v/v of monomer A and 75% of other monomer (1 to 16). The colour coding of

heat map makes a clear distinction between low and high bacterial attachment. A blue colour on the heat map represents a low bacterial attachment (low fluorescence intensity, au) and a red colour represents a high bacterial attachment (higher fluorescence intensity, au). From Figure 38, it is clear that co-polymers of monomers 1 to 16 with monomers A and B showed lower bacterial attachment compared with combinations with monomers C and D. Monomers A and B comprise of a short chain glycol groups compared with monomers C and D, that have long chain glycol groups (Figure 5). Monomer 5 showed higher bacterial attachment at all concentrations when mixed with monomers A to D. The results for each co-polymer, shown in Figure 38, are average of three repeats of each polymer material printed on same polymer microarray. Material compositions containing A and B showed lower *P. aeruginosa* attachment as compared with zwitterionic materials E, F and G.

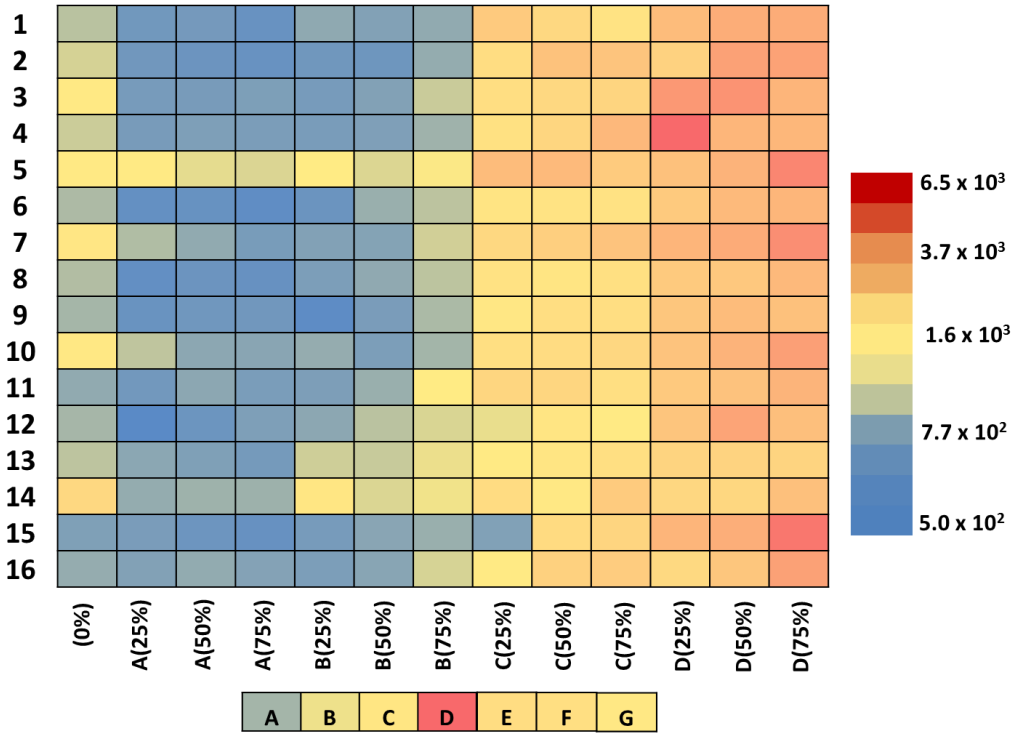


Figure 38: Heat map representation of *P. aeruginosa* (PA01-N) attachment on each polymer spot on the microarray measured by fluorescence intensity (au) using a fluorescence scanner (blue represents low and red represents higher bacterial attachment) (n=3 from three replicate blocks on same polymer microarray).

5.3.3 *Staphylococcus aureus* attachment assay

Similar to *P. aeruginosa*, the polymer microarray was also subjected to *S. aureus* attachment assays. Figure 39 shows the results of these experiments presented in a heat map format. *S. aureus* showed a similar pattern of attachment to *P. aeruginosa* in terms of a clear division between smaller (A and B) and longer chain glycol monomers (C and D). Most of the monomers showed good bacterial resistance as homopolymers and when co-polymerised with short chain glycol monomers as compared to zwitterionic materials E, F and G. The outlier seen in row 4 column D(25%) was an average of three replicates and the fluorescence reading was lower on all three readings.

However, bacterial attachment on each polymer spot, measured in three separate experiments would be ideal way of determining the reproducibility of these results.

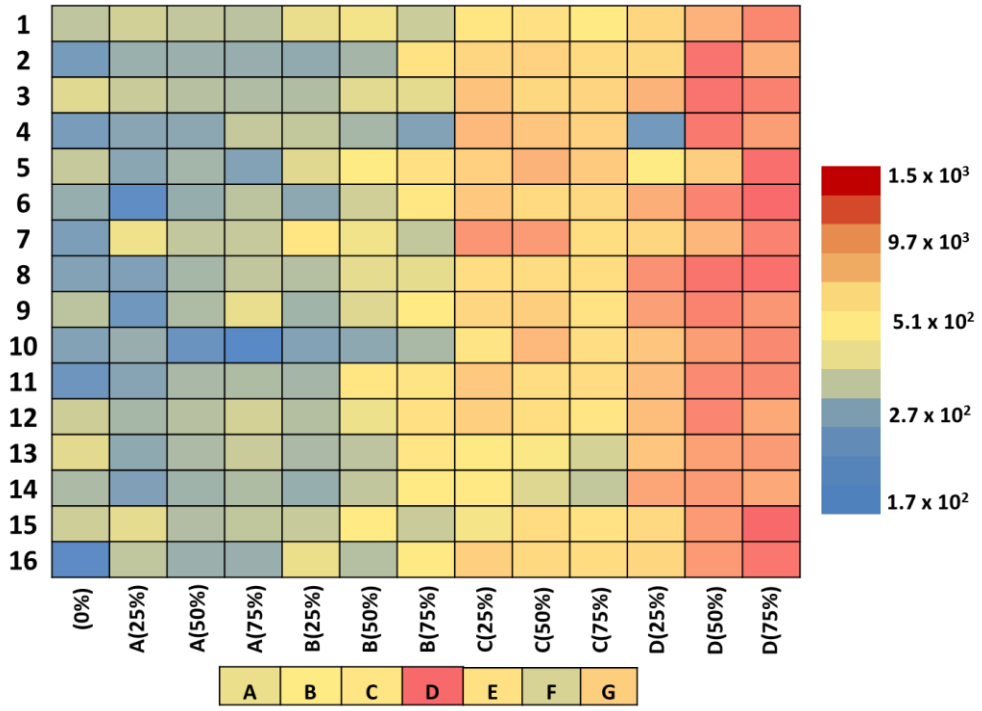


Figure 39: Heat map representation of *S. aureus* attachment on each polymer spot on the microarray measured by fluorescence intensity (au) using a fluorescence scanner. (n=3 from three replicate blocks on polymer microarray).

5.3.4 The relationship between surface bacterial attachment and wettability

The wettability of each polymer spot on the microarray was measured by water contact angle. The results of water contact angle plotted against bacterial attachment are shown in Figure 40 and Figure 41. There was no correlation between bacterial attachment on a surface and its respective wettability. *P.*

aeruginosa and *S. aureus* attachment appears to be independent of surface wettability.

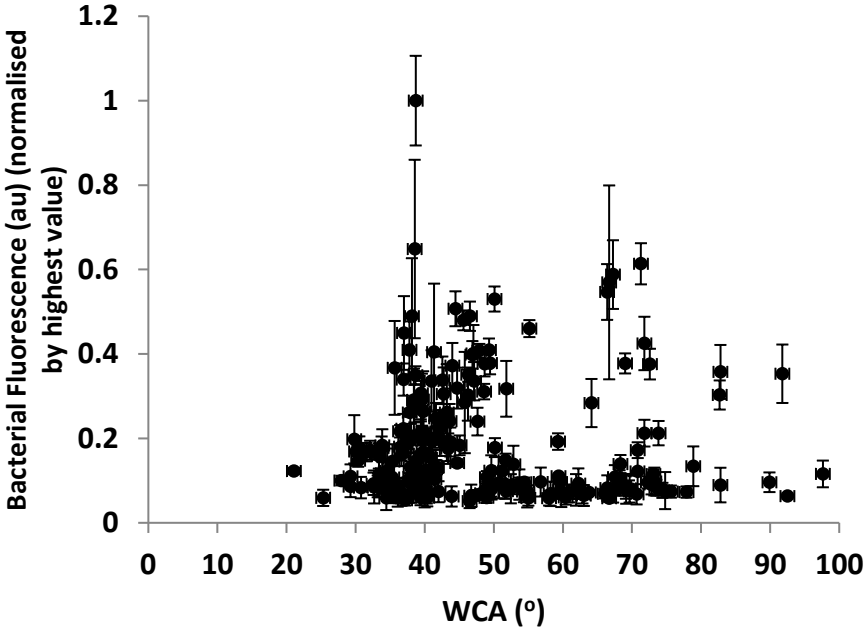


Figure 40: The effect of surface wettability on *P. aeruginosa* attachment. Microarray was incubated in human blood for 2 hours followed by incubation in RPMI-1640 media containing *P. aeruginosa* for 72 hours and imaged using a fluorescence array scanner (n=3).

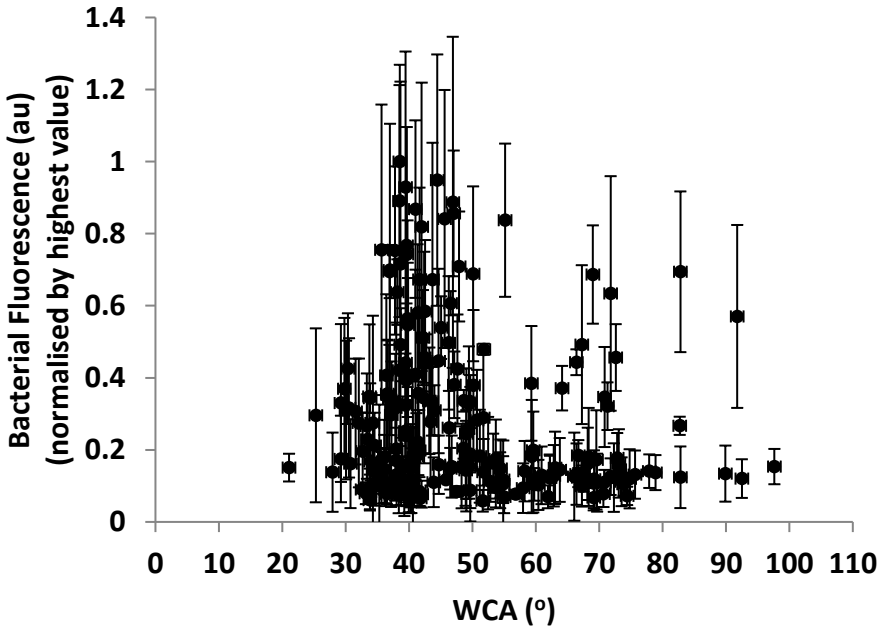


Figure 41: The effect of surface wettability on *S. aureus* attachment. Microarray was incubated in human blood for two hours followed by incubation in RPMI-1640 media containing *S. aureus* for 72 hours and imaged using a fluorescence array scanner (n=3).

5.3.5 Combining haemocompatibility and bacterial attachment results to identify hit materials from microarray screening

The high throughput microarray screening results obtained from haemocompatibility (Chapter 4) and bacterial assays were divided into three parts carrying equal weighing. These parts were bacterial (α), immune (β) and protein (γ) components of the results. The bacterial component was made up of bacterial attachment results from *P. aeruginosa* and *S. aureus* assays; the immune component was made up of an average of leukocyte, IgG and complement C3b results; the protein component was made up of combining fibrinogen adsorption and XPS protein overlayer thickness results. The combination (Ω) (average) of these three components is shown in Figure 42. Co-polymer of monomers 1 to 16 with monomers A and B showed a better haemocompatibility as well as lower bacterial coverage as compared with monomers C and D.

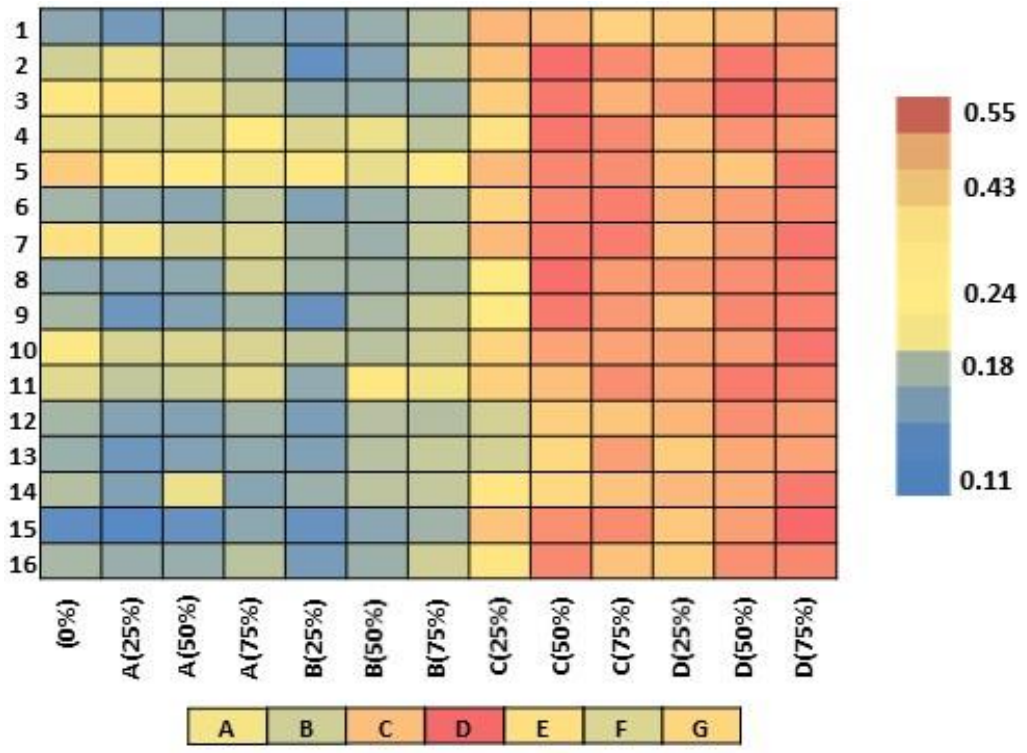
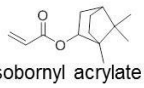
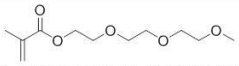
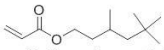
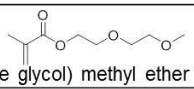
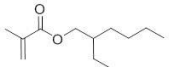
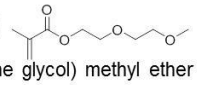
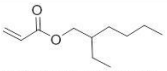
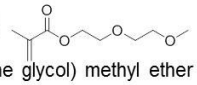
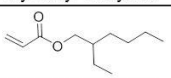
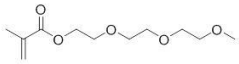
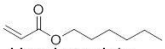
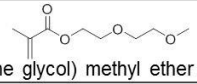
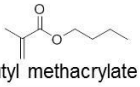
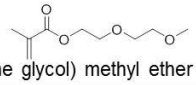
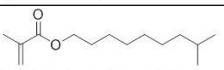
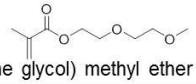
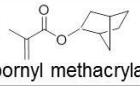
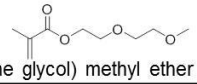


Figure 42: The combination (**Ω**) of bacterial (**α**), immune (**β**) and protein (**γ**) components to choose 'hit' materials from microarray screening. The values for each component (**α**, **β** and **γ**) were normalised to a range between 0 to 1 (au) and the combination values (au) were calculated by taking an average of three components **(Ω = (α+β+γ)/3)**.

The combined data from the entire microarray screening experiments was used to identify the top nine materials that were scaled up and used as coatings on silicone catheters. The list in Table 4 shows top nine material compositions from microarray screening chosen for scale up based on their bacterial resistance and haemocompatibility properties:

Table 4: Bacteria resistant haemocompatible 'hit' polymer compositions selected based upon their bacterial resistance and haemocompatibility properties from high throughput microarray screening for scale up studies. The combination of major monomers with short chain glycol monomers showed lower bacterial attachment as compared to longer chain glycols.

'Hit' Composition	Major Monomer (75%)	Minor Monomer (25%)
2(75%)B(25%)	(2)  Isobornyl acrylate	(B)  Tri(ethylene glycol) methyl ether methacrylate
6(75%)A(25%)	(6)  Trimethylhexyl acrylate	(A)  Di(ethylene glycol) methyl ether methacrylate
8(75%)A(25%)	(8)  Ethylhexyl methacrylate	(A)  Di(ethylene glycol) methyl ether methacrylate
9(75%)A(25%)	(9)  Ethylhexyl acrylate	(A)  Di(ethylene glycol) methyl ether methacrylate
9(75%)B(25%)	(9)  Ethylhexyl acrylate	(B)  Tri(ethylene glycol) methyl ether methacrylate
13(75%)A(25%)	(13)  Hexyl acrylate	(A)  Di(ethylene glycol) methyl ether methacrylate
14(75%)A(25%)	(14)  Butyl methacrylate	(A)  Di(ethylene glycol) methyl ether methacrylate
15(75%)A(25%)	(15)  Isodecyl methacrylate	(A)  Di(ethylene glycol) methyl ether methacrylate
16(75%)A(25%)	(16)  Norbornyl methacrylate	(A)  Di(ethylene glycol) methyl ether methacrylate

5.4 Discussion

5.4.1 Bacterial attachment assays

High-throughput screening of a library of materials was used to identify materials with a low bacterial attachment to the surface. The bacterial resistant monomers (1 to 16) were co-polymerised with glycol monomers of varying chain length (monomers A to D). *P. aeruginosa* and *S. aureus* attachment assays showed a clear distinction between co-polymers of short chain and long chain glycol monomers. The bacterial resistant performance of co-polymers (made up of monomers 1 to 16 mixed with monomers A to D) was compared with zwitterionic materials (E, F and G) [174, 175]. Zwitterionic materials have previously been reported to have antibacterial properties and are applied as coatings commercially, for example on contact lenses [176]. A number of hit materials showed lower bacterial attachment as compared to zwitterionic materials (E, F and G).

The bacterial resistant performance of materials 1 to 16 was enhanced by the addition of short chain glycol monomers (monomers A and B) (Figure 38 and Figure 39). This effect can be explained by the ability of glycols to reduce protein adsorption [177-179]. By reducing the protein adsorption on the surface, more of the bacterial resistant materials 1 to 16 are present on the surface and hence, reduced bacterial attachment. In contrast, the co-polymers with long chain glycols (monomers C and D) showed a higher bacterial attachment. This may be due to more of long glycol chains

present on the surface that may have negatively affected bacterial resistant performance of monomers 1 to 16.

5.4.2 The effect of surface wettability on bacterial attachment

Bacterial attachment on a surface is a complex process involving a range of bacterial surface factors including pili, fimbriae, flagella and other bacterial surface macromolecules [19, 69, 71, 180]. No relationship was observed between hydrophilicity / hydrophobicity of polymer surfaces and bacterial attachment (Figure 40 and Figure 41). These results are in agreement with some of previous studies of bacterial attachment on solid surfaces presented in the literature [181, 182]. On the other hand, in the case of a set of closely related materials, such as polystyrene and polyethylene terephthalate wettability may appear to be a controlling factor, when in fact it is simply a coincidence and the actual controlling factors is unknown [74, 183]. The monomers used in this project were chosen from a diverse library of materials with a range of physiochemical properties. This suggests that bacterial surface factors such as surface chemistry plays specific role in preventing surface attachment rather than attachment being simply dependent on surface water contact angle.

5.4.3 Selecting 'hit' polymer compositions via high-throughput screening

A number of haemocompatibility and bacterial attachment assays were carried out on polymer microarrays. These experiments yielded a substantial amount of experimental data. The challenging part of data analysis was to combine the data from all the experiments in a logical way to select top 'hit' haemocompatible, bacterial resistant polymers. To achieve this, the data from high throughput microarray experiments was divided into three components: bacterial attachment, immune response and protein adsorption. These three parameters were chosen as a basis for an ideal haemocompatible, non-immunogenic and bacterial resistant coating for application on blood-contacting medical devices. Resistance to protein adsorption is important as to maintain bacterial resistant properties of the coating material. Furthermore, bacteria use specific receptors such as von Willebrand factor binding protein, protein A [184, 185] and fibrinogen binding protein [186] on the surface of *S. aureus* to bind to adsorbed proteins and as a result can form biofilms on a surface with adsorbed proteins [26, 173]. On a similar note, an antibacterial coating must also be non-immunogenic and should have minimal interactions with the immune system. The limitation of giving bacterial, immune and protein components equal weighing is that there are some materials that showed good bacterial resistant properties, but activated immune response and therefore had good average overall score. However, as an initial screening platform, microarray data was given equal weighing for all three components.

Hence, by dividing the data in three components, focusing on bacterial, immune and protein adsorption, materials with bacterial resistant, haemocompatible and low-immunogenic properties were identified. Co-polymers of bacterial resistant monomers (1 to 16) with short chain glycols (A and B) showed a low bacterial attachment and protein adsorption and were less immunogenic when compared with longer chain glycols (C and D). Furthermore, the 'hit' materials showed less bacterial attachment and better haemocompatibility than zwitterionic materials.

5.5 Conclusions

- Co-polymers of monomers 1 to 16 with monomers A and B showed lower surface attachment of *P. aeruginosa* and *S. aureus* following whole blood incubation.
- There was no relationship between surface bacterial attachment and surface wettability.
- A total of nine bacterial resistant, haemocompatible 'hit' materials with low immunogenicity were chosen from high-throughput bacterial and haemocompatibility assays. The 'hit' compositions were co-polymers with short chain glycol monomers A and B.
- The 'hit' materials showed low bacterial attachment and good haemocompatibility as well as low immunogenicity when compared with zwitterionic materials.

6 Chapter 6 – Bacterial attachment and haemocompatibility testing of scaled-up 'hit' polymer compositions

6.1 Introduction

The high-throughput screening described in previous Chapters identified a number of candidate materials, from which the top nine bacterial resistant haemocompatible 'hit' materials were chosen. This Chapter deals with scaling up of these 'hit' material compositions as coatings on silicone catheters and testing them for haemocompatibility and bacterial resistance. Haemocompatibility of scaled up hit materials were tested against blood contact under static and flow conditions. It has been shown that hydrodynamic forces such as shear stress induced by blood flow causes unfolding of blood proteins such as von Willebrand factor (vWF) [187]. vWF plays an important role in blood clotting. vWF, an adhesive glycoprotein, binds and stabilises factor VIII in the circulation and protects factor VIII from degradation by activated protein C [188]. Factor VIII plays an important role in blood clotting cascade by activating Factor X (Figure 3). Furthermore, vWF binds to the receptors present on the platelet membrane. High fluid shear stress provides optimal conditions for vWF mediated platelet adhesion and clotting [189, 190]. vWF also binds to collagen (exposed by blood vessel injury) and localises factor VIII and platelets at the site of clot formation.

The bacterial attachment and haemocompatibility assays carried out on microarrays were repeated on scaled up

polymer materials. However, unlike microarray, where the activation of haemostasis and inflammatory markers by each polymer material were difficult to be determined due to the presence hundreds of materials on same slide, scaled up materials allowed detailed study of individual materials without the risk of cross reaction. The haemocompatibility experiments presented in this Chapter were divided into two categories, namely haemostasis and inflammation parameters. Haemostasis can be defined as body's co-ordinated cellular and plasmic response towards blood vessel injury [191]. The coagulation pathway is also activated by foreign surfaces such as insertion of a vascular catheter [37]. Hence, the interactions of the 'hit' polymer materials with various haemostatic parameters were investigated.

6.1.1 Coagulation activation (F1+2)

Prothrombin fragment 1+2 (F1+2) was used as a measure of coagulation activation. Fragment F1+2 is a product that is cleaved from amino-terminal end of prothrombin when prothrombin is converted to thrombin by factor Xa in the coagulation pathway [192] (starting from foreign surface (e.g. medical device such as catheter) contact with blood leading up to the formation of stable fibrin clot (Figure based on [37])

). Thereafter thrombin converts fibrinogen into fibrin that produces a stable blood clot. Therefore, by measuring F1+2 levels, the ability of a surface to activate the coagulation cascade can be determined.

6.1.2 Platelet and leukocyte decay and platelet-leukocyte conjugates

Leukocyte and platelet decay (a reduction in cell count after incubation with a surface) in the blood are mainly a reciprocal parameter of leukocyte and platelet adhesion. Platelets not only adhere to surfaces and stick together as aggregates but also to other cells such as leukocytes [193]. Furthermore, haemolysis can also result in a reduction in platelet count. Platelet adhesion onto other cells (conjugate formation) is mainly mediated by platelet surface receptors [193], thus it is a marker of platelet activation. Therefore, by measuring platelet and leukocyte decay, the ability of a surface to activate platelets and leukocytes can be estimated.

Similarly platelet-leukocyte conjugates can be used as a measure of coagulation and immune system activation by a surface. Flow cytometry can be used to investigate platelet-leukocyte conjugates by detecting the thrombocyte-specific surface marker CD41a on granulocytes and monocytes [37, 158, 194].

6.1.3 Platelet activation PF-4 (platelet factor 4)

PF-4 is a 7.8 kDa peptide stored as a tetramer complex in α-granules of blood platelets and it is released following platelet activation [195, 196]. PF-4 has been shown to bind and neutralise heparin [196]. However, in the experiments presented in this Chapter, PF-4 was used as a marker for blood platelet activation. PF-4 is present in plasma in very low

concentrations, which together with platelet specificity makes it a very sensitive marker of platelet degranulation and activation. According to one estimate, release of granule content from just one per 1000 platelets can double the plasma concentration of PF-4 [197].

6.1.4 Aim and objectives

The aim of these experiments was to assess the bacterial attachment and haemocompatibility of 'hit' materials identified from high throughput microarray screening following scale up. The objectives of this Chapter were:

1. Scale up 'hit' compositions to gram scale quantities using free radical polymerisation.
2. Dissolve scaled up polymers into a suitable solvent and dip coat silicone catheters with scaled up polymer materials.
3. Carry out bacterial attachment assays on coated catheters as per microarray assays using *P. aeruginosa* and *S. aureus* strains.
4. Compare the bacterial resistance performance of 'hit' materials against commercially available silicone and silver containing catheters.
5. Test haemocompatibility and immunogenicity of scaled up polymers under quasi-static and flow conditions.

6.2 Experimental

6.2.1 Materials

Rüsch Brillant Paediatric silicone catheters with size 8 Fr (2.7 mm) were purchased from Teleflex Medical. The catheters were first cut into 1 cm sections and further sliced horizontally to get a semi-circular lumen. MultiCath 2 Expert silver ion based 2-lumen XRO catheters used as control were purchased from Vygon UK Ltd. MultiCath 2 Expert uses AgION™ technology, which has silver (an antimicrobial agent) incorporated into the material from which the tube is made up of [198].

Teflon AF or Teflon Amorphous Fluoropolymers (a copolymer of tetrafluoroethylene and bis-2,2-trifluoromethyl-4,5-difluoro-1,2-dioxole) was used as a control for haemocompatibility testing due to its low thrombogenicity and good haemocompatibility properties [199-203].

6.2.2 Scale-up polymerisation of microarray 'hit' compositions

The scale up polymerisation was carried out using 2,2'-azobis-(2,4-dimethyl-4-methoxyvaleronitrile) (AIBN) mediated catalytic chain transfer polymerisation reaction as patented by David Borman and Derek Irvine [204]. The full reaction protocol is described in Appendix D. Briefly, in a 500 mL round bottom flask, 75.2 mL of major monomer was mixed with 20.8

mL of minor monomer (monomer A or B) together with 240 mg of AIBN and 100 mg of PhCoBF (bis(borondifluorodiphenylglyoximato) cobaltate (II)) (catalyst). Then 200 mL of toluene was added into the flask as a solvent for the reaction. The reaction was carried out at 80 ^{o}C for 18 h. Following completion, the polymer was precipitated in methanol and dried under vacuum to remove the solvent. The polymer was then dissolved in Dichloromethane DCM to make 30% w/v solution, which was used to dip coat silicone catheters.

6.2.3 Oxygen plasma treatment of silicone catheters and dip coating in polymer solution

Rusch Brilliant Paediatric silicone catheters (Teleflex Medical) size 8 FR , 3 mL and 31 cm length were cut into 1 cm length tubes, which was then further cut into semi-cylinders to expose the catheter lumen. These silicone semi-cylindrical pieces were then oxygen plasma treated in a T-shaped borosilicate chamber using a 13.56 MHz radio-frequency power source (Coaxial Power System Ltd.). Oxygen plasma oxidation was carried out at 50 W power and 300 mTorr working pressure for 10 minutes. Following plasma treatment, the catheter pieces were dip coated with 30% w/v polymer solution (in DCM). The dip coated catheter samples were then dried under vacuum for seven days to remove the solvent before carrying out bacterial assays.

6.2.4 Confocal microscopy bacterial attachment assay on hit material coated silicone catheters

Bacterial attachment assays were carried out on hit material coated silicone catheters as per the protocol described in Section 5.2.2. The experimental setup is shown in Figure 43. The polymer coating on the silicone catheter was confirmed using scanning electron microscopy as shown in Figure 43(b). Similar to the microarray bacterial attachment setup, the coated catheter sections were incubated in freshly taken human blood for two hours (Figure 43(c)). The catheter sections were then gently washed with PBS and water to remove unadsorbed blood proteins and cells, before transferring the catheter sections into a 50 mL Falcon tube containing RPMI-1640 media with bacteria (OD = 0.01) for 72 hours at 37 ^{o}C at 60 rpm. After 72 hours, the catheter sections were washed with PBS and water to remove unattached bacteria and imaged under confocal microscope (lumen side of the catheter) to obtain bacterial surface coverage data.

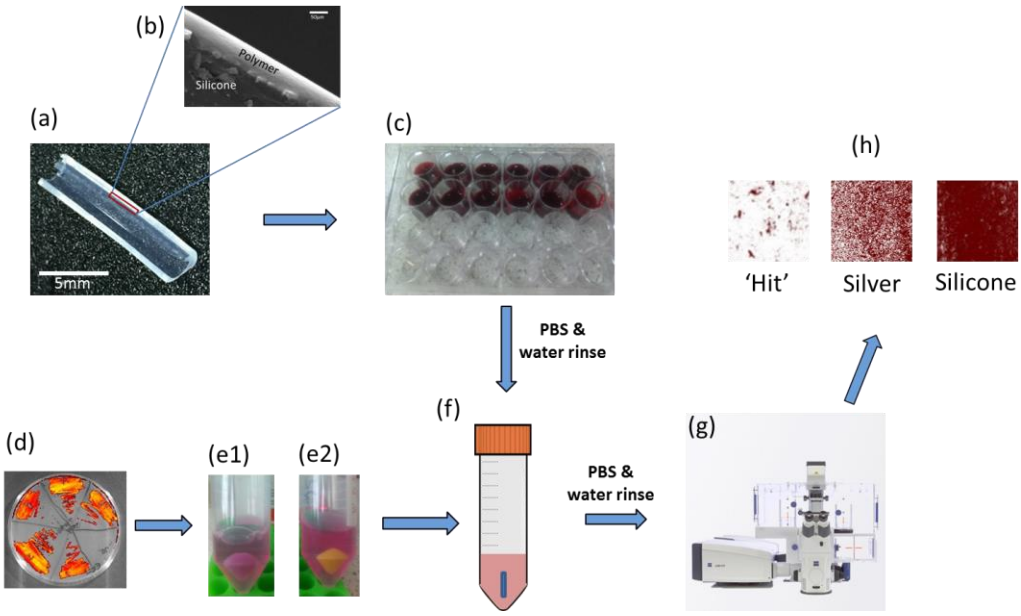


Figure 43: Blood incubation and bacterial attachment experimental setup on 'hit' material coated silicone catheter sample. **(a)** Polymer coated sliced silicone catheter section, **(b)** A scanning electron microscope image of polymer coating (thickness = 50 µm), **(c)** catheter sections incubated in freshly taken human blood in a 24-well plate, **(d)** Fluorescence image of mCherry labelled bacteria streaked on a 90 mm agar plate, **(e1)** and **(e2)** Overnight culture of *P. aeruginosa* (mCherry) and *S. aureus* (mKat), respectively in a 50 mL Falcone tube, **(f)** 72 hour bacterial attachment assay setup in RPMI-1640 media at 37 °C at 60 rpm, **(g)** Confocal microscopy to image bacterial attachment in the lumen of catheter sample , **(h)** Confocal images (625 x 625 µm) showing bacterial surface coverage on 'hit' material coated, silver and silicone uncoated catheters.

6.2.5 Whole blood incubation of scaled up materials under quasi-static conditions

Similar to the microarrays, the haemocompatibility of scaled up hit materials chosen from microarray studies was analysed using a quasi-static incubation chamber as shown in Figure 31. Round glass slides with a diameter of 25 mm (Schott, Germany) were plasma treated as per the protocol described in Section 6.2.3 and then dip coated in 30 %v/v polymer solution in DCM. The slides were dried under vacuum for seven days before carrying out quasi-static blood incubation

experiments as described in Section 4.2. In addition to standard immunochemical methods, soluble thrombotic and immunological components of the blood, on each surface were also measured. Blood samples retrieved from incubation chambers were mixed with recommended stabilisers for ELISA analysis of TAT (thrombin-antithrombin complex, Dade Behring GmbH, Germany), PF4 (platelet factor 4, Haemochrom Diagnostica GmbH, Germany) and C5a (complement fragment C5a, DRG Instruments GmbH, Germany). All the assays were carried out by following manufacturer's instructions. An automated cell counter (Coulter AcTdiff., Germany) was used to count red and white blood cells from EDTA (Ethylenediaminetetraacetic acid) anticoagulated blood samples.

Flow cytometry was performed on cells stained with 2.5 μL phycoerythrin labelled anti CD11b (clone ICRF44, Biozol, Eching, Germany) and 5 μL fluorescein labelled anti CD41a (Clone HIP8, BD/Pharmingen, Heidelberg, Germany) per 25 μL blood at room temperature for 30 minutes. A 0.1% NaN_3 (final concentration) was used to reduce cell activation during this incubation period [194]. The analysis and quantification of flow cytometry results was carried out as per the protocol described previously [131, 205].

6.2.6 Whole blood incubation of scaled up materials under flow conditions to evaluate haemocompatibility

To evaluate the effect of flow conditions, the hit material were dip coated onto Schott Nexterion Glass D slides (Schott, Germany) with dimensions 75.6 mm x 25 mm x 0.1 mm. The coated slides were dried under vacuum for seven days to evaporate the solvent prior to haemocompatibility experiments. Freshly obtained human blood was anticoagulated with 4 iu/mL heparin. The coated slides were placed in contact with blood under flow conditions in a custom made blood flow chamber as shown in Figure 44. The incubation was carried out under a shear rate of 300 s^{-1} for 30 minutes. The slides were then analysed for various blood proteins and cell attachment as per the protocols described in Section 4.2 and 6.2.5.

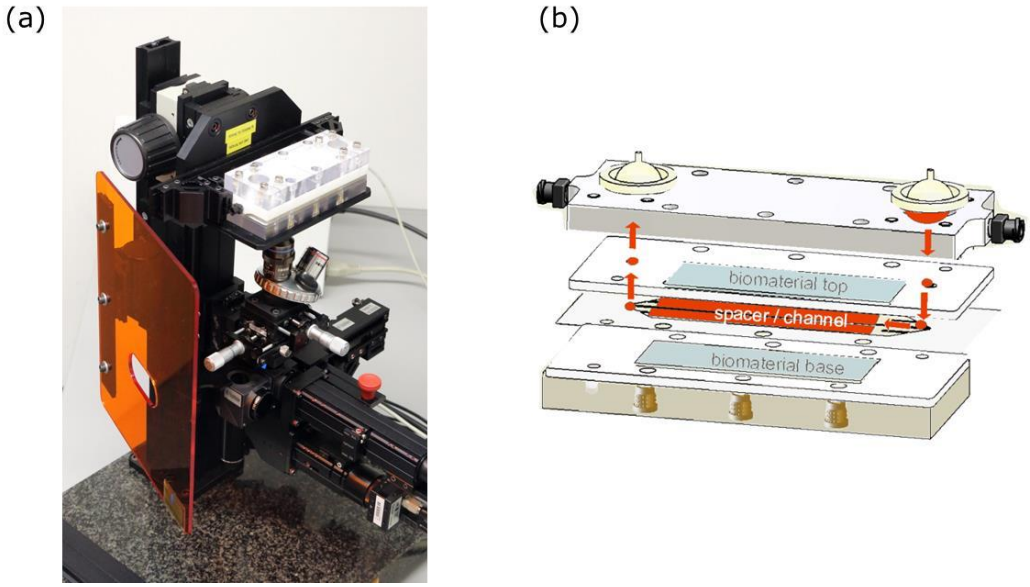


Figure 44: Custom made blood incubation flow chamber experimental setup **(a)** Blood flow chamber mounted on an inverted microscope, **(b)** a detailed schematic representation of various components of the flow chamber, spacer thickness = 150 μm.

6.2.7 LIVE/DEAD™ staining

Live/dead staining [206] was carried out using a LIVE/DEAD™ BacLight™ Bacterial Viability Kit (Molecular Probes) as per the manufacturer's instructions [207]. The kit consists of two dyes - SYTO® 9 green-fluorescent nucleic acid stain and propidium iodide, which is a red-fluorescent nucleic acid stain. Syto 9 dye penetrates both intact and damaged bacterial cells, therefore on its own stains both dead and live cells. In contrast, propidium iodide is unable to penetrate intact bacterial cells and only penetrates damaged membranes. When mixed together, propidium iodide causes a reduction in the SYTO 9 fluorescence in dead cells. Therefore, live bacteria fluoresce green, whereas dead bacteria fluoresce red. The excitation/emission maximum for SYTO 9 stain is 480 nm/500 nm and for propidium iodide is 490 nm/635 nm [207]. These dyes produced virtually no background fluorescence.

6.3 Results

6.3.1 Bacterial attachment assay on polymer coated silicone catheters

Silicone catheters were dip coated with hit materials and as with microarrays, bacterial attachment assays were carried out with *P. aeruginosa* and *S. aureus* strains. The bacterial attachment was analysed by confocal microscopy as shown in Figure 45. The percentage surface coverage of each bacterial strain on nine 'hit' materials estimated using *Image J* is shown in Figure 45. On scale up, all the hit materials from the micro array showed less bacterial surface coverage compared to silicone uncoated and commercial silver containing catheter. Polymer composition 2(75%)B(25%) and 16(75%)A(25%) showed least bacterial attachment for both *P. aeruginosa* and *S. aureus* out of all the 'hit' materials.

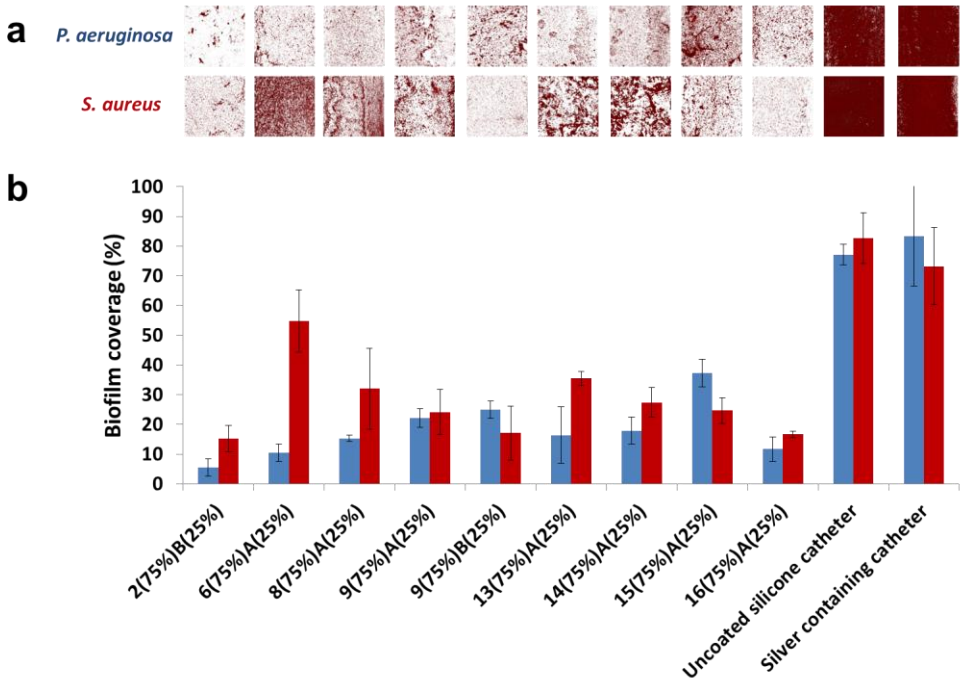


Figure 45: Bacterial attachment on 'hit' compositions coated silicone catheters as compared to silicone uncoated and commercially available silver containing catheters following 72 hour incubation in planktonic bacteria. **(a)** Confocal microscope images (625 x 625 μm) of mCherry labelled *P. aeruginosa* and mKat labelled *S. aureus* attached on hit polymer coated surfaces, uncoated silicone and silver containing catheters. **(b)** The quantification of biofilm coverage area (%) for *P. aeruginosa* (blue) and *S aureus* (red) on each material using the confocal images (n=3). The difference between bacterial attachment on hit materials and silicone and silver surfaces is statistically significant (p = 0.023)

6.3.2 LIVE/DEAD™ staining on hit material coating

The results so far showed that hit co-polymer composition reduced bacterial attachment on the surface, but the mechanism involved is not understood. To obtain further insight into the mechanism involved, a bacterial live/dead staining assay was carried out on coated and uncoated silicone catheters as shown in Figure 46. Green fluorescence indicates live bacteria and red fluorescence represents dead bacterial cells present on the surface. From Figure 46, it can be seen that most of bacterial cells present on hit material were live

(green fluorescence) together with the presence of some dead bacteria (red). In contrast silicone uncoated surface shows majority of live bacteria and virtually no dead bacteria on the surface. These results suggest an anti-attachment as principal mechanism rather than a killing mechanism of antibacterial activity of hit material. It should be noted that the unpolymerised monomers were removed from both microarray and scaled up polymers. After printing, the microarrays were placed under vacuum for seven days prior to bacterial and haemocompatibility assays to evaporate any unpolymerised monomers (most of the monomers were volatile). In case of scaled up polymerisation, the polymers were precipitated from the reaction mixture to remove unpolymerised monomers and subsequently dried under vacuum.

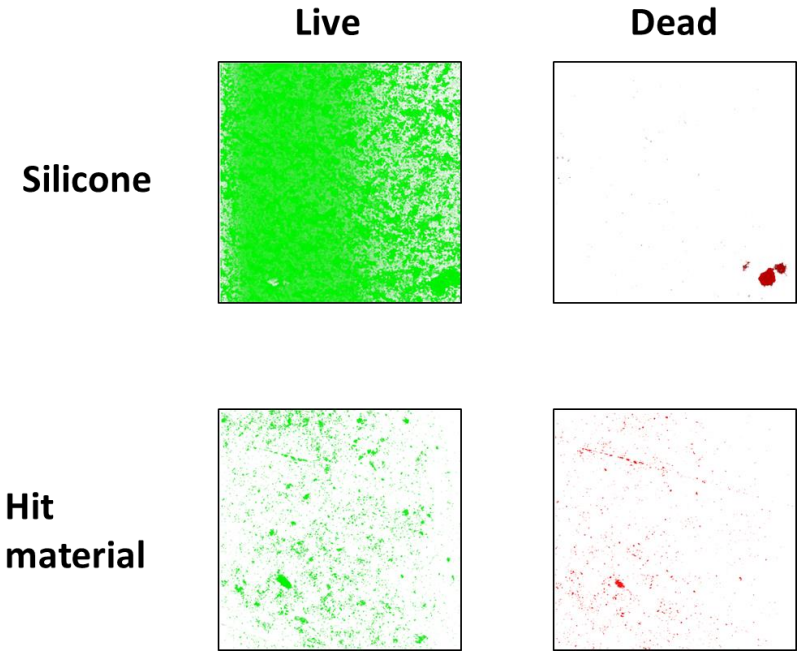


Figure 46: Live/dead staining on hit material (2(75%)B(25%)) coated and uncoated silicone catheters. The coated and uncoated silicone catheters were incubated in RPMI-1640 media containing *P. aeruginosa* for 72 hours. The surfaces were then stained using BacLight™ bacterial viability kit containing SYTO® 9 green-fluorescent nucleic acid stain (stains live bacteria) and propidium iodide, which is a red-fluorescent nucleic acid stain (stains dead bacteria). Each image is 625 x 625 µm.

6.3.3 Haemocompatibility assays on 'hit' polymers

Following bacterial attachment assays on 'hit' polymers, a range of haemocompatibility assays were carried out. Due to the limited capacity of incubation chambers, only six 'hit' material compositions (in triplicate) out of nine were chosen for haemocompatibility assays based upon bacterial resistance performance. These were divided into two categories namely haemostasis and inflammation parameters. The haemocompatibility assays were carried out under quasi-static and flow conditions.

6.3.3.1 Haemostasis parameter assays

Haemostasis is a complex process involving a range of different blood plasma proteins and cells. Coagulation and platelet activation as well as fibrinogen adsorption measured at each surface is shown in Figure 47. The performance of six 'hit' polymer surfaces together with Teflon AF (amorphous fluoroplastics) and glass were measured under quasi-static and flow conditions. Teflon AF is a haemocompatible material [203, 208] and has been extensively used for a range of biomedical applications [209]. Teflon is a hydrophobic, biologically inert polymer material that has been used in medical devices such as arterial grafts, sutures, venous catheters as well as surgical and cosmetic purposes [210]. In general blood flow conditions caused a greater platelet decay (Figure 47 (b)) and higher platelet activation (Figure 47 (c)) as compared with quasi-static conditions. All 'hit' surfaces

showed lower or similar platelet decay than Teflon AF under both flow and static conditions.

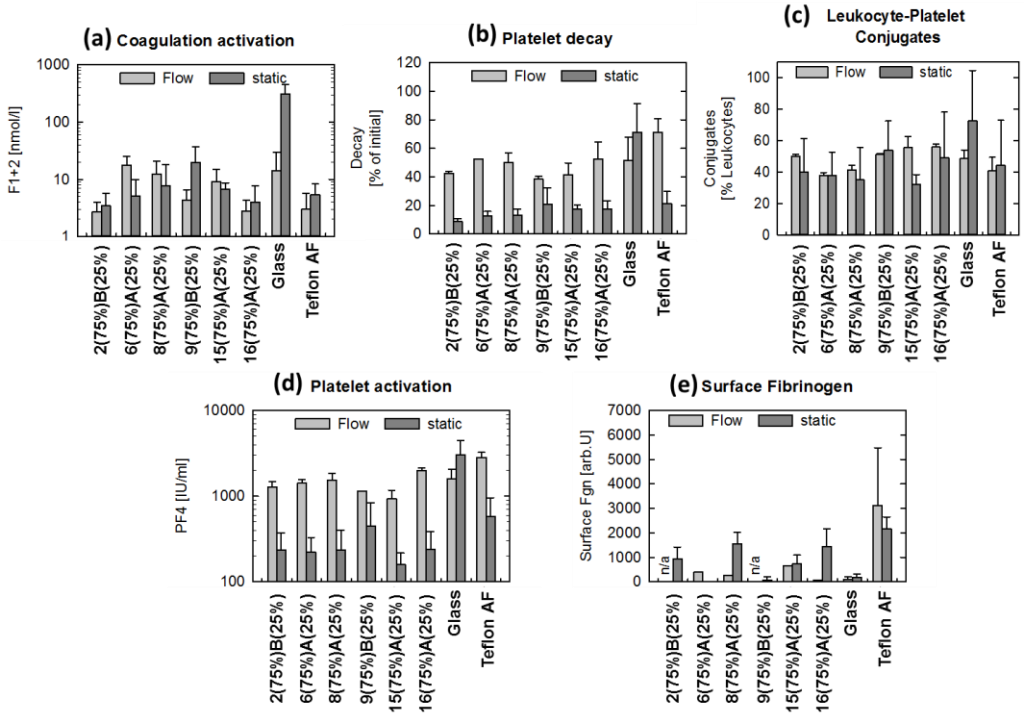


Figure 47: Haemostasis parameter assays to assess haemocompatibility of scaled up 'hit' materials under static and flow conditions. **(a)** Coagulation activation measured by Prothrombin fragment 1+2 (F1+2), **(b)** Platelet decay assay, **(c)** Leukocyte-Platelet conjugate assay, **(d)** Platelet activation measured by platelet factor 4 (PF4) and **(e)** Fibrinogen adsorption on test surfaces (n=3).

Most 'hit' materials showed a relatively low coagulation activation, similar to Teflon AF surface, based on prothrombin fragment F1+2 (Figure 47 (a)). 2(75%)B(25%) and 16(75%)A(25%) coated surfaces induced even lower coagulation activation than Teflon AF. Surface coating 9(75%)B(25%) showed higher coagulation activation out of all the 'hit' surfaces. Platelet activation (Figure 47 (d)) on all the 'hit' surfaces is generally lower than on the reference Teflon AF, but 9(75%)B(25%) induces slightly elevated platelet activation. This corresponds to the elevated coagulation at this surface. All of the surfaces showed lower fibrinogen adsorption

than Teflon AF surface (Figure 47 (e)) under quasi-static conditions. Interestingly, the glass surface showed highest coagulation and platelet activation but a very low surface fibrinogen under both quasi- static and flow conditions.

6.3.3.2 Inflammation parameter assays

The interactions of each 'hit' material with immune system were investigated using leukocyte, complement and IgG assays as shown in Figure 48. As a general trend, under blood flow conditions, all of the surfaces showed higher complement activation and higher leukocyte activation (Figure 48 (a) and (b)). In contrast, under flow conditions, there was elevated compelement activation for polymers 9(75%)B(25%) and 15(75%)A(25%), whereas no signs for elevated complement C5a under quasi-static conditions for these materials. All of the 'hit' material surfaces showed low leukocyte activation (Figure 48 (b)) as well as minimal leukocyte deacy (Figure 48 (c)) comparable to Teflon AF surface. The surface leukocyte density observed to be higher under static conditions compared to flow conditions on majority of surfaces tested (Figure 48 (d)). 2(75%)b(25%) and 8(75%)A(25%) showed a lower leukocyte density than Teflon AF surface under quasi-static conditions. Surface IgG and surface complement assays produced more variable results with half of the 'hit' materials showing a very low surface IgG than others (Figure 48 (e))

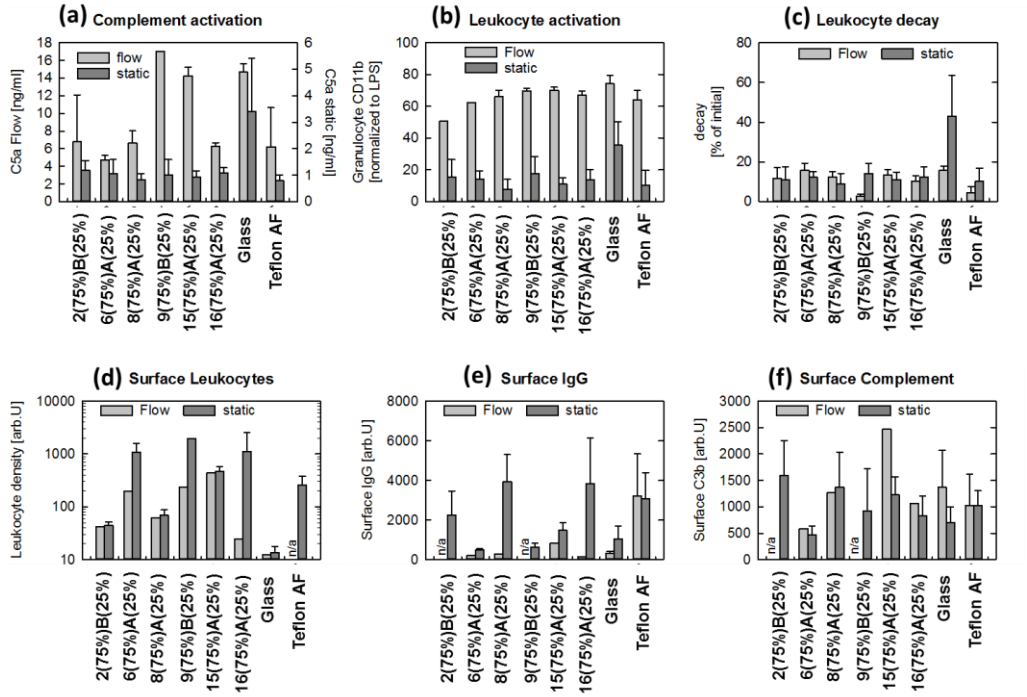


Figure 48: Inflammation parameter assays to assess immunogenicity of scaled up 'hit' materials under static and flow conditions. **(a)** Complement activation measured using C5a, **(b)** Leukocyte activation assay using Granulocyte CD11b marker, **(c)** Leukocyte decay assay, **(d)** Surface Leukocyte density measurement, **(e)** IgG adsorption on each surface, **(f)** Complement C3b adsorption on each surface (n=3).

6.3.4 Combining haemocompatibility data to identify the best performing material

Haemocompatibility experiments yielded a large dataset for each polymer material. To identify the best performing polymer material, Figure 49 rates the polymers (including Teflon AF reference), using most relevant parameters of the haemocompatibility test obtained in the quasi-static incubation. Measured values for every parameter were normalized to the range of 0 to 100 (using (Value – Minimum value)/ (Maximum value – Minimum value)%) and handled further with equal weighing. A low value indicates a good performance. All the haemostasis and inflammation

parameters were combined to get a mean haemostasis and mean inflammation values, respectively.

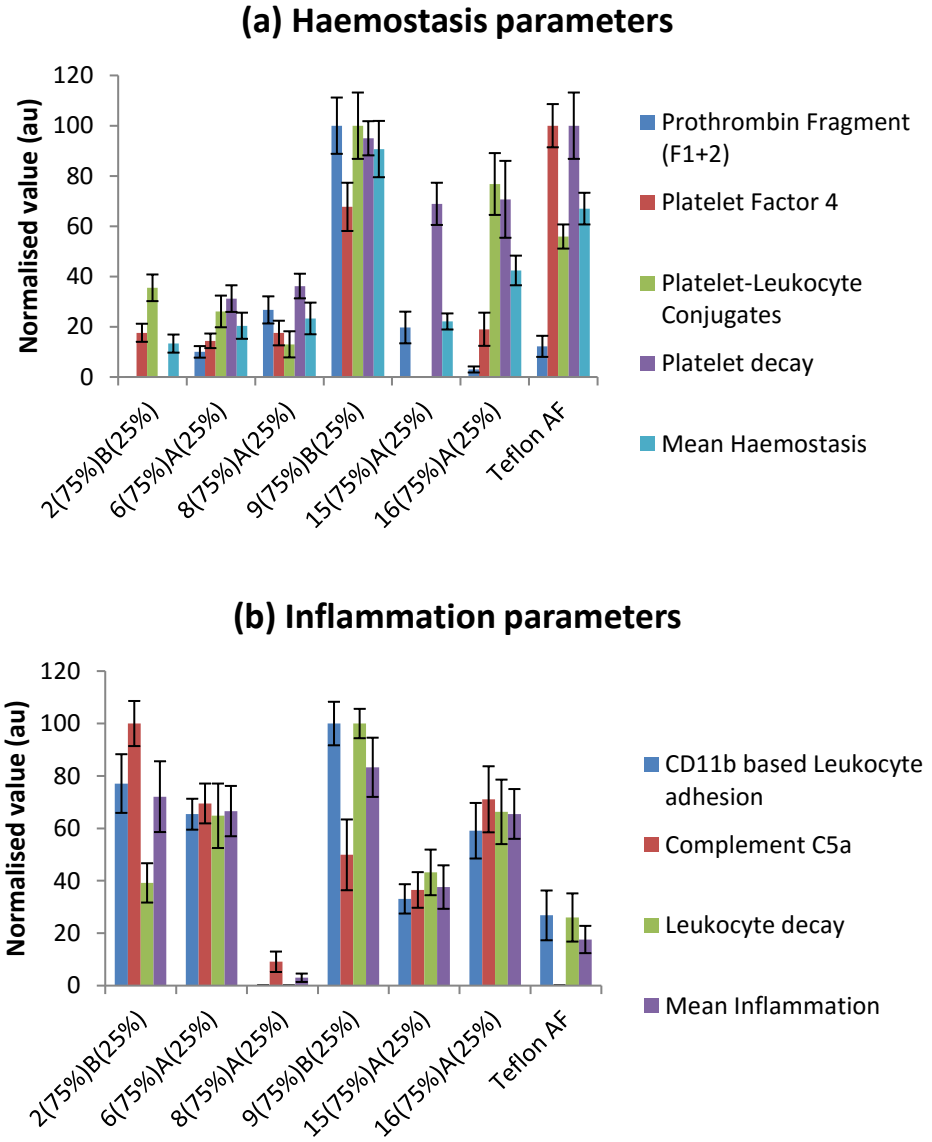


Figure 49: (a) Haemostasis and **(b)** Inflammation parameters to rate polymer performance using the most relevant parameters of the haemocompatibility test. Measured values for every parameter were normalized to the range of 0 to 100 and handled further with equal weight. Low values indicate good performance (n=3).

From the results shown in Figure 49 (a), Polymer 2(75%)B(25%) showed best score as a low-thrombogenic surface based on relevant haemostasis parameters. This surface also exhibited a low plasmatic clotting activation and

low platelet activation. However, 2(75%)B(25%) showed a much higher inflammatory response and leukocytes were observed on the surface by microscopy (Figure 49 (b)). Similarly the polymer 6(75%)A(25%) produced a low haemostasis, with coagulation activation (F1+2) similar to Teflon surface, but activated inflammatory parameters such as leukocytes and complement C5a.

Polymer 8(75%)A(25%) showed best score as low-inflammatory material and best total score out of all the polymer materials tested. Despite having higher coagulation activation than Teflon AF, a low platelet activation and decay was observed on this surface. In contrast polymer 9(75%)B(25%) has the poorest score in both coagulation and inflammation experiments including an elevated coagulation and blood platelet activation. A high level of complement activation was observed in the shear experiments.

Polymer 15(75%)A(25%) showed a higher coagulation than the Teflon AF surface, but a low platelet activation was observed on this surface as evident from Platelet Factor 4 (PF4) and conjugate results shown in Figure 49 (a). However, this surface showed a tendency to cause a higher inflammation than Teflon AF surface as evident from inflammation results. Interestingly, surface 16(75%)A(25%) produced low coagulation (F1+2) and platelet (PF4) activation, but a much higher platelet conjugation and decay was seen on this surface, together with a higher tendency to cause inflammation (leukocytes activation and C5a)

6.4 Discussion

6.4.1 Bacterial attachment on polymer coated catheters

All of the scaled up 'hit' material compositions from microarray screening showed a reduction in surface bacterial attachment, when compared with silicone and silver hydrogel catheters. Materials with cyclic functional group moieties: 2(75%)B(25%) and 16(75%)A(25%) had a lower bacterial surface coverage compared with linear or branched polymer materials. This observation is in line with the previous observation by Sanni *et.al.* [73], that polymer materials with a cyclic pendent group achieved a greater reduction in surface bacterial attachment compared to linear or aromatic pendent groups. This study showed that the molecular rigidity and polarity plays an important role in preventing bacterial attachment. As cyclic pendent groups are more rigid than the linear molecules, low bacterial attachment was observed on material with cyclic pendent groups [73]. Sanni *et.al.* [73] also concluded that nonpolar, molecularly rigid materials (e.g. cyclic pendent groups) prevent surface bacterial attachment. There was no difference between bacterial surface coverage on acrylate and methacrylate polymer materials, as both acrylate and methacrylate based materials showed a lower as well as a higher bacterial attachment [1]. Following exposure to whole blood, the majority of scaled up 'hit' materials (seven out of nine) showed a greater surface coverage with *S. aureus* strain as compared to *P. aeruginosa* strain. This can be explained by the presence of von Willebrand factor binding protein, protein A [184, 185] and fibrinogen binding protein [186] on the

surface of *S. aureus*. Therefore, adsorbed blood proteins promote *S. aureus* surface attachment.

The live-dead staining results (Figure 46) suggested that resistance to bacterial attachment is the main mechanism of action rather than killing of attached bacteria. There were some dead bacteria observed on the surface, but the majority of the attached bacteria were alive. This may be advantageous over a killing only mechanism, which is more likely to select for bacterial resistance due to the evolutionary pressures exerted on the bacteria as observed for antibiotic resistance [211]. However, further microbiology experiments, including single cell bacterial tracking and characterisation of the surface sensory transduction pathways involved, are required to determine the mechanism by which these materials prevent bacterial attachment.

6.4.2 Haemocompatibility assessment of scaled up polymer materials

Haemocompatibility is a key consideration for blood-contacting medical devices together with bacterial resistance properties. Haemocompatibility is a complex term involving various components of blood and immune system. The results presented in this Chapter examined haemocompatibility as haemostasis and activation of inflammation.

Leukocyte-platelet conjugate formation process is known to depend upon P-selectin (CD62P) expression on blood platelets and is driven by platelet activation rather than leukocyte activation [193, 212]. In general, platelet decay and platelet

activation was higher under flow conditions than under quasi-static conditions. In contrast, there was no significant difference in leukocyte-platelet conjugate formation under flow and quasi-static conditions. Interestingly the surface fibrinogen adsorption was higher under quasi-static conditions as compared to under flow conditions. This may be due to desorption of fibrinogen resulting from the flow of blood over the surfaces. Overall most of the polymer surfaces showed a lower or similar haemostasis than Teflon AF surface.

In general, immune system activation was higher under flow conditions as compared to quasi-static conditions as shown by complement C5a and leukocyte CD11b. In contrast, most of the surfaces showed a higher IgG adsorption and higher leukocyte attachment under static conditions as compared with flow conditions. However, leukocyte decay, which represents the loss of leukocytes from the blood after contact with blood, was similar under both flow and quasi-static conditions.

The combination of haemostasis and immune component results provided a better understanding of the interactions of each surface with blood. The polymer surface made up of 8(75%)A(25%) was found to be most haemocompatible out of all the scaled up polymer materials as well as the reference Teflon AF surface. Interestingly 2-ethylhexyl pendant group of monomer 8 is also present in bis(2-ethylhexyl) phthalate (DEHP), which is a widely used as a plasticiser in medical devices such as blood bags and dialysis equipment due to its excellent haemocompatibility [213]. Therefore, a good haemocompatibility shown by polymer 8(75%)A(25%) is due

to the presence of 2-ethylhexyl pendant group together with small chain ethylene glycol group.

6.5 Conclusions

- Scaled up polymer coated silicone catheters showed a lower bacterial attachment than uncoated and silver incorporated catheters.
- Co-polymer of isobornyl acrylate (75%) and tri(ethylene glycol) methyl ether methacrylate (25%) showed lowest bacterial attachment for both *P. aeruginosa* and *S. aureus.*
- Live/dead staining on one of the scaled up material indicates a resistance to bacterial attachment as the main mechanism rather than killing of the attached bacteria.
- Co-polymer of 2-ethylhexyl methacrylate (75%) and di(ethylene glycol) methyl ether methacrylate (25%) showed best haemocompatibility out of all the materials including Teflon AF.

7 Chapter 7 – *In-vivo* mouse infection model to assess hit material performance

7.1 Introduction

The *in-vitro* assessment of materials described in previous Chapters has identified the best performing bacterial resistant haemocompatible materials. However, the *in-vivo* environment is a lot more biologically complex than the *in-vitro* assay conditions. Furthermore, the tendency of a material to activate the immune system and induce an inflammatory response needs to be tested *in-vivo*.

As a medical device comes in contact with tissues and blood, non-specific protein adsorption occurs and the device is recognised as foreign material by the immune system using antibodies such as IgG, a process known as opsonisation [214, 215]. Opsonisation involves identification and labelling of foreign organisms such as bacteria or foreign surfaces in case of medical devices [136, 216]. The immune system then recognises the foreign surface and attacks the material in an attempt to isolate the material from the tissues [98, 217]. Macrophages recognise opsonised (protein-labelled) surfaces and attempt to phagocytose and digest them [76, 218]. However, due to the large size of the implanted material, individual macrophages are unable to phagocytose the material and consequently fuse together to form foreign-body giant cells. These giant macrophages then secrete cytokines and other chemotactic molecules to attract fibroblasts that deposit collagen on the surface of the implanted material [216,

219, 220]. This dense collagen layer isolates the device from rest of the tissues and causes the occlusion of the medical devices such as the lumen of a catheter. Furthermore, the foreign-body reaction usually leads to an increased inflammation at the device insertion site as well as reducing the working life-time of the device [136].

This Chapter investigates the *in-vivo* performance of the top hit material composition identified from the scaled up *in-vitro* testing described in Chapter 6. In order to progress towards the eventual clinical application of these bacterial resistant haemocompatible materials, good *in-vivo* performance is essential. In this Chapter, a mouse subcutaneous foreign-body infection model was used to test the bacterial resistance performance of best bacteria-resistant material, isobornyl acrylate-co-tri(ethylene glycol) methyl ether methacrylate (2(75%)B(25%)). The murine model used in this project was similar to that employed by Hook *et. al.* in 2012 [1].

7.1.1 Aim and objectives

The aim of these experiments was to assess the *in-vivo* bacterial resistance and biocompatibility of the best 'hit' material identified from scale-up studies. The objectives of the work described in this Chapter were as follows:

1. Test the immunogenicity of best bacteria-resistant material identified from Chapter 6.
2. Investigate the extent of the foreign-body reaction to the hit material.
3. Investigate the ability of the hit material identified from *in-vitro* assays to resist bacterial attachment *in-vivo*.
4. Test the viability of the 'hit' material as a coating on medical devices.

7.2 Experimental

7.2.1 Polymer coating on silicone catheters

Rusch Brilliant Paediatric silicone catheters (Teleflex Medical) size 8 FR, 3 mL and 31 cm length were cut into 0.75 cm length cylindrical sections. These sections were sonicated in acetone for 5 minutes. The washed catheter sections were dried and dip coated in MED1-161 silicone primer (NuSil Technology Ltd.) to improve adhesion of silicone to the polymer. The primer-coated sections were allowed to dry and activated for 15 minutes, after which the sections were dip-coated in a 30% w/v solution of polymer in DCM. The coated catheter sections were dried under vacuum at 70^{o}C for 24 hours and kept for a further five days under vacuum at room temperature to remove the solvent.

7.2.2 Mouse catheter implant model

A real-time, non-invasive catheter foreign-body implant model [221] was used to evaluate the *in-vivo* bacteria-resistant performance of hit materials. The *in-vivo* mouse infection model was used as per the licence reference 30/3238 approved by Home Office in a secure animal research facility located in Queens Medical Centre, Nottingham University hospital trust. Polymer-coated segments (0.75 cm), together with silicone uncoated segments (0.75 cm) were subcutaneously inserted into female BALB/c mice weighing 18-20 g (Charles River). The mice were allowed to recover for five

days with regular observations. After the recovery period, the animals were anaesthetized with isoflurane and injected with a bacterial inoculum in 50 µl of PBS containing either 2 x 10^6 CFUs (colony forming units) *Pseudomonas aeruginosa* (PA01-Lausanne *lux*) or 2 x 10^6 CFUs *Staphylococcus aureus* (Xen29-*lux*) (Caliper Life Sciences Inc), into the lumen of the catheter via a 29G needle and syringe. An IVIS spectrum camera (Caliper Ltd.) was used to image mice 10 minutes after injecting bacteria into the catheter lumen. Bioluminescence emitted by the bacteria inoculated into the catheters was determined every 24 hours for five days. All mice in the study were health assessed (scored) and weighed twice daily. The living image software package (Xenogen Corp.) was used to quantify the total photon emissions from the catheter implantation site over a five day period. The average radiance intensity was calculated by using the equation [p/s/cm²/sr], where p/s/cm^2 is photons ('p') per second ('s') per centimetre square (cm^2) area and 'sr' is a constant representing radiant flux on the arc emitted. The same size region of interest was used to calculate the area and quantify luminescence in all samples.

The mice were euthanised five days after bacterial inoculation and the catheter sections including the surrounding tissue were harvested. A Precellys 24 homogenizer was used to dissociate the bacteria from the tissues and biofilm from the catheter. The bacteria were removed from the catheter lumen by flushing with PBS. Viable bacterial counts (as CFUs) were generated from the tissue surrounding the infection site, bacteria associated with the catheter and bacteria internal to the lumen. All images were taken using the same acquisition parameter and scaled in the same way.

7.2.3 Scanning Electron Microscopy (SEM)

A Jeol 6060LV variable pressure scanning electron microscope (Jeol UK Ltd.) was used to scan the surface of the polymer-coated catheter sections to visualise surface topography. The samples were gold coated for four minutes prior to analysis using a Leica EM SCD005 sputter coater to achieve appropriate conductivity for the SEM to function.

7.3 Results

7.3.1 Foreign-body reaction on isobornyl acrylate (75%) tri(ethylene glycol) methyl ether methacrylate (25%) [2(75%)B(25%)]

The polymer coated and silicone uncoated catheter sections, respectively were subcutaneously implanted in mice to assess the 'foreign-body' reaction. The wound was allowed to heal for seven days and to allow a foreign-body response to occur. The mice were euthanized and the catheters were retrieved from the mice. The catheter sections were washed with PBS and analysed. The foreign-body reaction (a fibrous biological material) was observed on the silicone catheter, while the polymer-coated catheter remained largely unaffected as shown in Figure 50. The extent of the foreign-body reaction on polymer coated catheters compared with silicone can also be seen in the SEM images shown in Figure 54. In this figure, a substantially higher fibrous biological material deposition on the silicone surface is apparent compared with the polymer coating. These results show the ability of this novel polymer to prevent the foreign-body response and therefore device occlusion and inflammation compared with silicone. The polymer coating was well tolerated by the mice over the entire period of the experiments and there were no adverse immune responses observed in any of the mice used for this study.

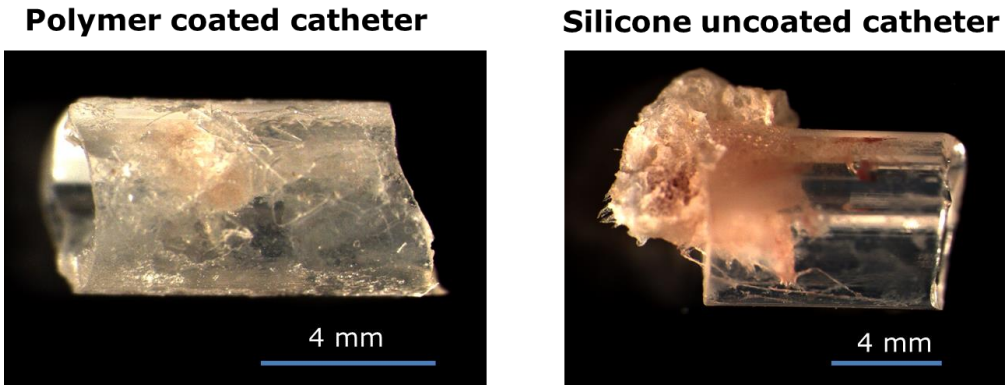


Figure 50: An optical microscope image of foreign-body reaction on subcutaneously implanted polymer (2(75%)B(25%)) coated and silicone uncoated catheters. A fibrous biological material was deposited on silicone uncoated catheter while the polymer coated catheter remained unaffected.

7.3.2 *In-vivo* bacterial attachment assays on isobornyl acrylate (75%) tri(ethylene glycol) methyl ether methacrylate (25%) [2(75%)B(25%)]

The bacterial attachment on each subcutaneously implanted catheter section colonised with *P. aeruginosa* (PA01-L) or *S. aureus* (Xen29) were imaged to detect bioluminescence as shown in Figures 51 and 52, respectively. The bioluminescence at the infection site was measured each day over a 5-day period. The body temperature of each mouse, recorded daily, was normal and no signs of sensitivity or inflammation observed at the catheter insertion site. The bioluminescence emitted from each sample was quantified by calculating average radiance (p/s/cm^2/sr) and compared with the silicone uncoated catheter. Identical average radiance (p/s/cm^2/sr) was observed for both silicone and polymer coatings on day 0 following bacterial inoculation as shown in Figures 51 and 52.

In the case of *P. aeruginosa*, on day 1 an overall reduction in average radiance was observed for both silicone and polymer coatings as shown in the top right graph in Figure 51.

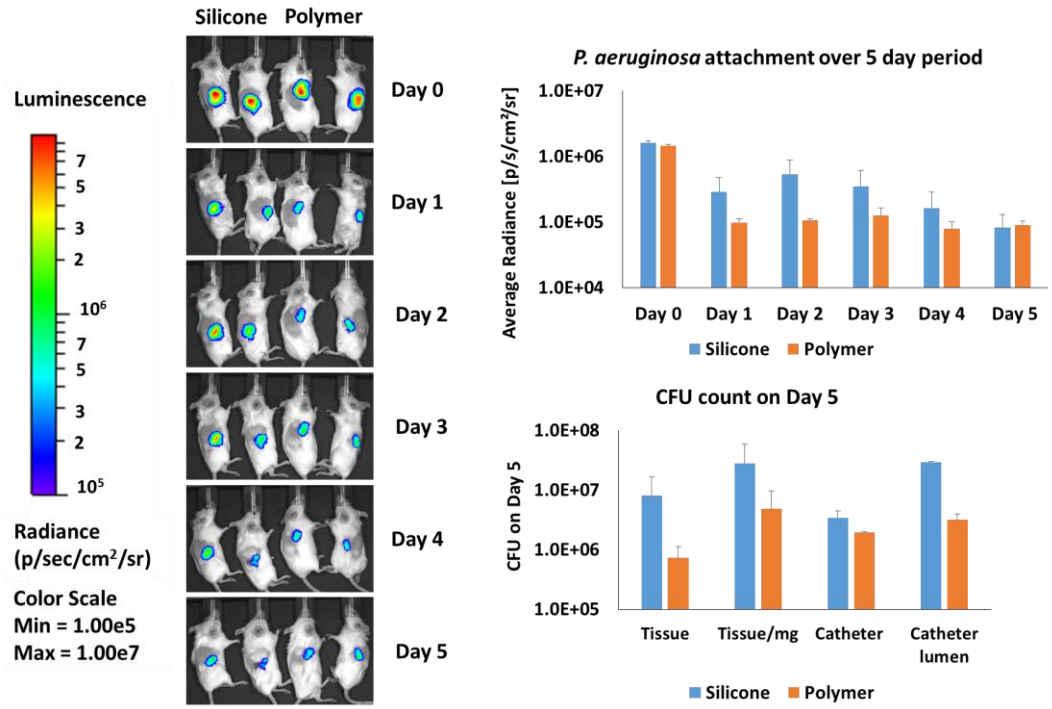


Figure 51: P. aeruginosa (PA01-L) bioluminescence measured on a polymer coated catheter compared with a silicone catheter in an in-vivo foreign-body mouse infection model over five-day period. The infection site can be seen as a fluorescence ring with varying intensity as shown by the intensity bar on the left. A blue colour represents a low luminescence and a red colour indicates higher luminescence. The bioluminescence was quantified as photons per second per cm^2. CFU were generated at day 5 and counted from the tissue around each catheter site, inside and outside the catheters. (*In-vivo* animal study was performed by Dr. Jeni Luckett).

A greater reduction in radiance was observed for the polymer-coated catheter as compared with silicone uncoated catheter. The measured average radiance on polymer-coated catheter stayed the same for next four measurements, while an increase in radiance was observed for silicone catheters. At day 5, the average radiance was similar on silicone and polymer-coated catheters. Similarly, viable count (CFUs)

measurements showed an order of magnitude lower number of PA01-L CFUs in the lumen as well as in the surrounding tissues of the polymer coated catheter as compared with silicone uncoated catheters. There was a statistically significant reduction ($p<0.05$) in bacterial viable count on the whole catheters.

In contrast to PA01-L, *S. aureus* Xen29 showed an overall increase in average radiance for both polymer-coated and silicone uncoated catheters from day 0 to day 1 as the infection established (Figure 52). The average radiance (hence, bacterial attachment) was an order of magnitude lower on polymer-coated catheters when compared with silicone uncoated catheters. This difference in average radiance stayed the same over the five day study period. Similar the PA01-L results, the polymer-coated catheter was associated with a two orders of magnitude lower viable count for Xen29 on the catheter surface as well as in the surrounding tissues when compared with silicone uncoated catheter as evident from the bottom right graph in Figure 52. In particular, the viable count was nearly two orders of magnitude lower in the surrounding tissue and on the polymer-coated catheter (as a whole) when compared with silicone surface. More importantly, a statistically significant reduction ($p<0.05$) in bacterial count was observed in the lumen of the polymer-coated catheter for *P. aeruginosa* and *S. aureus*.

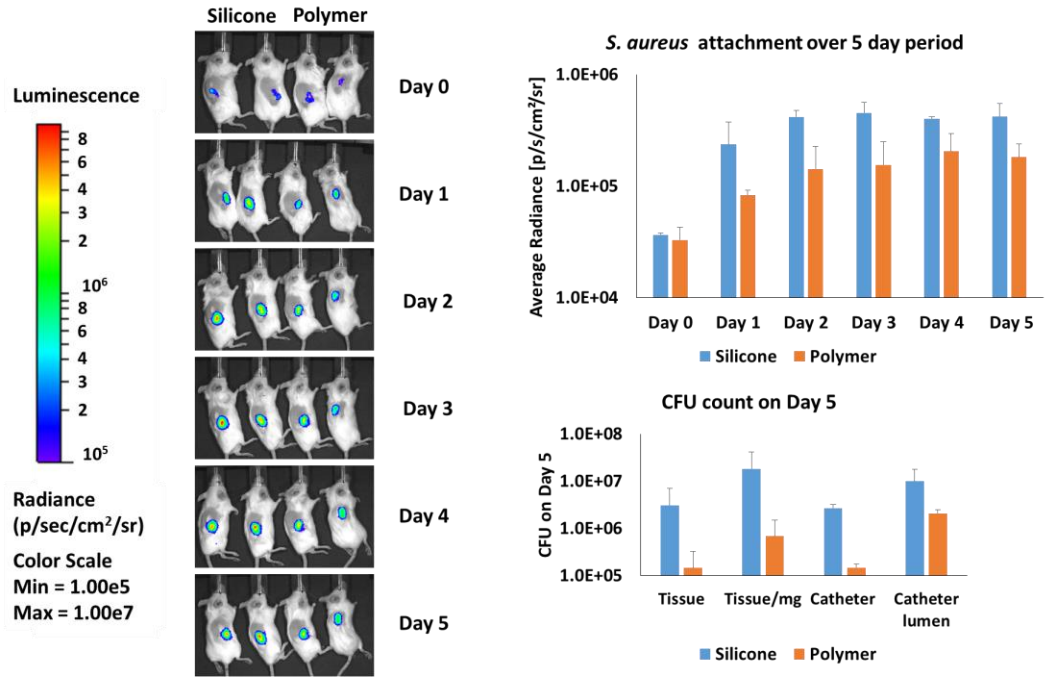


Figure 52: S. aureus (Xen29) bioluminescence from a polymer coated catheter compared with a silicone catheter in an in-vivo foreign-body mouse infection model over a five day period. The infection site can be seen as a fluorescence ring with varying intensities as shown by the intensity bar on the left. A blue colour represents low luminescence and a red colour indicates higher luminescence. The bioluminescence was quantified as photons per second per cm^2. CFU were generated at day 5 and counted from the tissue around each catheter site, inside and outside the catheters. (*In-vivo* animal study was performed by Dr. Jeni Luckett).

7.3.3 Viability of the 'hit' polymer coating on silicone catheter

To test the stability of the polymer coating, the catheter was placed in PBS at 37°C for seven days under static conditions and imaged using optical microscopy as shown in Figure 53. The coating appears uniform without major surface defects.

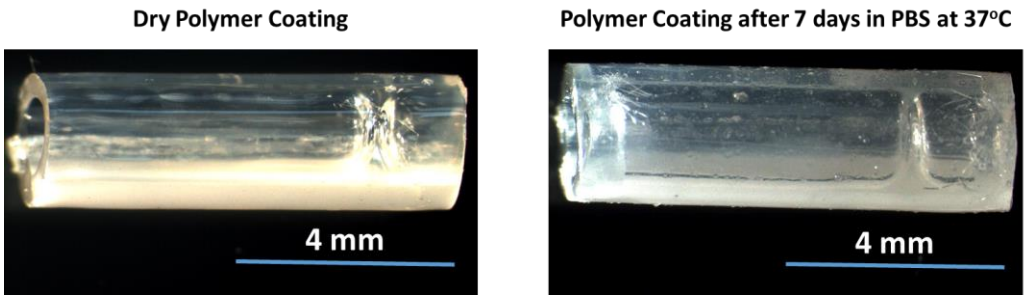


Figure 53: Isobornyl acrylate-co-tri(ethylene glycol) methyl ether methacrylate (75:25 %v/v) coated silicone catheter before and after seven days in PBS at 37°C under static conditions. The coating appears uniform without any cracks or deformation after seven days incubation. (The white reflection on dry polymer coating is due to a white guide line present on silicone catheter).

The *in-vitro* analysis of the stability of the polymer coating (Figure 53) showed no major changes in surface appearance of the coating. However, following subcutaneous implantation into mice over a seven day period, the retrieved polymer coated sample was cracked (Figure 50). The movement of mice and the compression of tissues around the implantation site may have caused the cracking. To further investigate this brittleness, a scanning electron microscope was used to obtain images of the polymer coating before and after subcutaneous implantation in mice over a two week period as shown in Figure 54. The dry polymer coating appears uniform and smooth before subcutaneous implantation without any surface defects. In contrast, cracks in the coating can be seen in the SEM images (second row in Figure 54) following a two week subcutaneous implantation. However, upon agitation with ceramic beads (used to remove bacteria from the catheters for CFU experiments), major surface defects in polymer coating can be seen in the SEM images (third row in Figure 54). These results indicate that the mechanical properties of the polymer coating needs to be optimised to act as a viable coating for medical devices.

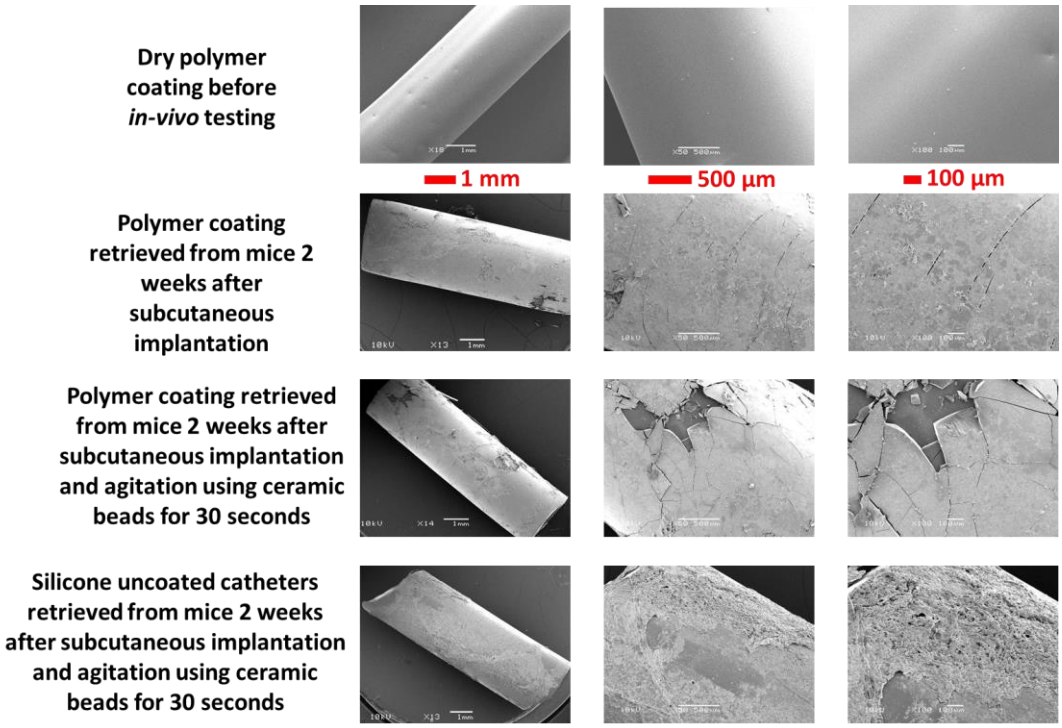


Figure 54: Scanning electron microscope images of the 'hit' polymer coating before and after in-vivo testing compared with silicone catheter. The cracks were visible upon retrieval of the coated catheters from mice after two weeks. The agitation with ceramic beads caused considerable damage to the coating as seen from the images in third row above. The agitation step was performed to remove bacteria from the catheter samples for viable count determination, but also indicate the durability of the coating under extreme conditions. A large amount of fibrous biological material was observed on silicone catheters compared with the polymer-coated samples. (Electron microscopy was performed by Mrs Christine Grainger-Boultby).

7.4 Discussion

7.4.1 Foreign-body response to the polymer coated catheter

Isobornyl acrylate (75%) tri(ethylene glycol) methyl ether methacrylate (25%) [2(75%)B(25%)] coated catheters were well tolerated by mice without any local or systemic adverse reactions. The lack of a foreign-body response on the coated catheters confirms the good biocompatibility of this polymer material. Foreign-body reaction is very common on implantable medical devices and by preventing this effect, biocompatibility and the device life-time can be improved [98, 136, 216]. Although the isobornyl acrylate - tri(ethylene glycol) methyl ether methacrylate co-polymer showed a tendency to activate the immune system in *in-vitro* experiments (Figure 49 (b)), this material did not show any adverse immune responses in an *in-vivo* mouse model based on twice daily health assessment scores. The *in-vitro* data for polymer 2(75%)B(25%) in Section 6.3.4 showed very low haemostasis, but a significantly higher surface leukocyte adhesion than Teflon AF (Figure 49), which has a tendency to activate the complement system. However, the *in-vivo* experiments showed good biocompatibility and minimal foreign-body reaction on this polymer coated surface.

7.4.2 *In-vivo* foreign-body infection model

Isobornyl acrylate (75%) tri(ethylene glycol) methyl ether methacrylate (25%) [2(75%)B(25%)] showed an order of magnitude reduction in bacterial attachment for both *P. aeruginosa* and *S. aureus* over a five day period, when compared with silicone. In the case of *P. aeruginosa* (Figure 51), similar radiance was observed on silicone and polymer coated catheters on day 5. As the radiance value measures total luminescence from the inoculation site, this measurement does not reflect the bacteria attached to the catheter or the surrounding tissues. Therefore, a viable count estimation was carried out to determine bacterial numbers on the catheter, in the catheter lumen and on the tissue surrounding the catheter. The tissues harvested around the implanted catheters showed an order of magnitude reduction in CFU count on the polymer-coated catheter as compared with silicone. One important point to note is that the inoculum used (2×10^6 CFU) is likely to be several orders of magnitude higher than a device is likely to be exposed to in a clinical setting. The inoculum dose was also 20 times higher than used by Hook *et. al.*[1], who observed nearly two orders of magnitude reduction in bacterial numbers on the 'hit' polymer-coated catheter when compared to silicone as shown in Figure 55. The polymer-coated catheter also showed an order of magnitude reduction in bacteria viable counts in the tissues surrounding the implant, spleen and kidneys.

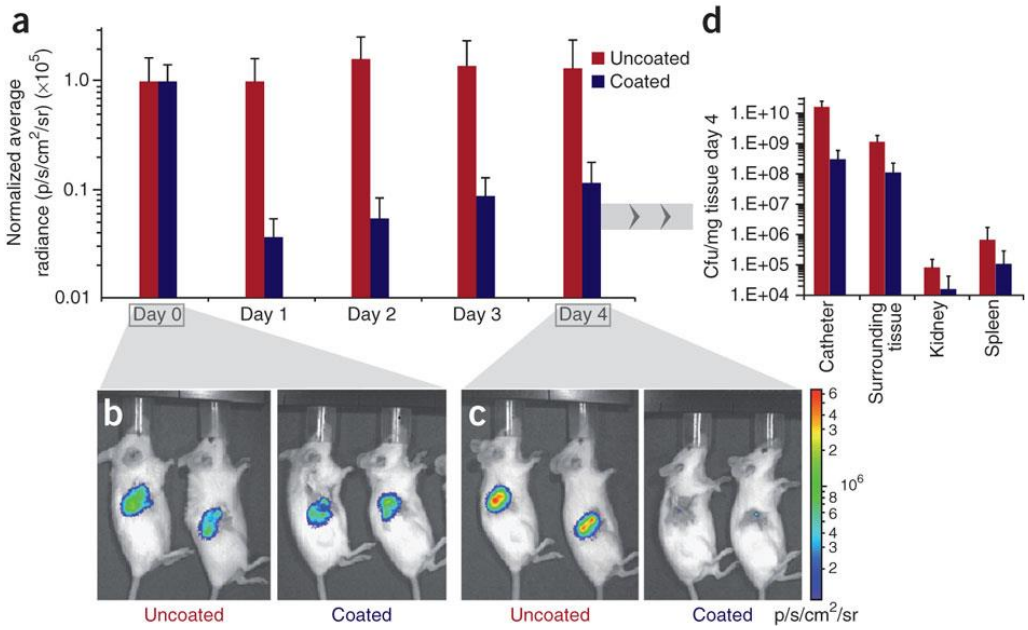


Figure 55: *In-vivo* performance of polymer material in a foreign-body response model used by Hook *et. al.* for a comparison with the 'hit' polymer material used in this thesis.

Furthermore, the infection model described in this thesis using isobornyl acrylate-co-tri(ethylene glycol) methyl ether methacrylate was tested over a five day period compared with the four day period used by Hook *et. al.* [1]. Even after day 5, a significant reduction in bacterial attachment was observed both on the catheter as well as in the surrounding tissues. Furthermore, even after day 5, the *S. aureus* viable count on the hit material tested in this thesis (Figure 52) is three orders of magnitude lower ($1x10^5$ vs $1x10^8$) than the material tested in Hook *et. al*. (Figure 55 d). This demonstrates the bacteria resistant properties of the isobornyl acrylate-co-tri(ethylene glycol) methyl ether methacrylate. As this polymer is optimised to be applied as a coating on blood-contacting medical devices, the bacterial resistance performance of this material needs to be tested under blood flow conditions in a suitable *in-vivo* model such as a rat model used by Chauhan *et. al.* [46].

7.4.3 Suitability of the 'hit' polymer as a coating on medical devices

Bacterial attachment and haemocompatibility experiments have identified a number of haemocompatible materials with good bacteria attachment resistance. However, the mechanical properties of these polymer materials needs to be taken into account when choosing a polymer for coating medical devices. For example the glass transition temperature (Tg) of a polymer is an important parameter that determines the brittleness of a coating [222]. The glass transition temperature of a polymer is the temperature below which a material becomes hard and brittle like glass and above Tg the material turns into soft, flexible rubbery material [223].

A polymer coating on a vascular catheter must be flexible and not brittle. Furthermore the coating must be durable and able to bear the stresses of device sterilisation, transportation, handling by healthcare practitioners and biological conditions inside the human body. As an example, polymer material isobornyl acrylate (75%) tri(ethylene glycol) methyl ether methacrylate (25%) showed excellent bacterial resistance and haemocompatibility, however, the predicted Tg of this polymer (using Fox Equation - $1/Tg = W1/Tg1 + W2/Tg2 + \ldots$ (where W is weight fractions of each monomers and Tg's are in Kelvin) [224]) is 50 ^{o}C [225]. This means that the polymer coating is likely to be glassy and brittle at body temperature. Therefore, the mechanical properties of the coatings need to be optimised before choosing a haemocompatible bacterial resistant material for application on blood-contacting medical devices. The flexibility of a coating can be fine-tuned by co-

polymerising the monomer with a low Tg material to achieve an overall lower Tg. As an example, Adlington *et. al.* [226] used diethylene glycol methyl ether methacrylate (DEGMA) to lower the Tg of five bacteria resistant (meth)acrylate materials, including isobornyl methacrylate. This study showed that the flexibility of (meth)acrylate polymers can be fine-tuned to a similar level as silicone catheter using a low Tg monomer, while retaining the bacterial resistant properties. The measured Tg of isobornyl methacrylate/DEGMA (75:25 %v/v) was 74 ^{o}C, which was reduced to 25 ^{o}C at 50:50 and -10 ^{o}C at 75:25 composition. The *in-vitro* percentage bacterial coverage of isobornyl methacrylate/DEGMA at 75:25 ratio was less than 0.5% for *P. aeruginosa*, *S. aureus* and *E. coli*. There was a general increase in % bacterial coverage as the DEGMA ratio was increased from 25 to 75 %v/v and was measured to be ~5% at 50:50 and ~10% at 25:75 (isobornyl methacrylate:DEGMA), which was significantly lower than silicone surface (~30%). This study indicated that there is a fine balance between addition of an inert low Tg material to achieve desired physical properties while retaining the bacterial resistance properties.

7.5 Conclusions

- Isobornyl acrylate-co-tri(ethylene glycol) methyl ether methacrylate (75:25) showed good biocompatibility and was well tolerated in an *in-vivo* mouse subcutaneous model.
- The polymer coating on silicone catheter prevented the foreign-body reaction as evident from optical and electron microscopy.
- Polymer coating showed an order of magnitude lower surface bacterial counts for both *P. aeruginosa* and *S. aureus* bacteria when compared with silicone.
- The polymer coating showed signs of cracking following two week subcutaneous implantation in mice.
- The mechanical properties and response to bodily fluids (leaching) of the scaled up polymers needs to be tested *in-vivo* to assess suitability as a coating on medical devices such as vascular catheters.

8 Chapter 8 – Conclusions and future work

8.1 Summary

Biofilm formation on blood-contacting medical devices is a major healthcare problem causing a significant mortality and morbidity in hospitalised patients. The current clinical practice measures such as the use of antibiotics are insufficient to prevent biofilm formation. The replacement of an infected device proves costly as well as a significant discomfort for the patient. Furthermore, the currently used blood-contacting medical devices such as vascular catheters are prone to thrombosis formation leading to device occlusion, reducing the working life-time of a device. Due to ever increasing antibiotic resistance and a fear of post-antibiotic era, novel biomaterials that resist surface bacterial attachment and biofilm formation are needed. However, the mechanism of bacteria-surface interactions is not fully understood yet. Therefore, a high-throughput material microarray technique allows hundreds of novel biomaterials to be screened efficiently.

Following the successful optimisation and printing of a polymer microarray, the next step was to test haemocompatibility of these materials. Haemocompatibility is an umbrella term covering the interactions of a material with various blood proteins, cells and immune components. It has been shown that the presence of blood proteins on a surface leads to increased bacterial attachment and biofilm formation [16, 17, 102, 173, 227] as shown in Section 5.3.1. The microarray was incubated in human blood and the interaction of each material

with blood proteins such as fibrinogen, blood cells e.g. platelets, immune cells such as leukocytes and antibodies as well as complement system were studied as described in Chapter 4. Co-polymer compositions made up of small chain glycol monomers showed better haemocompatibility than longer chain glycol monomers and zwitterionic materials. Similarly, the co-polymers of monomers 1 to 16 with short chain glycols, showed a lower bacterial attachment as compared to longer chain oligoethylene glycols and zwitterionic materials. There was no correlation between wettability of a surface and its relative bacterial attachment in this diverse materials library. This reinforced the previous finding that bacterial attachment is a complex process depending on a range of different surface properties.

By collating the bacterial and haemocompatibility results, nine 'hit' materials were identified for scale up polymerisation. The scaled up materials were then used to coat silicone venous catheters and were tested for *in-vitro* haemocompatibility and surface bacterial attachment as presented in Chapter 6. All of the scaled up materials showed a lower bacterial attachment than silicone uncoated catheters and commercial silver containing catheter. The live-dead staining results indicated that a resistance to bacterial attachment rather than killing the attached bacteria, is responsible for a low bacterial attachment on 'hit' surfaces. Haemocompatibility testing on scaled up 'hit' materials showed varying trends with some surfaces showing a low coagulation but higher immunogenicity and *vice-versa*. Polymer composition isobornyl acrylate-co-tri(ethylene glycol) methyl ether methacrylate (75:25) showed lowest bacterial attachment for *P. aeruginosa* and *S. aureus* out of all nine 'hit' materials. Polymer composition 2-ethylhexyl methacrylate-co-

di(ethylene glycol) methyl ether methacrylate (75:25) showed excellent haemocompatibility by having a low haemostasis as well as a very low immunogenicity.

In-vivo mice foreign-body infection results were promising with polymer composition isobornyl acrylate-co-tri(ethylene glycol) methyl ether methacrylate (75:25) showing minimal foreign-body fibrous deposition when compared with silicone surface. The polymer coating also showed a good biocompatibility without any local or systemic adverse events when subcutaneously implanted in mice. The foreign-body infection model showed an order of magnitude lower bacterial attachment on the surface of polymer coated catheter as compared to silicone catheter surface. Furthermore, the CFU results showed an order of magnitude lower bacteria viable counts in the surrounding tissues for both *P. aeruginosa* and *S. aureus* bacterial strains.

8.2 Recommendations for future work

The high-throughput screening approach developed in this thesis has identified a number of bacterial resistant haemocompatible materials. These 'hit' materials were chosen based upon low surface attachment with two bacterial species: *P. aeruginosa* and *S. aureus*. These novel polymer materials need to be tested with other biofilm forming bacterial strains and clinical isolates. The *in-vivo* foreign-body infection model results were promising with Isobornyl acrylate – tri(ethylene glycol) methyl ether methacrylate co-polymer showing good biocompatibility and a statistically significant reduction in surface bacterial attachment than silicone surface. The

histology data from foreign body infection model is still needs to be analysed to establish the extent of inflammation at the catheter insertion site.

The application of 'hit' material on blood-contacting medical devices requires the evaluation of the *in-vivo* performance of these materials under blood flow conditions, using a suitable animal model such as a rat blood flow model [46, 99]. The polymer coated catheter ideally needs to be placed in central vein of an animal and inoculated with *P. aeruginosa* or *S. aureus* bacterial strains to test the bacterial resistant efficacy under blood flow conditions.

The mechanical properties of 'hit' material requires optimisation to prevent brittleness and cracking as a bacterial resistant coating on medical devices such as venous catheter. The mechanical properties such as Tg of a polymer can be lowered by mixing it with an inert low Tg material as shown by Adlington *et. al.* [226]. However, this method of adding inert material can reduce bacterial resistant ability of 'hit' material and may lead to reduced biological performance. Another approach is to chemically linking the 'hit' material onto the surface of a device by 'grafting to' or 'grafting from' method using thiol-ene chemistry as shown by Magennis *et. al*. [228]. These chemical grafting methods modify the surface of a medical device and deposit monolayers of the 'hit' material on the surface. The advantage of this chemically modification is that the device retains its mechanical properties and as a result there is no cracking of the polymer material as seen with dip coating method, which apply 50-100 µm thick surface coating.

The exact cellular and molecular level mechanism of bacterial resistant properties of these materials needs to be further investigated. As the initial attachment of bacteria on a surface is a key step in biofilm formation, further understanding of this step is essential to understand the mechanism of action of anti-attachment properties of these surfaces. Differential Interference Contrast (DIC) and Total Internal Reflective Fluorescence (TIRF) microscopy can be used to track the motility of a single bacterial cell on a surface. Understanding these initial bacterial interactions with surfaces will provide novel insights into mechanism of bacterial resistant properties of surfaces. This will contribute to the design of novel anti-attachment surfaces based on structure-activity relationship.

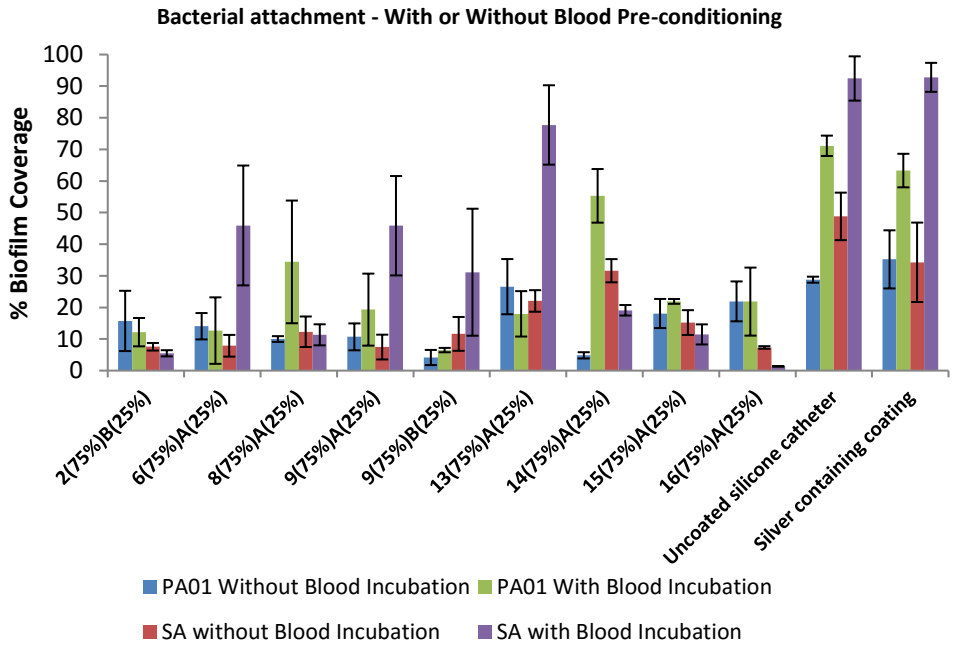
ToF-SIMS surface analysis of polymer microarray spots has yielded vast amount of data in the form of ion fragments for each polymer material. ToF-SIMS data, together with bacterial attachment data, can be used to perform multivariate analysis such as Partial Least Square regression (PLS). PLS analysis allows to link the surface chemistry with biological performance in the form of a statistical model. Therefore, PLS model can be used predict biological performance of various chemical functionalities within a 'hit' material molecule. This would then permit structure activity relationship analysis for chemical functionalities important for preventing bacterial attachment and help to design novel bacterial resistant materials. The knowledge of key chemical functionalities that prevent bacterial attachment and biofilm formation would allow *in-silico* design of novel bacterial resistant polymer materials for biomedical applications.

Furthermore, the polymer materials with high bacterial attachment can be used to screen for other biomedical applications such as stem cell attachment and as a platform for stem cell growth and differentiation. To a similar note, materials with high surface bacterial attachment can be further developed as surfaces to remove bacteria from a fluid such as blood during dialysis by flowing the fluid over these surfaces that attract bacteria.

9 Appendices

9.1 Appendix A: Bacterial attachment on scaled up polymer materials, silicone and silver containing catheters with and without blood pre-incubation.

The effect of blood incubation step prior to biofilm setup can be seen in figure below. In general there was higher biofilm coverage on blood pre-conditioned surfaces as compared to the surfaces without blood incubation step (n=3).



9.2 Appendix B: *In-vivo* bacterial attachment on 2-ethylhexyl methacrylate (75%) di(ethylene glycol) methyl ether methacrylate (25%) [8(75%)A(25%)]

Subcutaneously implanted polymer coated catheter sections colonised with *P. aeruginosa* (PA01-L) and *S. aureus* (Xen29) were imaged to detect bioluminescence from each sample as shown in Figure 56. The bioluminescence at the infection site was measured each day over five day period. The body temperature of each mouse, recorded daily, was normal and these were no sign of sensitivity or inflammation overserved at the catheter insertion site. The bioluminescence detected from each sample was quantified by calculating p/s/cm^2/sr and compared as shown in Figure 57. There was no significant difference in bioluminescence detected from polymer coated samples when compared with the silicone uncoated samples for material 8(75%)A(25%). These results indicated that the best haemocompatible material identified from a high throughput screening was biocompatible but failed to reduce bacterial attachment *in-vivo* when compared with silicone catheter.

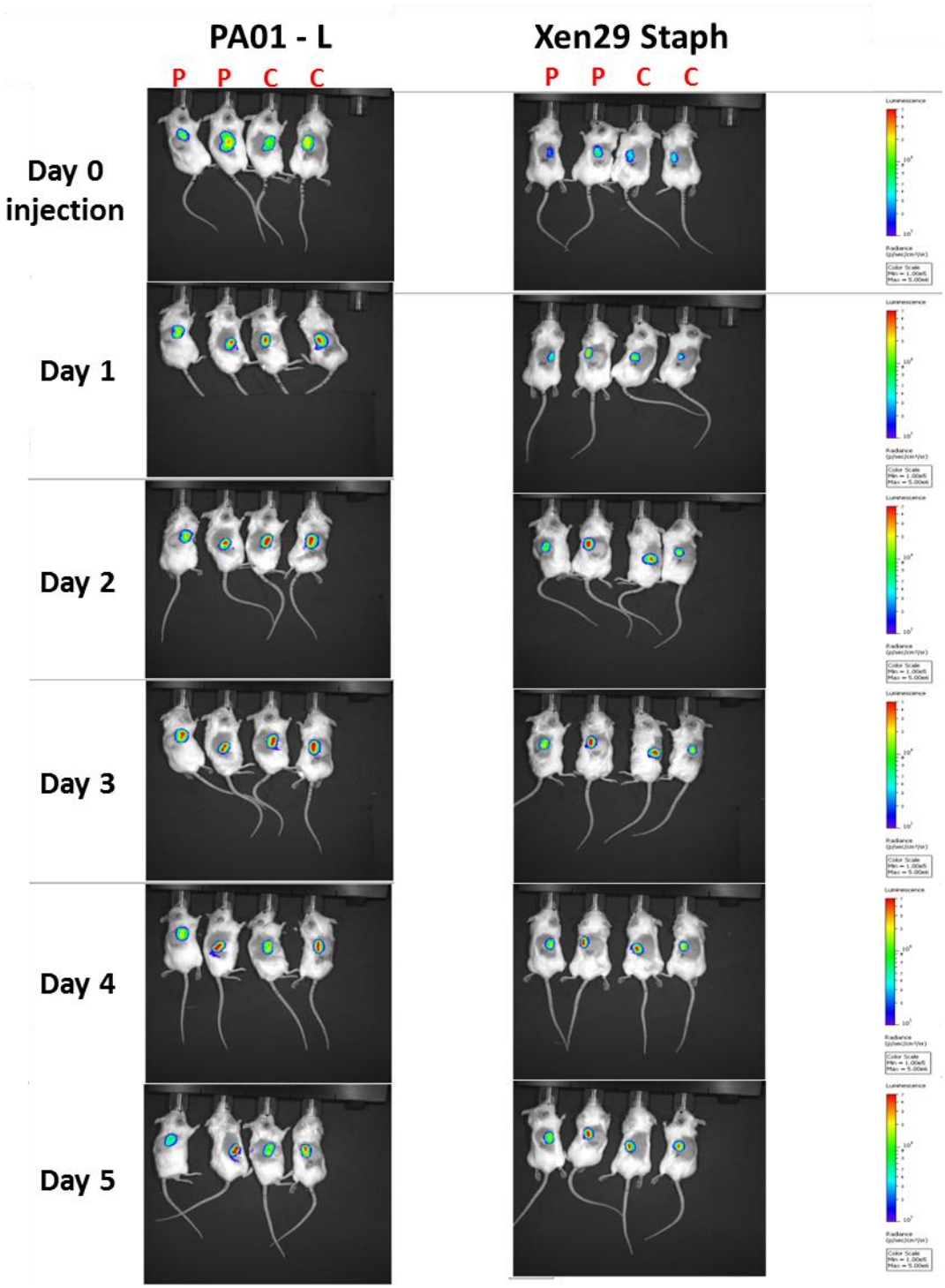


Figure 56: IVIS scanner images showing *in-vivo* biofilm experimental setup for polymer 8(75%)A(25%) over five day period. The infection site can be seen as a fluorescence ring with varying intensity as shown by the intensity bar on the right. A blue colour represents a low luminescence and a red colour indicates higher luminescence. Two repeats of polymer coated samples (labelled as 'P') and control silicone uncoated catheters (labelled as 'C') were used for each bacterial strain.

The overall bioluminescence was appear to increase from day 1 to day 5 as bacteria colonise the catheter and multiply to form biofilms. This trend is more evident for Xen 29 *S. aureus* strain than PA01 strain.

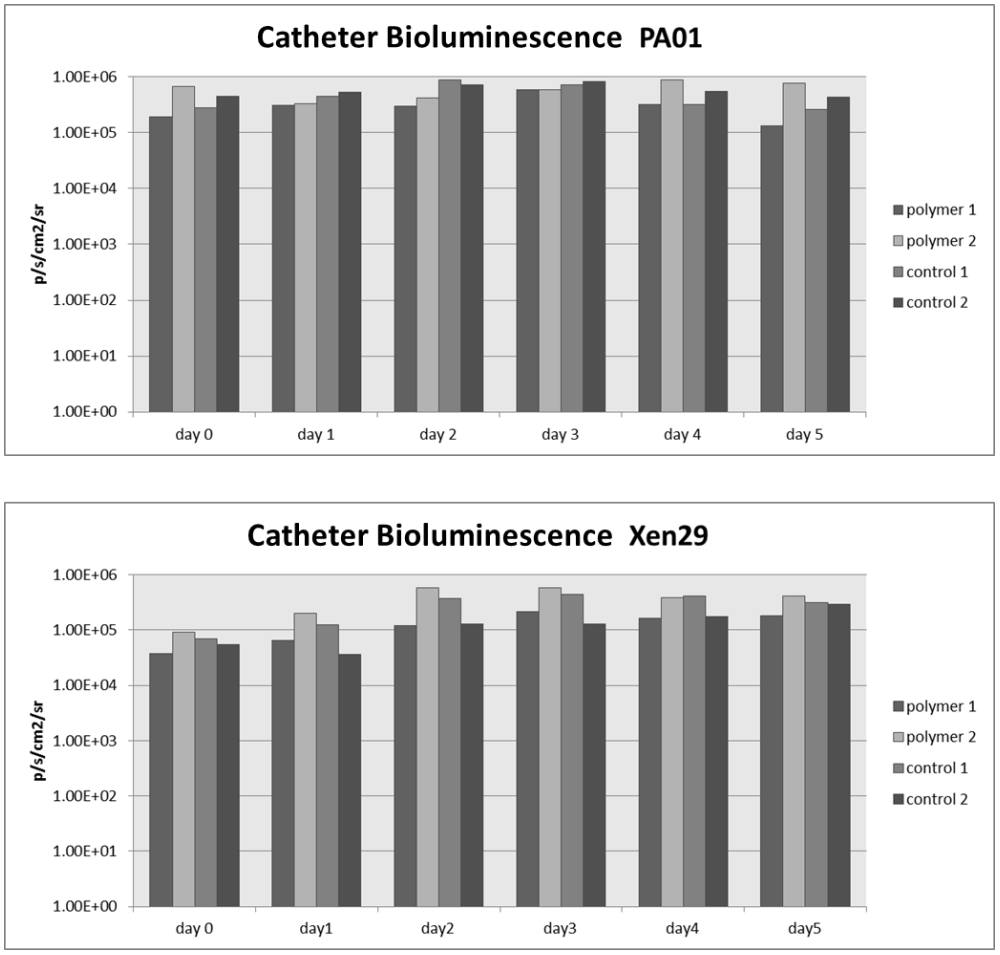


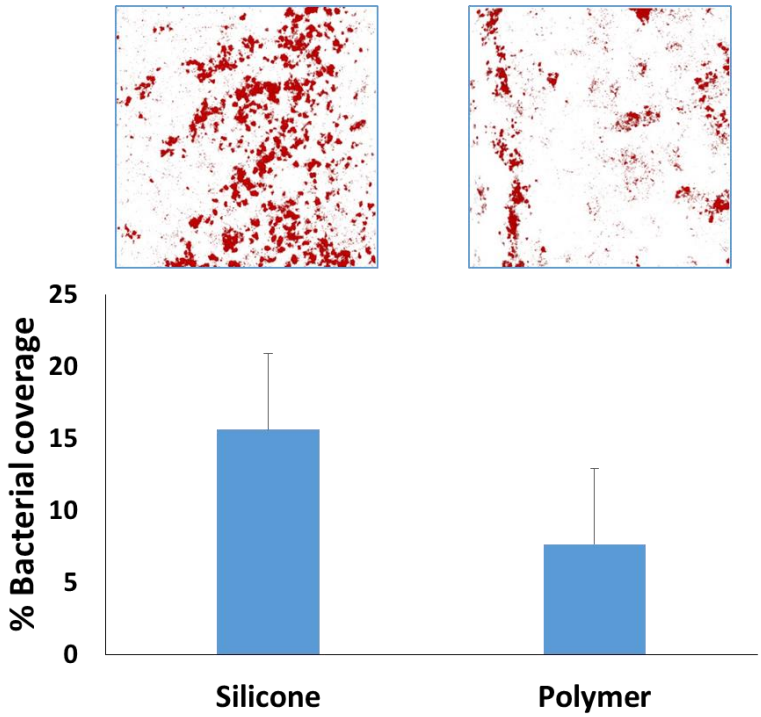
Figure 57: Bioluminescence from two repeats of polymer coated and control samples subcutaneously implanted in mice, measured using an IVIS spectrum camera and quantified using living image software package over five day period. PA01 represents *P. aeruginosa* and Xen29 is a *S. aureus* strain.

9.3 Appendix C: Comparison of foreign-body response pre-conditioning vs whole blood pre-conditioning on *in-vitro* biofilm formation

To look at the effect of foreign-body response pre-conditioning step on biofilm formation, polymer coated and silicone uncoated catheters were subcutaneously inserted in mice for five days to allow the wound healing. After day 5, the catheters were harvested from mice and incubated in *P. aeruginosa* (PA01-L) in RPMI media at 37^{o}C for 72 hours as per the *in-vitro* biofilm protocol described in Section 5.2.2. The results show a lower % surface coverage of PA01-L on silicone after subcutaneous condition as compared to whole blood incubation step. However, the thickness of biofilm was double on subcutaneously conditioned silicon than on blood conditioned silicone and polymer coated catheters, as shown below.

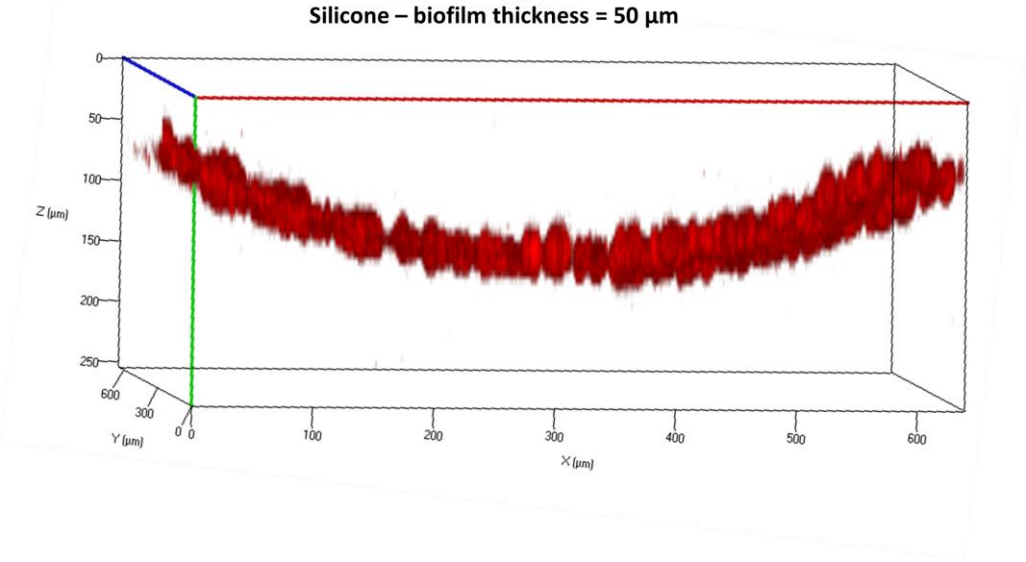
PA01-L 72 hours biofilm following 7 day subcutaneous insertion in mice pre-conditioning step

- **Small difference in surface coverage**
- **Double the thickness on silicone than polymer**



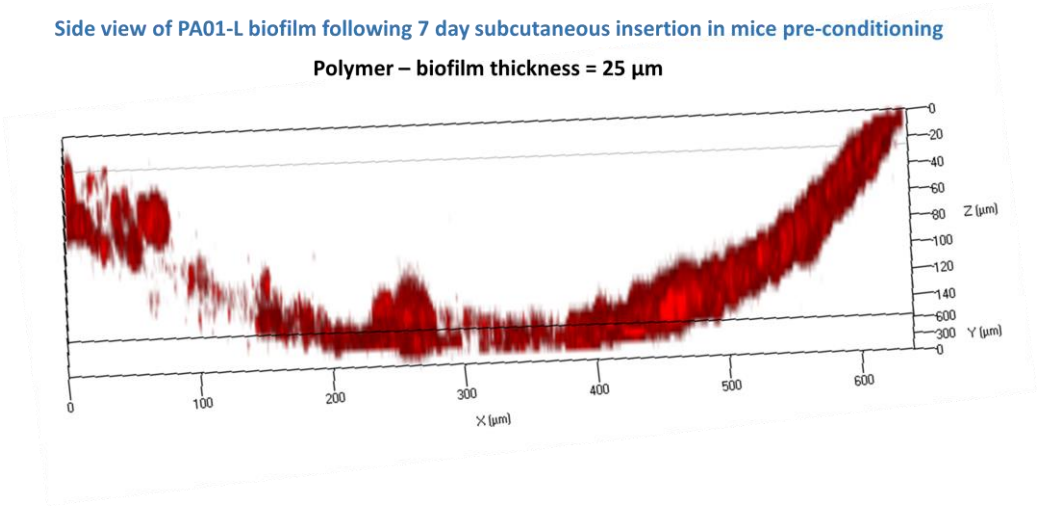
Side view of PA01-L biofilm following 7 day subcutaneous insertion in mice pre-conditioning

Silicone – biofilm thickness = 50 µm



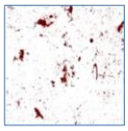
Side view of PA01-L biofilm following 7 day subcutaneous insertion in mice pre-conditioning

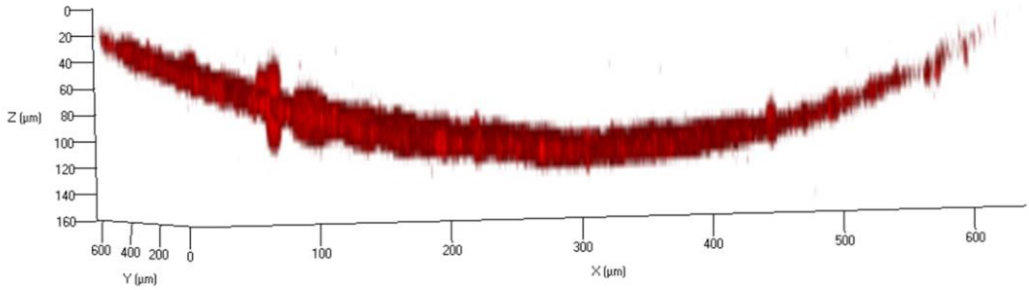
Polymer – biofilm thickness = 25 µm



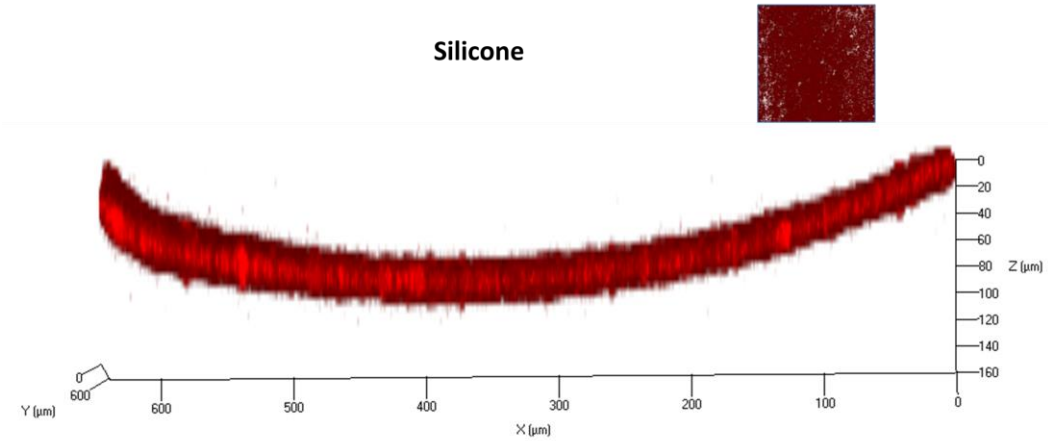
Side view of PA01-L biofilm – Following whole blood pre-conditioning

Isobornyl acrylate-co-TEGMA (75:25)

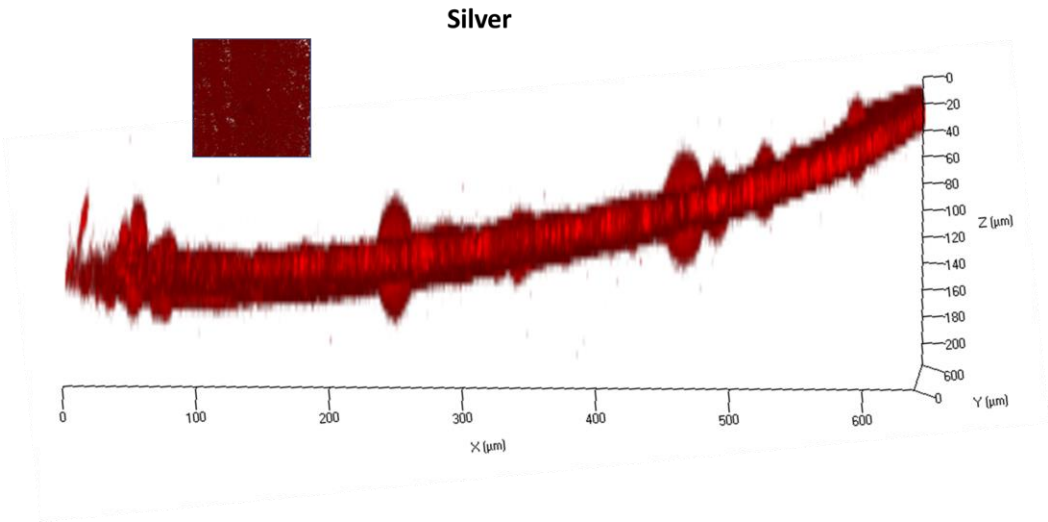




Side view of PA01-L biofilm – Following whole blood pre-conditioning



Side view of PA01-L biofilm – Following whole blood pre-conditioning



9.4 Appendix D: AIBN mediated polymerisation to scale up 'hit' compositions

Materials:

- Major Monomer – 75.2 mL
- Minor Monomer – 20.8 mL

- AIBN (Initiator) – 240 mg
- PhCoBF (Catalyst) – 10 mg
- Toluene (Solvent) – 200 mL
- Total Reaction Volume = 300 mL (Recalculate volumes/quantities for other volumes)
- Hexane (For precipitation after polymerisation)
- Round bottom flask OR Schlenk tube

Method:

- Weigh out / measure all the materials in required quantities as listed above
- Add a stirring magnet into a round bottom flask or a Schlenk tube (depending in polymerisation volume)
- Add AIBN and PhCoBF into a round a bottom flask or Schlenk tube
- Add major monomer (more volume) into the flask or Schlenk tube first followed by minor monomer (less volume)
- Then add the required volume of Toluene into the same flask or tube
- Cover the neck of flask or tube with a rubber septum
- Insert a long needle attached to Nitrogen or Argon through the septum and insert a smaller needle into the septum to release the pressure
- Turn on gas and allow a steady flow of gas through the mixture in the flask or tube for 30 minutes
- After 30 minutes, remove long needle and attach a balloon filled with Argon or Nitrogen to the smaller needle for positive flow of inert gas in the reaction mixture
- Lower the flask or tube into the paraffin oil bath at 80^{o}C (turned on and stabilised 30 minutes before starting),

stirring at a constant speed with oil level two mm below the liquid level in the flask or tube

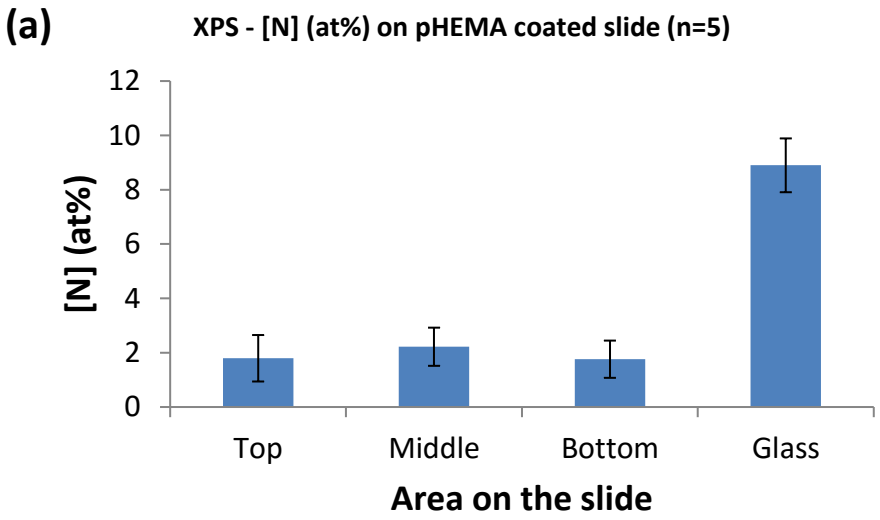
- Leave the reaction running overnight for completion (takes about 8 hours to complete)
- Following overnight polymerisation reaction, take the flask or tube out of the oil bath and leave for a few minutes for oil from outside of the flask to drip into the oil bath
- Keep small volume of polymer solution to do GPC and NMR to confirm polymerisation
- Put Hexane in a 500 mL beaker (4 x volume of polymer in flask or Schlenk tube) along with a magnetic stirrer
- Put the Hexane in ICE tub and allow it to cool down
- Transfer the polymer solution from flask or tube into a separation funnel
- While stirring at a high speed, add the polymer solution into the Hexane in a dripwise manner.
- The polymer should precipitate as white coloured substance and any unpolymerised monomer will dissolve in hexane
- Continue the step 17 until all the polymer solution has transferred from separation funnel into the Hexane
- Keep the hexane beaker with precipitated polymer still at room temperature for 30 minutes for polymer to settle down at the bottom of the beaker
- Decant the hexane and dispose via appropriate waste route and allow the remaining hexane to evaporate in the fume hood for two hours
- Dry the polymer in the vacuum oven for two hours
- Once dry, dissolve the polymer in DCM to make 20%-30% w/v solution to dip coat silicone catheters

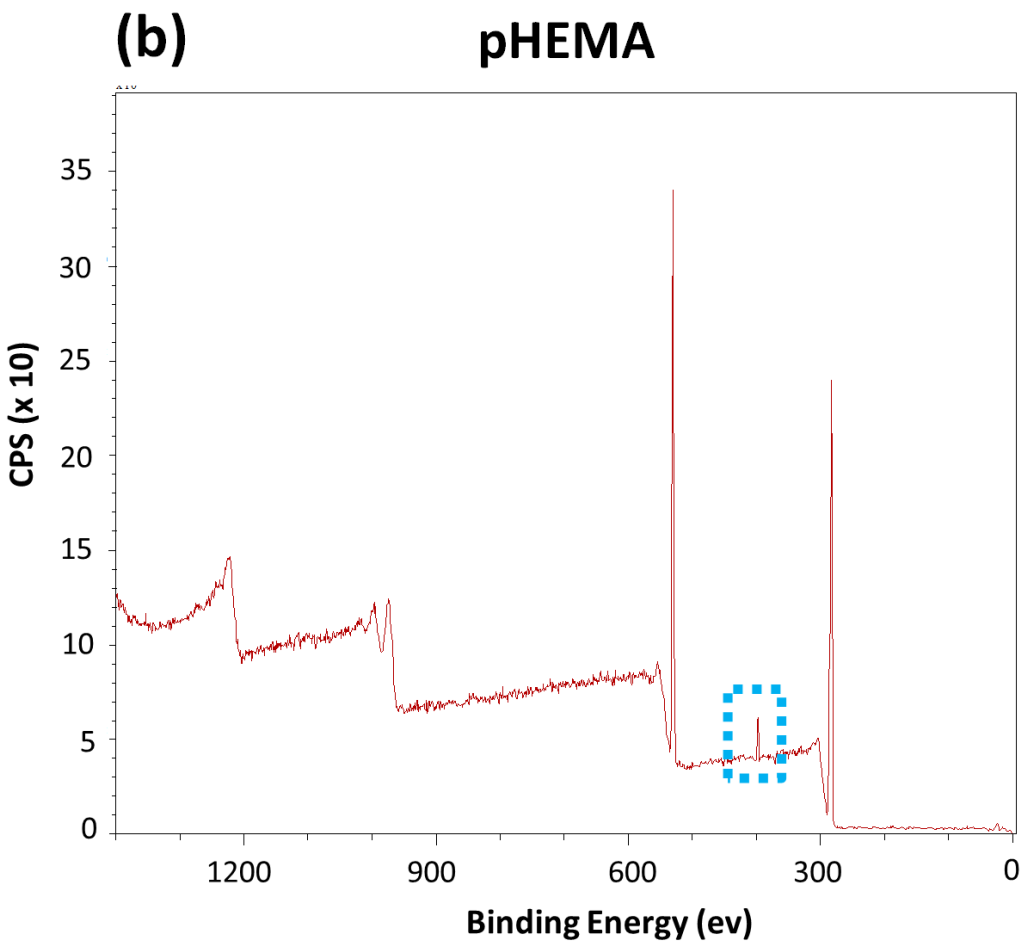
9.5 Appendix E: Polymerisation % conversion and molecular weights

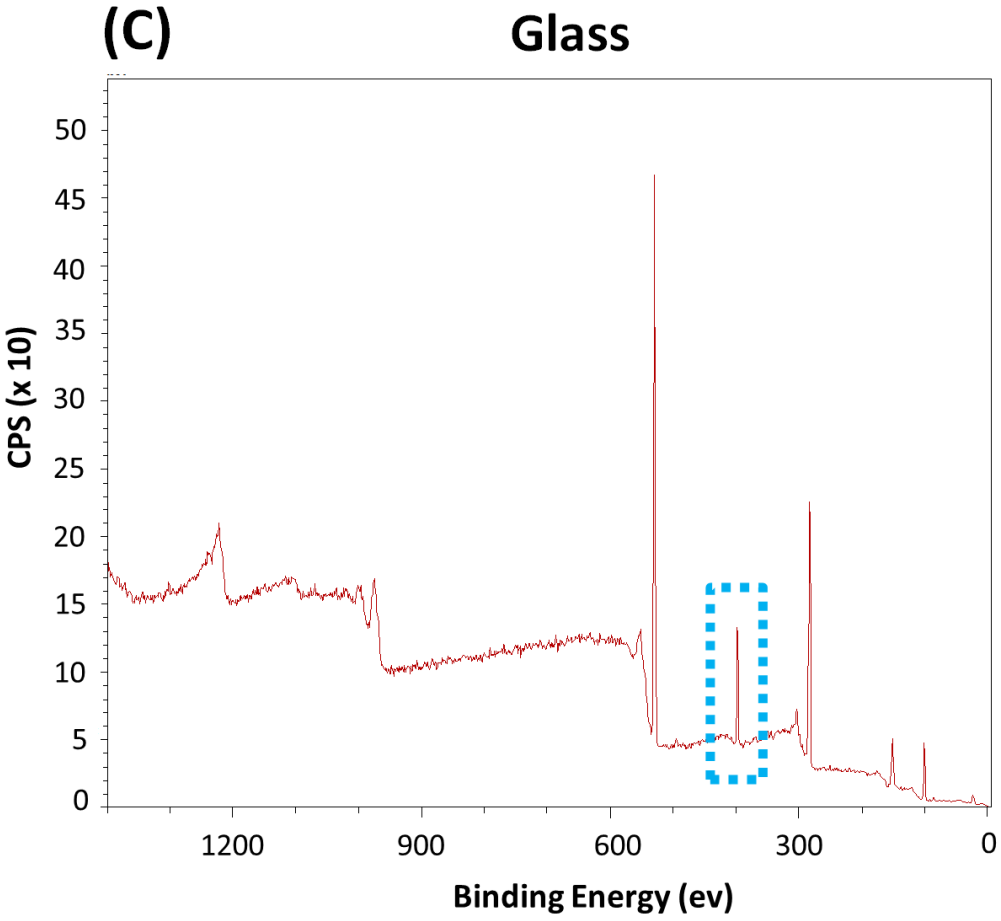
'Hit' material composition	NMR data	GPC data
2(75%)B(25%)	% Conversion = 53%	Mw = 21934, Mn = 5834, PD = 3.75968
6(75%)A(25%)	% Conversion = 83%	Mw = 29507, Mn = 11003, PD = 2.68172
8(75%)A(25%)	% Conversion = 79%	Mw = 13438, Mn = 8221, PD = 1.63459
9(75%)A(25%)	% Conversion = 75%	Mw = 11667, Mn = 5316, PD = 2.1947
9(75%)B(25%)	% Conversion = 68%	Mw = 20074, Mn = 8872, PD = 2.26262
13(75%)A(25%)	% Conversion = 88%	Mw = 94719, Mn = 16875, PD = 5.61298
14(75%)A(25%)	% Conversion = 82%	Mw = 12512, Mn = 7501, PD = 1.66804
15(75%)A(25%)	% Conversion = 55%	Mw = 14378, Mn = 8253, PD = 1.74215
16(75%)A(25%)	% Conversion = 93%	Mw = 15762, Mn = 8191 , PD = 1.92431

9.6 Appendix F: The effectiveness of washing procedure following plasma/blood incubation

A pHEMA coated slide was incubated in plasma for two hours and washed with PBS and water. The slide was analysed by XPS to determine [N] (at%) at top, middle and bottom of the slide to determine the variability in [N] (at%). The pHEMA uncoated end of glass slide was also analysed. Any variability in measurements at three different areas of the slide would be due to washing step. This was important to make sure that the washing step would not affect the XPS measurements. Figure (a) below shows the average XPS [N] (at%) at three different areas on pHEMA slide compared to uncoated glass. The measurements emphasise the low-fouling properties of pHEMA surface. Figures (b) and (c) show the XPS spectrum taken from of pHEMA and glass surface after plasma incubation with Nitrogen peak highlighted.

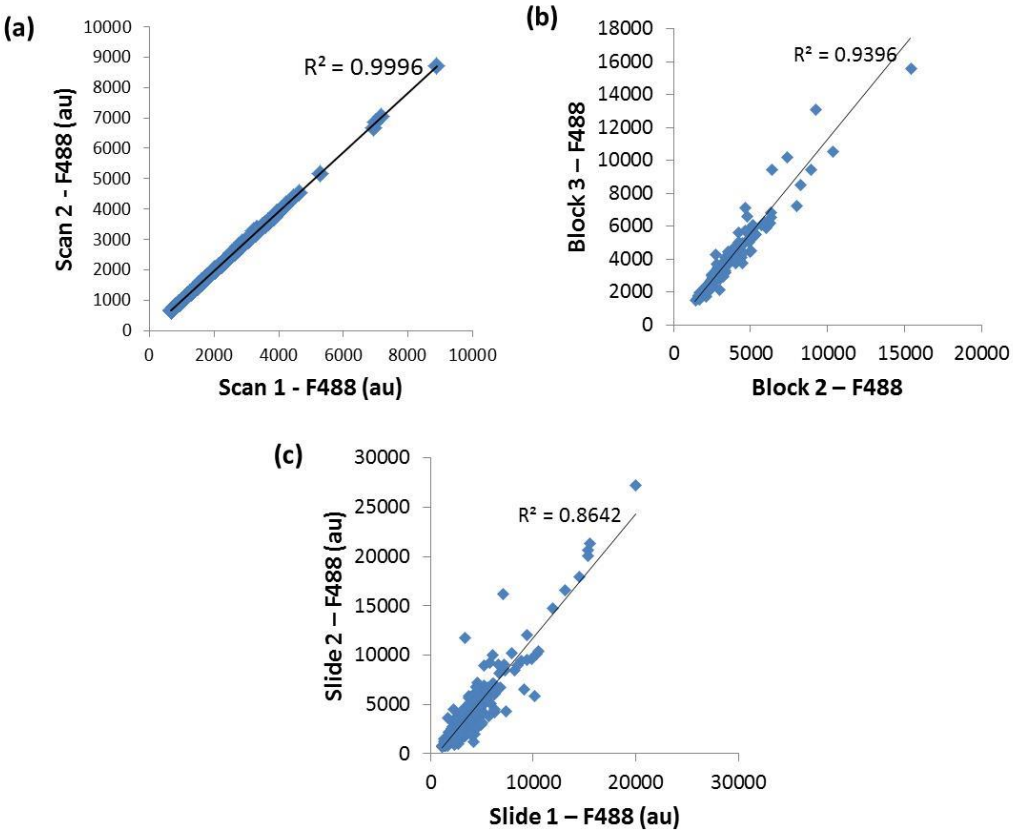



(b)
pHEMA
CPS (x 10)
35
30
25
20
15
10
5
0
1200
900
600
300
0
Binding Energy (ev)


(C)
Glass
CPS (x 10)
50
45
40
35
30
25
20
15
10
5
0
1200
900
600
300
0
Binding Energy (ev)

9.7 Appendix G: Fluorescence scanner and software reproducibility test

To test the reproducibility of the scanner, software as well as the printed microarray, the replicate blocks on same slide were scanned. Two different microarrays printed under same conditions were also scanned to investigate intra-slide variations. (a) Same block scanned twice and analysed using Genepix Pro software, (b) Two replicates printed on same slide scanned for inter-slide variations, (c) Two microarray slides printed under same conditions for intra-slide variations.



10 References

[1] Hook, A.L.; Chang, C.Y.; Yang, J.; Luckett, J.; Cockayne, A.; Atkinson, S.; Mei, Y.; Bayston, R.; Irvine, D.J.; Langer, R.; Anderson, D.G.; Williams, P.; Davies, M.C.; Alexander, M.R., Combinatorial discovery of polymers resistant to bacterial attachment. *Nature Biotechnology,* **2012**, *30*, (9), 868-U899.

[2] Hook, A.L.; Chang, C.-Y.; Yang, J.; Luckett, J.; Cockayne, A.; Atkinson, S.; Mei, Y.; Bayston, R.; Irvine, D.; Langer, R.; Anderson, D.G.; Williams, P.; Davies, M.C.; Alexander, M.R., Combinatorial discovery of polymers resistant to bacterial attachment. *Nature Biotechnology,* **2012**, *30*, (9), 868-875.

[3] Hook, A.L.; Chang, C.Y.; Yang, J.; Atkinson, S.; Langer, R.; Anderson, D.G.; Davies, M.C.; Williams, P.; Alexander, M.R., Discovery of novel materials with broad resistance to bacterial attachment using combinatorial polymer microarrays. *Advanced Materials,* **2013**, *25*, (18), 2542-2547.

[4] Guggenbichler, J.P.; Assadian, O.; Boeswald, M.; Kramer, A., Incidence and clinical implication of nosocomial infections associated with implantable biomaterials - catheters, ventilator-associated pneumonia, urinary tract infections. *GMS Krankenhaushygiene interdisziplinar,* **2011**, *6*, (1), Doc18.

[5] Baskin, J.L.; Pui, C.-H.; Reiss, U.; Wilimas, J.A.; Metzger, M.L.; Ribeiro, R.C.; Howard, S.C., Management of occlusion and thrombosis associated with long-term indwelling central venous catheters. *Lancet,* **2009**, *374*, (9684), 159-169.

[6] Hartkamp, A.; van Boxtel, A.J.H.; Zonnenberg, B.A.; Witteveen, P.O., Totally implantable venous access devices: evaluation of complications and a prospective comparative study of two different port systems. *Netherlands Journal of Medicine,* **2000**, *57*, (6), 215-223.

[7] Bouza, E.; Burillo, A.; Munoz, P., Catheter-related infections: diagnosis and intravascular treatment. *Clinical Microbiology and Infection,* **2002**, *8*, (5), 265-274.

[8] Stone, P.W., Economic burden of healthcare-associated infections: an American perspective. *Expert review of pharmacoeconomics & outcomes research,* **2009**, *9*, (5), 417-422.

[9] Davies, D., Understanding biofilm resistance to antibacterial agents. *Nature Reviews Drug Discovery,* **2003**, *2*, (2).

[10] Donlan, R.M., Biofilms and device-associated infections. *Emerging Infectious Diseases,* **2001**, *7*, (2), 277-281.

[11] O'Grady, N.P.; Alexander, M.; Dellinger, E.P.; Gerberding, J.L.; Heard, S.O.; Maki, D.G.; Masur, H.; McCormick, R.D.; Mermel, L.A.; Pearson, M.L.; Raad, II; Randolph, A.; Weinstein, R.A., Guidelines for the prevention of intravascular catheter-related infections. *American Journal of Infection Control,* **2002**, *30*, (8), 476-489.
[12] Tacconelli, E.; Smith, G.; Hieke, K.; Lafuma, A.; Bastide, P., Epidemiology, medical outcomes and costs of catheter-related bloodstream infections in intensive care units of four European countries: literature- and registry-based estimates. *Journal of Hospital Infection,* **2009**, *72*, (2), 97-103.
[13] NHS Scotland (Accessed 13/10/2012) www.nes.scot.nhs.uk/education-and-training/by-theme-initiative/healthcare-associated-infections/online-short-courses/preventing-catheter-related-bloodstream-infections.aspx.
[14] Donlan, R.M., Biofilm formation: A clinically relevant microbiological process. *Clinical Infectious Diseases,* **2001**, *33*, (8), 1387-1392.
[15] Donlan, R.M., Biofilms on central venous catheters: Is eradication possible? *Bacterial Biofilms,* **2008**, *322*.
[16] Aoki, E.E.; Pizzolitto, A.C.; Garcia, L.B.; Pizzolitto, E.L., Stpahylococcus aureus biofilms on central venous haemodialysis catheters. *Brazilian Journal of Microbiology,* **2005**, *36*, (4).
[17] Crump, J.A.; Collignon, P.J., Intravascular catheter-associated infections. *European Journal of Clinical Microbiology & Infectious Diseases,* **2000**, *19*, (1).
[18] O'Gara, J.P.; Humphreys, H., Staphylococcus epidermidis biofilms: importance and implications. *Journal of Medical Microbiology,* **2001**, *50*, (7).
[19] Costerton, J.W.; Lewandowski, Z.; Caldwell, D.E.; Korber, D.R.; Lappinscott, H.M., Microbial biofilms. *Annual Review of Microbiology,* **1995**, *49*, 711-745.
[20] Donlan, R.M., Biofilms: Microbial life on surfaces. *Emerging Infectious Diseases,* **2002**, *8*, (9), 881-890.
[21] Donelli, G.; De Paoli, P.; Fadda, G.; Marone, P.; Nicoletti, G.; Varaldo, P.E.; Grp, C.V.C.S., A multicenter study on central venous catheter-associated infections in Italy. *Journal of Chemotherapy,* **2001**, *13*.
[22] Weiss, R.L., Structure and occurrence of pili (fimbriae) on pseudomonas aeruginosa. *Journal of General Microbiology,* **1971**, *67*, (AUG), 135-&.
[23] Keizer, D.W.; Slupsky, C.M.; Kalisiak, M.; Campbell, A.P.; Crump, M.P.; Sastry, P.A.; Hazes, B.; Irvin, R.T.; Sykes, B.D., Structure of a pilin monomer from Pseudomonas aeruginosa - Implications for the assembly of pili. *Journal of Biological Chemistry,* **2001**, *276*, (26), 24186-24193.

[24] Folkhard, W.; Marvin, D.A.; Watts, T.H.; Paranchych, W., Structure of polar pili from pseudomonas aeruginosa strain-K and strain-O. *Journal of Molecular Biology,* **1981**, *149*, (1), 79-93.
[25] Donelli, G., Vascular catheter-related infection and sepsis. *Surgical infections,* **2006**, *7 Suppl 2*.
[26] Casey, A.L.; Mermel, L.A.; Nightingale, P.; Elliott, T.S.J., Antimicrobial central venous catheters in adults: a systematic review and meta-analysis. *Lancet Infectious Diseases,* **2008**, *8*, (12).
[27] Souza Antunes, A.L.; Bonfanti, J.W.; Rodrigues Perez, L.R.; Ferreira Pinto, C.C.; Peixoto de Freitas, A.L.; Macedo, A.J.; Barth, A.L., High vancomycin resistance among biofilms produced by Staphylococcus species isolated from central venous catheters. *Memorias Do Instituto Oswaldo Cruz,* **2011**, *106*, (1).
[28] Costerton, J.W.; Stewart, P.S.; Greenberg, E.P., Bacterial biofilms: A common cause of persistent infections. *Science,* **1999**, *284*, (5418), 1318-1322.
[29] Smith, A.W., Biofilms and antibiotic therapy: Is there a role for combating bacterial resistance by the use of novel drug delivery systems? *Advanced Drug Delivery Reviews,* **2005**, *57*, (10).
[30] Dwyer, A., Surface-treated catheters - a review. *Seminars in Dialysis,* **2008**, *21*, (6).
[31] Davies, D.G.; Geesey, G.G., Regulation of the alginate biosynthesis gene ALGC in pseudomonas-aeruginosa during biofilm development in continuous-culture. *Applied and Environmental Microbiology,* **1995**, *61*, (3), 860-867.
[32] Becker, P.; Hufnagle, W.; Peters, G.; Herrmann, M., Detection of differential gene expression in biofilm-forming versus planktonic populations of Staphylococcus aureus using micro-representational-difference analysis. *Applied and Environmental Microbiology,* **2001**, *67*, (7), 2958-2965.
[33] Prigent-Combaret, C.; Vidal, O.; Dorel, C.; Lejeune, P., Abiotic surface sensing and biofilm-dependent regulation of gene expression in Escherichia coli. *Journal of Bacteriology,* **1999**, *181*, (19), 5993-6002.
[34] Ryan, M.L.; Thorson, C.M.; King, D.R.; Van Haren, R.M.; Manning, R.J.; Andrews, D.M.; Livingstone, A.S.; Proctor, K.G., Insertion of central venous catheters induces a hypercoagulable state. *Journal of Trauma and Acute Care Surgery,* **2012**, *73*, (2).
[35] Burns, K.E.A.; McLaren, A., A critical review of thromboembolic complications associated with central venous catheters. *Canadian Journal of Anaesthesia-Journal Canadien D Anesthesie,* **2008**, *55*, (8).

[36] Kuter, D.J., Thrombotic complications of central venous catheters in cancer patients. *Oncologist,* **2004**, *9*, (2).
[37] Gorbet, M.B.; Sefton, M.V., Biomaterial-associated thrombosis: roles of coagulation factors, complement, platelets and leukocytes. *Biomaterials,* **2004**, *25*, (26), 5681-5703.
[38] Nygren, H., Initial reactions of whole blood with hydrophilic and hydrophobic titanium surfaces. *Colloids and Surfaces B-Biointerfaces,* **1996**, *6*, (4-5), 329-333.
[39] Nygren, H.; Tengvall, P.; Lundstrom, I., The initial reactions of TiO2 with blood. *Journal of Biomedical Materials Research,* **1997**, *34*, (4), 487-492.
[40] Vroman, L.; Adams, A.L., Findings with recording ellipsometer suggesting rapid exchange of specific plasma proteins at liquid/solid interfaces. *Surface Science,* **1969**, *16*, 438-&.
[41] Vroman, L.; Adams, A.L., Identification of rapid changes at plasma-solid interfaces. *Journal of biomedical materials research,* **1969**, *3*, (1), 43-67.
[42] Hirsh, S.L.; McKenzie, D.R.; Nosworthy, N.J.; Denman, J.A.; Sezerman, O.U.; Bilek, M.M.M., The Vroman effect: Competitive protein exchange with dynamic multilayer protein aggregates. *Colloids and Surfaces B-Biointerfaces,* **2013**, *103*, 395-404.
[43] Zelzer, M.; Albutt, D.; Alexander, M.R.; Russell, N.A., The Role of Albumin and Fibronectin in the Adhesion of Fibroblasts to Plasma Polymer Surfaces. *Plasma Processes and Polymers,* **2012**, *9*, (2), 149-156.
[44] Davenport, A., What are the anticoagulation options for intermittent hemodialysis? *Nature Reviews Nephrology,* **2011**, *7*, (9), 499-508.
[45] Ademovic, Z.; Wei, J.; Winther-Jensen, B.; Hou, X.L.; Kingshott, P., Surface modification of PET films using pulsed AC plasma polymerisation aimed at preventing protein adsorption. *Plasma Processes and Polymers,* **2005**, *2*, (1), 53-63.
[46] Chauhan, A.; Bernardin, A.; Mussard, W.; Kriegel, I.; Esteve, M.; Ghigo, J.-M.; Beloin, C.; Semetey, V., Preventing biofilm formation and associated occlusion by biomimetic glycocalyxlike polymer in central venous catheters. *Journal of Infectious Diseases,* **2014**, *210*, (9), 1347-1356.
[47] Mermel, L.A.; Allon, M.; Bouza, E., Clinical practice guidelines for the diagnosis and management of intravascular catheter-related infection: 2009 update by the Infectious Diseases Society of America (vol 49, pg 1, 2009). *Clinical Infectious Diseases,* **2010**, *50*, (7), 1079-1079.

[48] Justo, J.A.; Bookstaver, P.B., Antibiotic lock therapy: review of technique and logistical challenges. *Infection and drug resistance,* **2014**, *7*, 343-363.
[49] Safdar, N.; Maki, D.G., The commonality of risk factors for nosocomial colonization and infection with antimicrobial-resistant Staphylococcus aureus, enterococcus, gram-negative bacilli, Clostridium difficile, and Candida. *Annals of Internal Medicine,* **2002**, *136*, (11), 834-844.
[50] Safdar, N.; Maki, D.G., Use of vancomycin-containing lock or flush solutions for prevention of bloodstream infection associated with central venous access devices: A meta-analysis of prospective, randomized trials. *Clinical Infectious Diseases,* **2006**, *43*, (4), 474-484.
[51] Ferreira Chacon, J.M.; de Almeida, E.H.; Simoes, R.d.L.; Ozorio, V.L.C.; Alves, B.C.; Mello de Andrea, M.L.; Biernat, M.S.; Biernat, J.C., Randomized study of minocycline and edetic acid as a locking solution for central line (Port-A-Cath) in children with cancer. *Chemotherapy,* **2011**, *57*, (4), 285-291.
[52] Raad, I.I.; Fang, X.; Keutgen, X.M.; Jiang, Y.; Sherertz, R.; Hachem, R., The role of chelators in preventing biofilm formation and catheter-related bloodstream infections. *Current Opinion in Infectious Diseases,* **2008**, *21*, (4).
[53] Carcao, M.D.; Connolly, B.L.; Chait, P.; Stain, A.M.; Acebes, M.; Massicotte, P.; Blanchette, V.S., Central venous catheter-related thrombosis presenting as superior vena cava syndrome in a haemophilic patient with inhibitors. *Haemophilia,* **2003**, *9*, (5).
[54] Talsma, S.S., Biofilms on medical devices. *Home healthcare nurse,* **2007**, *25*, (9).
[55] Bayston, R.; Grove, N.; Siegel, J.; Lawellin, D.; Barsham, S., Prevention of hydrocephalus shunt catheter colonization in-vitro by impregnation with antimicrobials. *Journal of Neurology Neurosurgery and Psychiatry,* **1989**, *52*, (5), 605-609.
[56] Bayston, R.; Fisher, L.E.; Weber, K., An antimicrobial modified silicone peritoneal catheter with activity against both Gram positive and Gram negative bacteria. *Biomaterials,* **2009**, *30*, (18), 3167-3173.
[57] Medtronic Ares antibiotic-impregnated catheters. (28/07/2016),
[58] Heard, S.O.; Wagle, M.; Vijayakumar, E.; McLean, S.; Brueggemann, A.; Napolitano, L.M.; Edwards, L.P.; O'Connell, F.M.; Puyana, J.C.; Doern, G.V., Influence of triple-lumen central venous catheters coated with chlorhexidine and silver sulfadiazine on the incidence of catheter-related bacteremia. *Archives of Internal Medicine,* **1998**, *158*, (1), 81-87.

[59] Weng, M.; Zhu, M.; Chen, W.; Miao, C., Life-threatening anaphylactic shock due to chlorhexidine on the central venous catheter: a case series. *International Journal of Clinical and Experimental Medicine,* **2014**, *7*, (12), 5930-5936.
[60] Guleri, A.; Kumar, A.; Morgan, R.J.M.; Hartley, M.; Roberts, D.H., Anaphylaxis to chlorhexidine-coated central venous catheters: a case series and review of the literature. *Surgical Infections,* **2012**, *13*, (3), 171-174.
[61] FDA http://www.fda.gov/MedicalDevices/Safety/AlertsandNotices/PublicHealthNotifications/ucm062306.htm (30/11),
[62] Moffat, C.F.; Long, W.F.; Williamson, F.B., Chemically modified heparins of defined structure. *Thrombosis Research,* **1986**, 92-92.
[63] Casu, B., Structure of heparins and their fragments. *Nouvelle Revue Francaise D Hematologie,* **1984**, *26*, (4), 211-219.
[64] Liang, O.D.; Ascencio, F.; Fransson, L.A.; Wadstrom, T., BINDING OF HEPARAN-SULFATE TO STAPHYLOCOCCUS-AUREUS. *Infection and Immunity,* **1992**, *60*, (3), 899-906.
[65] Wu, H.; Moser, C.; Wang, H.-Z.; Hoiby, N.; Song, Z.-J., Strategies for combating bacterial biofilm infections. *International Journal of Oral Science,* **2015**, *7*, (1), 1-7.
[66] Dubern, J.-F.; Diggle, S.P., Quorum sensing by 2-alkyl-4-quinolones in Pseudomonas aeruginosa and other bacterial species. *Molecular Biosystems,* **2008**, *4*, (9), 882-888.
[67] O'Loughlin, C.T.; Miller, L.C.; Siryaporn, A.; Drescher, K.; Semmelhack, M.F.; Bassler, B.L., A quorum-sensing inhibitor blocks Pseudomonas aeruginosa virulence and biofilm formation. *Proceedings of the National Academy of Sciences of the United States of America,* **2013**, *110*, (44), 17981-17986.
[68] Cevizci, R.; Duzlu, M.; Dundar, Y.; Noyanalpan, N.; Sultan, N.; Tutar, H.; Bayazit, Y.A., Preliminary results of a novel quorum sensing inhibitor against pneumococcal infection and biofilm formation with special interest to otitis media and cochlear implantation. *European Archives of Oto-Rhino-Laryngology,* **2015**, *272*, (6), 1389-1393.
[69] Kalia, D.; Merey, G.; Nakayama, S.; Zheng, Y.; Zhou, J.; Luo, Y.; Guo, M.; Roembke, B.T.; Sintim, H.O., Nucleotide, c-di-GMP, c-di-AMP, cGMP, cAMP, (p)ppGpp signaling in bacteria and implications in pathogenesis. *Chemical Society Reviews,* **2013**, *42*, (1), 305-341.
[70] Romling, U.; Galperin, M.Y.; Gomelsky, M., Cyclic di-GMP: the first 25 years of a universal bacterial second messenger. *Microbiology and Molecular Biology Reviews,* **2013**, *77*, (1), 1-52.
[71] Hengge, R., Principles of c-di-GMP signalling in bacteria. *Nature Reviews Microbiology,* **2009**, *7*, (4), 263-273.

[72] Sampath, L.A.; Tambe, S.M.; Modak, S.M., In vitro and in vivo efficacy of catheters impregnated with antiseptics or antibiotics: Evaluation of the risk of bacterial resistance to the antimicrobials in the catheters. *Infection Control and Hospital Epidemiology,* **2001**, *22*, (10), 640-646.
[73] Sanni, O.; Chang, C.-Y.; Anderson, D.G.; Langer, R.; Davies, M.C.; Williams, P.M.; Williams, P.; Alexander, M.R.; Hook, A.L., Bacterial attachment to polymeric materials correlates with molecular flexibility and hydrophilicity. *Advanced Healthcare Materials,* **2015**, *4*, (5), 695-701.
[74] Wiencek, K.M.; Fletcher, M., Bacterial adhesion to hydroxyl-terminated and methyl-terminated alkanethiol self-assembled monolayers. *Journal of Bacteriology,* **1995**, *177*, (8), 1959-1966.
[75] Hook, A.L.; Anderson, D.G.; Langer, R.; Williams, P.; Davies, M.C.; Alexander, M.R., High throughput methods applied in biomaterial development and discovery. *Biomaterials,* **2010**, *31*, (2), 187-198.
[76] Smith, R.S.; Zhang, Z.; Bouchard, M.; Li, J.; Lapp, H.S.; Brotske, G.R.; Lucchino, D.L.; Weaver, D.; Roth, L.A.; Coury, A.; Biggerstaff, J.; Sukavaneshvar, S.; Langer, R.; Loose, C., Vascular catheters with a nonleaching poly-sulfobetaine surface modification reduce thrombus formation and microbial attachment. *Science Translational Medicine,* **2012**, *4*, (153), 10.
[77] Li, P.; Poon, Y.F.; Li, W.F.; Zhu, H.Y.; Yeap, S.H.; Cao, Y.; Qi, X.B.; Zhou, C.C.; Lamrani, M.; Beuerman, R.W.; Kang, E.T.; Mu, Y.G.; Li, C.M.; Chang, M.W.; Leong, S.S.J.; Chan-Park, M.B., A polycationic antimicrobial and biocompatible hydrogel with microbe membrane suctioning ability. *Nature Materials,* **2011**, *10*, (2), 149-156.
[78] Jia, Z.S.; Shen, D.F.; Xu, W.L., Synthesis and antibacterial activities of quaternary ammonium salt of chitosan. *Carbohydrate Research,* **2001**, *333*, (1), 1-6.
[79] Heller, M.J., DNA microarray technology: Devices, systems, and applications. *Annual Review of Biomedical Engineering,* **2002**, *4*, 129-153.
[80] Yang, L.N.; Guo, S.J.; Li, Y.; Zhou, S.M.; Tao, S.C., Protein microarrays for systems biology. *Acta Biochimica Et Biophysica Sinica,* **2011**, *43*, (3), 161-171.
[81] Venkatasubbarao, S., Microarrays - status and prospects. *Trends in Biotechnology,* **2004**, *22*, (12), 630-637.
[82] Anderson, D.G.; Levenberg, S.; Langer, R., Nanoliter-scale synthesis of arrayed biomaterials and application to human embryonic stem cells. *Nature Biotechnology,* **2004**, *22*, (7), 863-866.
[83] Anderson, D.G.; Putnam, D.; Lavik, E.B.; Mahmood, T.A.; Langer, R., Biomaterial microarrays: rapid, microscale

screening of polymer-cell interaction. *Biomaterials,* **2005**, *26*, (23), 4892-4897.
[84] Diaz-Mochon, J.J.; Tourniaire, G.; Bradley, M., Microarray platforms for enzymatic and cell-based assays. *Chemical Society Reviews,* **2007**, *36*, (3), 449-457.
[85] Khan, F.; Tare, R.S.; Kanczler, J.M.; Oreffo, R.O.C.; Bradley, M., Strategies for cell manipulation and skeletal tissue engineering using high-throughput polymer blend formulation and microarray techniques. *Biomaterials,* **2010**, *31*, (8), 2216-2228.
[86] Tare, R.S.; Khan, F.; Tourniaire, G.; Morgan, S.M.; Bradley, M.; Oreffo, R.O.C., Selection of human mesenchymal osteoprogenitors from bone marrow stromal cell populations using polymer microarrays. *Tissue Engineering,* **2007**, *13*, (7), 1754-1754.
[87] Tourniaire, G.; Collins, J.; Campbell, S.; Mizomoto, H.; Ogawa, S.; Thaburet, J.F.; Bradley, M., Polymer microarrays for cellular adhesion. *Chemical Communications,* **2006**, (20), 2118-2120.
[88] Pernagallo, S.; Wu, M.; Gallagher, M.P.; Bradley, M., Colonising new frontiers-microarrays reveal biofilm modulating polymers. *Journal of Materials Chemistry,* **2011**, *21*, (1), 96-101.
[89] Quinlan, G.J.; Martin, G.S.; Evans, T.W., Albumin: Biochemical properties and therapeutic potential. *Hepatology,* **2005**, *41*, (6), 1211-1219.
[90] Meyer, D.; Girma, J.P., von Willebrand factor - structure and function. *Thrombosis and Haemostasis,* **1993**, *70*, (1), 99-104.
[91] Ruggeri, Z.M., Structure and function of von Willebrand factor. *Thrombosis and Haemostasis,* **1999**, *82*, (2), 576-584.
[92] Furlan, M., von Willebrand factor: molecular size and functional activity. *Annals of Hematology,* **1996**, *72*, (6), 341-348.
[93] Rodriguez, E.; Nan, R.; Li, K.Y.; Gor, J.; Perkins, S.J., A revised mechanism for the activation of Complement C3 to C3b - a molecular explanation of a disease-associated polymorphism. *Journal of Biological Chemistry,* **2015**, *290*, (4), 2334-2350.
[94] Tan, Y.H.; Liu, M.; Nolting, B.; Go, J.G.; Gervay-Hague, J.; Liu, G.Y., A nanoengineering approach for investigation and regulation of protein immobilization. *Acs Nano,* **2008**, *2*, (11), 2374-2384.
[95] Au, H.Y.N.; Brand, S.; Hutchinson, D.W.; Matejtschuk, P., Structure and ligand-binding properties of human-serum albumins. *Biochemical Society Transactions,* **1984**, *12*, (4), 659-660.

[96] De Ceunynck, K.; De Meyer, S.F.; Vanhoorelbeke, K., Unwinding the von Willebrand factor strings puzzle. *Blood,* **2013**, *121*, (2), 270-277.
[97] Zhang, Z.; Chen, S.F.; Jiang, S.Y., Dual-functional biomimetic materials: Nonfouling poly(carboxybetaine) with active functional groups for protein immobilization. *Biomacromolecules,* **2006**, *7*, (12), 3311-3315.
[98] Zhang, L.; Cao, Z.; Bai, T.; Carr, L.; Ella-Menye, J.-R.; Irvin, C.; Ratner, B.D.; Jiang, S., Zwitterionic hydrogels implanted in mice resist the foreign-body reaction. *Nature Biotechnology,* **2013**, *31*, (6), 553-+.
[99] Chauhan, A.; Lebeaux, D.; Decante, B.; Kriegel, I.; Escande, M.-C.; Ghigo, J.-M.; Beloin, C., A rat model of central venous catheter to study establishment of long-term bacterial biofilm and related acute and chronic infections. *PloS one,* **2012**, *7*, (5).
[100] Zhao, C.; Li, L.Y.; Wang, Q.M.; Yu, Q.M.; Zheng, J., Effect of Film Thickness on the Antifouling Performance of Poly(hydroxy-functional methacrylates) Grafted Surfaces. *Langmuir,* **2011**, *27*, (8), 4906-4913.
[101] Yu, Q.A.; Zhang, Y.X.; Wang, H.W.; Brash, J.; Chen, H., Anti-fouling bioactive surfaces. *Acta Biomaterialia,* **2011**, *7*, (4), 1550-1557.
[102] Passerini, L.; Lam, K.; Costerton, J.W.; King, E.G., Biofilms on indwelling vascular catheters. *Critical Care Medicine,* **1992**, *20*, (5).
[103] Dubois, J.; Rypens, F.; Garel, L.; David, M.; Lacroix, J.; Gauvin, F., Incidence of deep vein thrombosis related to peripherally inserted central catheters in children and adolescents. *Canadian Medical Association Journal,* **2007**, *177*, (10).
[104] Vickerman, J.C.; Gilmore, I.S. *Surface Analysis The Principal Techniques*. Second ed. John Wiley & Sons Ltd.: United Kingdom, **2009**.
[105] D, B. *Surface Analysis of Polymers by XPS and Static SIMS*. Cambridge University Press: Cambridge, **1998**.
[106] C., V.J.; S, G.I., Eds. *Surface Analysis: The Principal Techniques*. Second Edition ed. John Wiley & Sons Ltd.: United Kingdom, **2009**.
[107] Electronics, P. http://www.phi.com/surface-analysis-techniques/tof-sims.html [accessed 29 Jan 2013].
[108] Vickerman, J.C., Ed. *Surface Analysis - The Principal Techniques*. John Wiley & Sons: Chichester, **2003**.
[109] Watts, J.F. *An Introduction to Surface Analysis by Electron Spectroscopy*. Oxford University Press: New York, **1990**.

[110] Ista, L.K.; Mendez, S.; Lopez, G.P., Attachment and detachment of bacteria on surfaces with tunable and switchable wettability. *Biofouling,* **2010**, *26*, (1), 111-118.
[111] Cunliffe, D.; Alarcon, C.D.; Peters, V.; Smith, J.R.; Alexander, C., Thermoresponsive surface-grafted poly(N-isopropylacrylamide) copolymers: Effect of phase transitions on protein and bacterial attachment. *Langmuir,* **2003**, *19*, (7), 2888-2899.
[112] Taylor, M.; Urquhart, A.J.; Zelzer, M.; Davies, M.C.; Alexander, M.R., Picoliter water contact angle measurement on polymers. *Langmuir,* **2007**, *23*, (13), 6875-6878.
[113] Taylor, M. Surface analysis of polymer microarrays. The University of Nottingham, 2008.
[114] Schenk, S.; Laddaga, R.A., Improved method for electroporation of staphylococcus-aureus. *Abstracts of the General Meeting of the American Society for Microbiology,* **1992**, *92*, 223-223.
[115] Nwaneshiudu, A.; Kuschal, C.; Sakamoto, F.H.; Anderson, R.R.; Schwarzenberger, K.; Young, R.C., Introduction to Confocal Microscopy. *Journal of Investigative Dermatology,* **2012**, *132*, (12), 1-5.
[116] Olympus http://www.olympusfluoview.com/theory/index.html (17/09/2015),
[117] Hook, A.L.; Scurr, D.J.; Burley, J.C.; Langer, R.; Anderson, D.G.; Davies, M.C.; Alexander, M.R., Analysis and prediction of defects in UV photo-initiated polymer microarrays. *Journal of Materials Chemistry B,* **2013**, *1*, (7), 1035-1043.
[118] Hook, A.L.; Yang, J.; Chen, X.Y.; Roberts, C.J.; Mei, Y.; Anderson, D.G.; Langer, R.; Alexander, M.R.; Davies, M.C., Polymers with hydro-responsive topography identified using high throughput AFM of an acrylate microarray. *Soft Matter,* **2011**, *7*, (16), 7194-7197.
[119] LookChem http://www.lookchem.com/ (12/06/2014),
[120] ChemSpider http://www.chemspider.com/Chemical-Structure (12/06/2014),
[121] Surface tension values. http://www.surface-tension.de/ (01/06/2014),
[122] Accudyne. http://www.accudynetest.com/polytable_01_print.html (10/06/2014),
[123] Davies, M.C.; Alexander, M.R.; Hook, A.L.; Yang, J.; Mei, Y.; Taylor, M.; Urquhart, A.J.; Langer, R.; Anderson, D.G., High throughput surface characterization: A review of a new tool for screening prospective biomedical material arrays. *Journal of Drug Targeting,* **2010**, *18*, (10), 741-751.

[124] Weng, L.T.; Ng, K.M.; Cheung, Z.L.; Lei, Y.G.; Chan, C.M., Quantitative analysis of styrene-pentafluorostyrene random copolymers by ToF-SIMS and XPS. *Surface and Interface Analysis,* **2006**, *38*, (1), 32-43.
[125] Ferrari, S.; Ratner, B.D., ToF-SIMS quantification of albumin adsorbed on plasma-deposited fluoropolymers by partial least-squares regression. *Surface and Interface Analysis,* **2000**, *29*, (12), 837-844.
[126] Celiz, A.D.; Smith, J.G.W.; Patel, A.K.; Langer, R.; Anderson, D.G.; Barrett, D.A.; Young, L.E.; Davies, M.C.; Denning, C.; Alexander, M.R., Chemically diverse polymer microarrays and high throughput surface characterisation: a method for discovery of materials for stem cell culture. *Biomaterials Science,* **2014**, *2*, (11), 1604-1611.
[127] 194, T.; International Organization for Standardisation (ISO), **2002**.
[128] Seyfert, U.T.; Biehl, V.; Schenk, J., In vitro hemocompatibility testing of biomaterials according to the ISO 10993-4. *Biomolecular Engineering,* **2002**, *19*, (2-6), 91-96.
[129] Holmlin, R.E.; Chen, X.X.; Chapman, R.G.; Takayama, S.; Whitesides, G.M., Zwitterionic SAMs that resist nonspecific adsorption of protein from aqueous buffer. *Langmuir,* **2001**, *17*, (9), 2841-2850.
[130] Dunkelberger, J.R.; Song, W.-C., Complement and its role in innate and adaptive immune responses. *Cell Research,* **2010**, *20*, (1), 34-50.
[131] Streller, U.; Sperling, C.; Hubner, J.; Hanke, R.; Werner, C., Design and evaluation of novel blood incubation systems for in vitro hemocompatibility assessment of planar solid surfaces. *Journal of Biomedical Materials Research Part B-Applied Biomaterials,* **2003**, *66B*, (1), 379-390.
[132] Ray, S.; Shard, A.G., Quantitative analysis of adsorbed proteins by X-ray photoelectron spectroscopy. *Analytical Chemistry,* **2011**, *83*, (22), 8659-8666.
[133] Peters, T., Serum-albumin. *Advances in Protein Chemistry,* **1985**, *37*, 161-245.
[134] Kiselev, M.A.; Gryzunov, Y.A.; Dobretsov, G.E.; Komarova, M.N., The size of human serum albumin molecules in solution. *Biofizika,* **2001**, *46*, (3), 423-427.
[135] Nimmerjahn, F.; Ravetch, J.V., Fc gamma receptors as regulators of immune responses. *Nature Reviews Immunology,* **2008**, *8*, (1), 34-47.
[136] Anderson, J.M., Mechanisms of inflammation and infection with implanted devices. *Cardiovascular Pathology,* **1993**, *2*, (3), S33-S41.
[137] Zhang, Z.; Zhang, M.; Chen, S.F.; Horbetta, T.A.; Ratner, B.D.; Jiang, S.Y., Blood compatibility of surfaces with

superlow protein adsorption. *Biomaterials,* **2008**, *29*, (32), 4285-4291.
[138] Anderson, N.L.; Anderson, N.G., The human plasma proteome - History, character, and diagnostic prospects. *Molecular & Cellular Proteomics,* **2002**, *1*, (11), 845-867.
[139] Horbett, T.A., Protein adsorption on biomaterials. *Advances in Chemistry Series,* **1982**, (199), 233-244.
[140] Horbett, T.A.; Bohnert, J.L.; Slack, S.; Rapoza, R., Mechanisms of protein adsorption. *Abstracts of Papers of the American Chemical Society,* **1986**, *192*, 87-COLL.
[141] Yanagisawa, N.; Li, D.Q.; Ljungh, A., Protein adsorption on ex vivo catheters and polymers exposed to peritoneal dialysis effluent. *Peritoneal Dialysis International,* **2004**, *24*, (3), 264-273.
[142] Tengvall, P.; Lundstrom, I.; Liedberg, B., Protein adsorption studies on model organic surfaces: an ellipsometric and infrared spectroscopic approach. *Biomaterials,* **1998**, *19*, (4-5), 407-422.
[143] Taylor, M.; Urquhart, A.J.; Anderson, D.G.; Williams, P.M.; Langer, R.; Alexander, M.R.; Davies, M.C., A methodology for investigating protein adhesion and adsorption to microarrayed combinatorial polymers. *Macromolecular Rapid Communications,* **2008**, *29*, (15), 1298-1302.
[144] Bergstrand, A.; Rahmani-Monfared, G.; Ostlund, A.; Nyden, M.; Holmberg, K., Comparison of PEI-PEG and PLL-PEG copolymer coatings on the prevention of protein fouling. *Journal of Biomedical Materials Research Part A,* **2009**, *88A*, (3), 608-615.
[145] Deible, C.R.; Petrosko, P.; Johnson, P.C.; Beckman, E.J.; Russell, A.J.; Wagner, W.R., Molecular barriers to biomaterial thrombosis by modification of surface proteins with polyethylene glycol. *Biomaterials,* **1999**, *20*, (2), 101-109.
[146] Kenausis, G.L.; Voros, J.; Elbert, D.L.; Huang, N.P.; Hofer, R.; Ruiz-Taylor, L.; Textor, M.; Hubbell, J.A.; Spencer, N.D., Poly(L-lysine)-g-poly(ethylene glycol) layers on metal oxide surfaces: Attachment mechanism and effects of polymer architecture on resistance to protein adsorption. *Journal of Physical Chemistry B,* **2000**, *104*, (14), 3298-3309.
[147] Kingshott, P.; Thissen, H.; Griesser, H.J., Effects of cloud-point grafting, chain length, and density of PEG layers on competitive adsorption of ocular proteins. *Biomaterials,* **2002**, *23*, (9), 2043-2056.
[148] Li, D.; Chen, H.; McClung, W.G.; Brash, J.L., Lysine-PEG-modified polyurethane as a fibrinolytic surface: Effect of PEG chain length on protein interactions, platelet interactions and clot lysis. *Acta Biomaterialia,* **2009**, *5*, (6), 1864-1871.
[149] Ma, C.; Zhou, G.; Zhang, G., Protein Resistance of Polyurethane with Hydrophilic and Hydrophobic Soft

Segments. *Journal of Polymer Science Part B-Polymer Physics,* **2010**, *48*, (18), 1987-1993.
[150] Wilson, C.J.; Clegg, R.E.; Leavesley, D.I.; Pearcy, M.J., Mediation of biomaterial-cell interactions by adsorbed proteins: A review. *Tissue Engineering,* **2005**, *11*, (1-2), 1-18.
[151] Tsai, W.B.; Grunkemeier, J.M.; McFarland, C.D.; Horbett, T.A., Platelet adhesion to polystyrene-based surfaces preadsorbed with plasmas selectively depleted in fibrinogen, fibronectin, vitronectin, or von Willebrand's factor. *Journal of Biomedical Materials Research,* **2002**, *60*, (3), 348-359.
[152] Wettero, J.; Tengvall, P.; Bengtsson, T., Platelets stimulated by IgG-coated surfaces bind and activate neutrophils through a selectin-dependent pathway. *Biomaterials,* **2003**, *24*, (9), 1559-1573.
[153] Grunkemeier, J.M.; Tsai, W.B.; McFarland, C.D.; Horbett, T.A., The effect of adsorbed fibrinogen, fibronectin, von Willebrand factor and vitronectin on the procoagulant state of adherent platelets. *Biomaterials,* **2000**, *21*, (22), 2243-2252.
[154] Vogler, E.A., Protein adsorption in three dimensions. *Biomaterials,* **2012**, *33*, (5), 1201-1237.
[155] Sivaraman, B.; Latour, R.A., The relationship between platelet adhesion on surfaces and the structure versus the amount of adsorbed fibrinogen. *Biomaterials,* **2010**, *31*, (5), 832-839.
[156] Passirani, C.; Barratt, G.; Devissaguet, J.P.; Labarre, D., Interactions of nanoparticles bearing heparin or dextran covalently bound to poly(methyl methacrylate) with the complement system. *Life Sciences,* **1998**, *62*, (8), 775-785.
[157] Carroll, M.V.; Sim, R.B., Complement in health and disease. *Advanced Drug Delivery Reviews,* **2011**, *63*, (12), 965-975.
[158] Chang, C.C.; Lieberman, S.M.; Moghe, P.V., Leukocyte spreading behavior on vascular biomaterial surfaces: consequences of chemoattractant stimulation. *Biomaterials,* **1999**, *20*, (3), 273-281.
[159] Wettero, J.; Askendal, A.; Bengtsson, T.; Tengvall, P., On the binding of complement to solid artificial surfaces in vitro. *Biomaterials,* **2002**, *23*, (4), 981-991.
[160] Arvidsson, S.; Askendal, A.; Tengvall, P., Blood plasma contact activation on silicon, titanium and aluminium. *Biomaterials,* **2007**, *28*, (7), 1346-1354.
[161] Arima, Y.; Toda, M.; Iwata, H., Complement activation on surfaces modified with ethylene glycol units. *Biomaterials,* **2008**, *29*, (5), 551-560.
[162] Hirata, I.; Morimoto, Y.; Murakami, Y.; Iwata, H.; Kitano, E.; Kitamura, H.; Ikada, Y., Study of complement activation on well-defined surfaces using surface plasmon

resonance. *Colloids and Surfaces B-Biointerfaces,* **2000**, *18*, (3-4), 285-292.
[163] Jang, H.S.; Ryu, K.E.; Ahn, W.S.; Chun, H.J.; Dal Park, H.; Park, K.D.; Kim, Y.H., Complement activation by sulfonated poly(ethylene glycol)-acrylate copolymers through alternative pathway. *Colloids and Surfaces B-Biointerfaces,* **2006**, *50*, (2), 141-146.
[164] Chen, M.; Yu, Q.; Sun, H., Novel strategies for the prevention and treatment of biofilm related infections. *International Journal of Molecular Sciences,* **2013**, *14*, (9), 18488-18501.
[165] Malaty, J.; Antonelli, P.J., Effect of blood and mucus on tympanostomy tube biofilm formation. *Laryngoscope,* **2008**, *118*, (5), 867-870.
[166] Samaranayake, Y.H.; Cheung, B.P.K.; Yau, J.Y.Y.; Yeung, S.K.W.; Samaranayake, L.P., Human serum promotes Candida albicans biofilm growth and virulence gene expression on silicone biomaterial. *Plos One,* **2013**, *8*, (5).
[167] Shadeed, M.; AlMogbel, M.S.; Al-Hazimi, A.; Hossain, A., Influence of normal human serum on production of biofilm by acinetobacter baumannii. *Journal of Pure and Applied Microbiology,* **2014**, *8*, (1), 273-278.
[168] Menzies, B.E., The role of fibronectin binding proteins in the pathogenesis of Staphylococcus aureus infections. *Current Opinion in Infectious Diseases,* **2003**, *16*, (3), 225-229.
[169] Switalski, L.M.; Patti, J.M.; Butcher, W.; Gristina, A.G.; Speziale, P.; Hook, M., A collagen receptor on staphylococcus-aureus strains isolated from patients with septic arthritis mediates adhesion to cartilage. *Molecular Microbiology,* **1993**, *7*, (1), 99-107.
[170] Eidhin, D.N.; Perkins, S.; Francois, P.; Vaudaux, P.; Hook, M.; Foster, T.J., Clumping factor B (ClfB), a new surface-located fibrinogen-binding adhesin of Staphylococcus aureus. *Molecular Microbiology,* **1998**, *30*, (2), 245-257.
[171] McDevitt, D.; Nanavaty, T.; HousePompeo, K.; Bell, E.; Turner, N.; McIntire, L.; Foster, T.; Hook, M., Characterization of the interaction between the Staphylococcus aureus clumping factor (ClfA) and fibrinogen. *European Journal of Biochemistry,* **1997**, *247*, (1), 416-424.
[172] Fehrmann, C.; Jurk, K.; Bertling, A.; Seidel, G.; Fegeler, W.; Kehrel, B.E.; Peters, G.; Becker, K.; Heilmann, C., Role for the fibrinogen-binding proteins Coagulase and Efb in the Staphylococcus aureus-Candida interaction. *International Journal of Medical Microbiology,* **2013**, *303*, (5), 230-238.
[173] Wagner, C.; Aytac, S.; Hansch, G.M., Biofilm growth on implants: bacteria prefer plasma coats. *International Journal of Artificial Organs,* **2011**, *34*, (9), 811-817.

[174] Cheng, G.; Zhang, Z.; Chen, S.; Bryers, J.D.; Jiang, S., Inhibition of bacterial adhesion and biofilm formation on zwitterionic surfaces. *Biomaterials,* **2007**, *28*, (29), 4192-4199.
[175] Cheng, G.; Xite, H.; Zhang, Z.; Chen, S.F.; Jiang, S.Y., A Switchable Biocompatible Polymer Surface with Self-Sterilizing and Nonfouling Capabilities. *Angewandte Chemie-International Edition,* **2008**, *47*, (46), 8831-8834.
[176] Xu, L.N.; Ma, P.P.; Yuan, B.; Chen, Q.; Lin, S.C.; Chen, X.; Hua, Z.C.; Shen, J., Anti-biofouling contact lenses bearing surface-immobilized layers of zwitterionic polymer by one-step modification. *Rsc Advances,* **2014**, *4*, (29), 15030-15035.
[177] Roosjen, A.; Kaper, H.J.; van der Mei, H.C.; Norde, W.; Busscher, H.J., Inhibition of adhesion of yeasts and bacteria by poly(ethylene oxide)-brushes on glass in a parallel plate flow chamber. *Microbiology-Sgm,* **2003**, *149*, 3239-3246.
[178] Roosjen, A.; van der Mei, H.C.; Busscher, H.J.; Norde, W., Microbial adhesion to poly(ethylene oxide) brushes: Influence of polymer chain length and temperature. *Langmuir,* **2004**, *20*, (25), 10949-10955.
[179] Rosenhahn, A.; Schilp, S.; Kreuzer, H.J.; Grunze, M., The role of "inert'' surface chemistry in marine biofouling prevention. *Physical Chemistry Chemical Physics,* **2010**, *12*, (17), 4275-4286.
[180] Hall-Stoodley, L.; Stoodley, P., Evolving concepts in biofilm infections. *Cellular Microbiology,* **2009**, *11*, (7), 1034-1043.
[181] Lorenzetti, M.; Dogsa, I.; Stosicki, T.; Stopar, D.; Kalin, M.; Kobe, S.; Novak, S., The Influence of Surface Modification on Bacterial Adhesion to Titanium-Based Substrates. *Acs Applied Materials & Interfaces,* **2015**, *7*, (3), 1644-1651.
[182] Boulangepetermann, L.; Baroux, B.; Bellonfontaine, M.N., The influence of metallic surface wettability on bacterial adhesion. *Journal of Adhesion Science and Technology,* **1993**, *7*, (3), 221-230.
[183] Fletcher, M.; Loeb, G.I., Influence of substratum characteristics on the attachment of a marine pseudomonad to solid-surfaces. *Applied and Environmental Microbiology,* **1979**, *37*, (1), 67-72.
[184] Bjerketorp, J.; Nilsson, M.; Ljungh, A.; Flock, J.I.; Jacobsson, K.; Frykberg, L., A novel von Willebrand factor binding protein expressed by Staphylococcus aureus. *Microbiology-Sgm,* **2002**, *148*, 2037-2044.
[185] O'Seaghdha, M.; van Schooten, C.J.; Kerrigan, S.W.; Emsley, J.; Silverman, G.J.; Cox, D.; Lenting, P.J.; Foster, T.J., Staphylococcus aureus protein A binding to von Willebrand factor A1 domain is mediated by conserved IgG binding regions. *Febs Journal,* **2006**, *273*, (21), 4831-4841.

[186] Cheung, A.L.; Krishnan, M.; Jaffe, E.A.; Fischetti, V.A., Fibrinogen acts as a bridging molecule in the adherence of staphylococcus-aureus to cultured human endothelial-cells. *Journal of Clinical Investigation,* **1991**, *87*, (6), 2236-2245.
[187] Schneider, S.W.; Nuschele, S.; Wixforth, A.; Gorzelanny, C.; Alexander-Katz, A.; Netz, R.R.; Schneider, M.F., Shear-induced unfolding triggers adhesion of von Willebrand factor fibers. *Proceedings of the National Academy of Sciences of the United States of America,* **2007**, *104*, (19), 7899-7903.
[188] Koppelman, S.J.; vanHoeij, M.; Vink, T.; Lankhof, H.; Schiphorst, M.E.; Damas, C.; Vlot, A.J.; Wise, R.; Bouma, B.N.; Sixma, J.J., Requirements of von willebrand factor to protect factor VIII from inactivation by activated protein C. *Blood,* **1996**, *87*, (6), 2292-2300.
[189] Peyvandi, F.; Garagiola, I.; Baronciani, L., Role of von Willebrand factor in the haemostasis. *Blood Transfusion,* **2011**, *9*, S3-S8.
[190] Sperling, C.; Fischer, M.; Maitz, M.F.; Werner, C., Blood coagulation on biomaterials requires the combination of distinct activation processes. *Biomaterials,* **2009**, *30*, (27), 4447-4456.
[191] Scharf, R.E.; Adams, H.A.; Baumann, G.; Cascorbi, I.; Emmel, M.; Fischer, D.; Flohe, S.; Fries, D.; Gaensslen, A.; Geiger, S.; Heller, A.R.; Hildebrand, F.; Klar, E.; Klippe, H.J.; Lampl, L.; Prange, H.; Rolle, U.; Sarrafzadeh, A.; Standl, T.; Teske, W.; Werner, G.; Zander, R.; Divi, Haemostasis in shock Part 2: physiology of haemostasis. *Anasthesiologie & Intensivmedizin,* **2014**, *55*, 272-+.
[192] Aronson, D.L.; Stevan, L.; Ball, A.P.; Franza, B.R.; Finlayson, J.S., Generation of combined prothrombin activation peptide (f1.2) during clotting of blood and plasma. *Journal of Clinical Investigation,* **1977**, *60*, (6), 1410-1418.
[193] Pidard D., S.-T.M., Chignard M., M.C. Berndt. *Neutrophil-platelet interactions, in: Platelets, thrombosis and the vessel wall*. Harwood Academic Publishers: Amsterdam, **2000**.
[194] Yeo, E.L.; Sheppard, J.A.I.; Feuerstein, I.A., Role of p-selectin and leukocyte activation in polymorphonuclear cell-adhesion to surface adherent activated platelets under physiological shear conditions (an injury vessel wall model). *Blood,* **1994**, *83*, (9), 2498-2507.
[195] Capitanio, A.M.; Niewiarowski, S.; Rucinski, B.; Tuszynski, G.P.; Cierniewski, C.S.; Hershock, D.; Kornecki, E., Interaction of platelet factor-4 with human-platelets. *Biochimica Et Biophysica Acta,* **1985**, *839*, (2), 161-173.
[196] Rucinski, B.; Poggi, A.; James, P.; Holt, J.C.; Niewiarowski, S., Purification of 2 heparin-binding proteins

from porcine platelets and their homology with human secreted platelet proteins. *Blood,* **1983**, *61*, (6), 1072-1080.
[197] Ashby B., C.R.W., Daniel J.L., Kunapuli S.P., Smith J.B. *Platelet stimulatory and inhibitory receptors, in: Hemostasis and thrombosis. Basic prin-ciples and clinical practice*. 4th ed. Lippincott Williams & Wilkins: Philadelphia, Baltimore., **2001**.
[198] https://www.vygon.com/catalog/multicath-expert-2_923_008157167, V.-. Double lumen Multicath Expert. https://www.vygon.com/catalog/multicath-expert-2_923_008157167 (04/01/2016),
[199] Ahmed, A.-F.; Zakaria, K.M., Synthesis, characterization, and biocompatibility of poly (acrylic acid/methyl methacrylate)-grafted-poly (ethylene-co-tetrafluoroethylene) film for prosthetic cardiac valves. *Colloid and Polymer Science,* **2014**, *292*, (12), 3301-3310.
[200] Duncan M. Paton, T.R.A., Roshan Maini Fluorinating Polymer Surfaces ;US Patent: US5356668 A. 1991.
[201] Young H. Kim, D.K.H. Perfluorocarbon-grafted polyurethane with improved blood compatibility and process for their preparation; US Patent: US5242995 A. 1993.
[202] Pathak, C.P. Implantable medical devices with fluorinated polymer coatings, and methods of coating thereof ; Patent no: WO2005061023 A1. 2005.
[203] Pathak, C.P., Implantable medical devices with fluorinated polymer coatings, and methods of coating thereof. *Official Gazette of the United States Patent and Trademark Office Patents,* **2009**.
[204] Borman Christopher David, I.D.J. Production of vinylic polymers; International Patent no.: WO2000034345 A1. Jun 15, 2000.
[205] Seib, F.P.; Maitz, M.F.; Hu, X.; Werner, C.; Kaplan, D.L., Impact of processing parameters on the haemocompatibility of Bombyx mori silk films. *Biomaterials,* **2012**, *33*, (4), 1017-1023.
[206] Berney, M.; Hammes, F.; Bosshard, F.; Weilenmann, H.U.; Egli, T., Assessment and interpretation of bacterial viability by using the LIVE/DEAD BacLight kit in combination with flow cytometry. *Applied and Environmental Microbiology,* **2007**, *73*, (10), 3283-3290.
[207] https://tools.thermofisher.com/content/sfs/manuals/mp07007.pdf, B.-. https://tools.thermofisher.com/content/sfs/manuals/mp07007.pdf
[208] Martz, H.; Paynter, R.; Losier, M.; Domurado, D.; Forest, J.C.; Guidoin, R., Blood hemolysis by PTFE and polyurethane vascular prostheses in an in-vitro circuit. *Journal of Biomedical Materials Research,* **1987**, *21*, (10), 1187-1196.

[209] Anamelechi, C.C.; Truskey, G.A.; Reichert, W.M., Mylar (TM) and Teflon-AF (TM) as cell culture substrates for studying endothelial cell adhesion. *Biomaterials,* **2005**, *26*, (34), 6887-6896.
[210] Ratner BD, H.A., Schoen FJ, Lemons JE. *Biomaterials Science: An Introduction to Materials in Medicine*. 2nd ed. ed. London: Elsevier Academic Press, **2004**.
[211] Davies, J.; Davies, D., Origins and Evolution of Antibiotic Resistance. *Microbiology and Molecular Biology Reviews,* **2010**, *74*, (3), 417-+.
[212] McEver R.P., P.-s. *Platelets, thrombosis and the vessel wall*. Harwood Academic Publishers: Amsterdam, **2000**.
[213] plasticisers.org http://www.plasticisers.org/plasticisers/bis-2-ethylhexyl-phthalate-dehp. http://www.plasticisers.org/plasticisers/bis-2-ethylhexyl-phthalate-dehp (26/11/2015),
[214] Jackson, J.K.; Springate, C.M.K.; Hunter, W.L.; Burt, H.M., Neutrophil activation by plasma opsonized polymeric microspheres: inhibitory effect of Pluronic F127. *Biomaterials,* **2000**, *21*, (14), 1483-1491.
[215] Sun, D.H.; Trindade, M.C.D.; Nakashima, Y.; Maloney, W.J.; Goodman, S.B.; Schurman, D.J.; Smith, R.L., Human serum opsonization of orthopedic biomaterial particles: Protein-binding and monocyte/macrophage activation in vitro. *Journal of Biomedical Materials Research Part A,* **2003**, *65A*, (2), 290-298.
[216] Anderson, J.M.; Rodriguez, A.; Chang, D.T., Foreign body reaction to biomaterials. *Seminars in Immunology,* **2008**, *20*, (2), 86-100.
[217] Langer, R.; Tirrell, D.A., Designing materials for biology and medicine. *Nature,* **2004**, *428*, (6982), 487-492.
[218] Peppas, N.A.; Langer, R., New challenges in biomaterials. *Science,* **1994**, *263*, (5154), 1715-1720.
[219] Hetrick, E.M.; Prichard, H.L.; Klitzman, B.; Schoenfisch, M.H., Reduced foreign body response at nitric oxide-releasing subcutaneous implants. *Biomaterials,* **2007**, *28*, (31), 4571-4580.
[220] Ratner, B.D., Reducing capsular thickness and enhancing angiogenesis around implant drug release systems. *Journal of Controlled Release,* **2002**, *78*, (1-3), 211-218.
[221] Kuklin, N.A.; Pancari, G.D.; Tobery, T.W.; Cope, L.; Jackson, J.; Gill, C.; Overbye, K.; Francis, K.P.; Yu, J.; Montgomery, D.; Anderson, A.S.; McClements, W.; Jansen, K.U., Real-time monitoring of bacterial infection in vivo: Development of bioluminescent staphylococcal foreign-body and deep-thigh-wound mouse infection models. *Antimicrobial Agents and Chemotherapy,* **2003**, *47*, (9), 2740-2748.

[222] Overney, R.M.; Buenviaje, C.; Luginbuhl, R.; Dinelli, F., Glass and structural transitions measured at polymer surfaces on the nanoscale. *Journal of Thermal Analysis and Calorimetry,* **2000**, *59*, (1-2), 205-225.
[223] de Gennes, P.G., Glass transitions in thin polymer films. *European Physical Journal E,* **2000**, *2*, (3), 201-203.
[224] Fox, T.G.; *Bull. Am. Phys. Soc*, **1956**; Vol. *1*.
[225] Aldrich, S. https://www.sigmaaldrich.com/content/dam/sigma-aldrich/docs/Aldrich/General_Information/thermal_transitions_of_homopolymers.pdf. https://www.sigmaaldrich.com/content/dam/sigma-aldrich/docs/Aldrich/General_Information/thermal_transitions_of_homopolymers.pdf (27/11/2015),
[226] Adlington K, E.E., yang J ing, Chang Chien YI, Li Jianing, Gower Alexandra, Stimpson Amy, Anderson Daniel G, Langer Robert, Davies Martyn C, Hook Andrew L, Williams Paul, Alexander Morgan R and Irvine Derek J, Application of targeted molecular and material property optimization to bacterial attachment-resistant (meth)acrylate polymers. *Biomacromolecules,* **2016**.
[227] Murga, R.; Miller, J.M.; Donlan, R.M., Biofilm formation by gram-negative bacteria on central venous catheter connectors: Effect of conditioning films in a laboratory model. *Journal of Clinical Microbiology,* **2001**, *39*, (6).
[228] Magennis, P.E.; Hook, A.L.; Alexander, M.R.; Williams, P., Making silicone rubber highly resistant to bacterial attachment using thiol-ene grafting. *ACS Applied Materials & Interfaces,* **2016**.